INTEGRATED GEOCHEMICAL, MECHANICAL, AND LITHOLOGICAL CHARACTERIZATION OF THE MARCELLUS SHALE, PENNSYLVANIA

by

CHIEKE GREGORY OFFURUM

Bachelor of Science, 2004

University of Port Harcourt

Nigeria

Submitted to the Graduate Faculty of the

Colleges of Science and Engineering

Texas Christian University

in partial fulfillment of the requirements

for the degree of

Master of Science

December 2016

ACKNOWLEDGEMENTS

Firstly, I would like to thank my thesis advisor Dr. Helge Alsleben for all his continued support and guidance throughout this study. I would also like to thank my committee members Milton Enderlin for sharing his petrophysical expertise with me and Dr. Cheyenne Xie for teaching me the processes involved in sedimentary basin formation and evolution.

Secondly, I would like to thank EOG Resources, Inc. for allowing me to embark on this study and providing the cores and core analysis results required for this graduate work. I especially want to thank Michael Shultz, Fort Worth Division Exploration Manager, for his support and guidance throughout this process especially his continued mentorship which has enhanced my geological knowledge and the quality of this graduate work. I would also like to thank my colleagues at EOG, Denton O'Neal, Hannah Durkee, and Shadiya Bello for their support, ideas and suggestions to this work.

Finally, I would like to thank my wife Adanna for her support during this process. I am extremely grateful for your encouragement, patience, love, and assistance especially with our infant son. This thesis would not have been possible without you and I dedicate it to you.

TABLE OF CONTENTS

LIST OF FIGURES

LIST OF TABLES

CHAPTER 1
INTRODUCTION

The Appalachian basin in North America is an asymmetric foreland trough that formed in the early Paleozoic during the Taconic orogeny (Ver Straeten et al., 2011). It is a northeast to southwest trending basin that extends from Quebec to Alabama. The basin is bounded by the Acadian mountains to the east, and to the west by the Nashville Dome, Jessamine Dome, Cincinnati Arch, and Findlay Arch (Fig. 1.1) (Reed et al., 2007). The basin covers 185,500 mi^2 (480,000 km^2) and is approximately 1,075 miles (1,730 km) long by 170 miles (270 km) wide (Ryder, 2008).

Within the Appalachian basin, the Marcellus Shale Formation has become a prolific shale-gas reservoir in the United States and more than 3,600 wells are producing approximately 18 Bcf (billion cubic feet) per day of gas as of July 2016 (U.S EIA, 2016). The Marcellus Shale interval (Middle Devonian) is the basal unit of the Hamilton Group. It consists of two shale intervals, the lower Union Springs Shale and the upper Oatka Creek Shale, which are separated by the Cherry Valley Limestone (Zagorski et al., 2012). It is bounded above by the Middle Devonian Mahantango Formation and below by the Lower Devonian Onondaga Limestone (Fig. 1.2).

Despite its often homogenous and fine grained appearance, the Marcellus Shale was deposited under varying environmental conditions, which can lead to subtle differences in fabric and texture not readily identifiable by conventional low-resolution sampling and analysis methods. The main purpose of this study is to identify and understand the heterogeneity in the Marcellus Shale by using high-resolution chemostratigraphy and mechanical stratigraphy. The project has three main goals: 1) to perform detailed lithological, chemical, and mechanical analysis on the Marcellus Shale, 2) to understand the heterogeneity in lithology, mineralogy, and rock strength in

the formation, and 3) to compare the geochemical and geomechanical results with petrophysical logs.

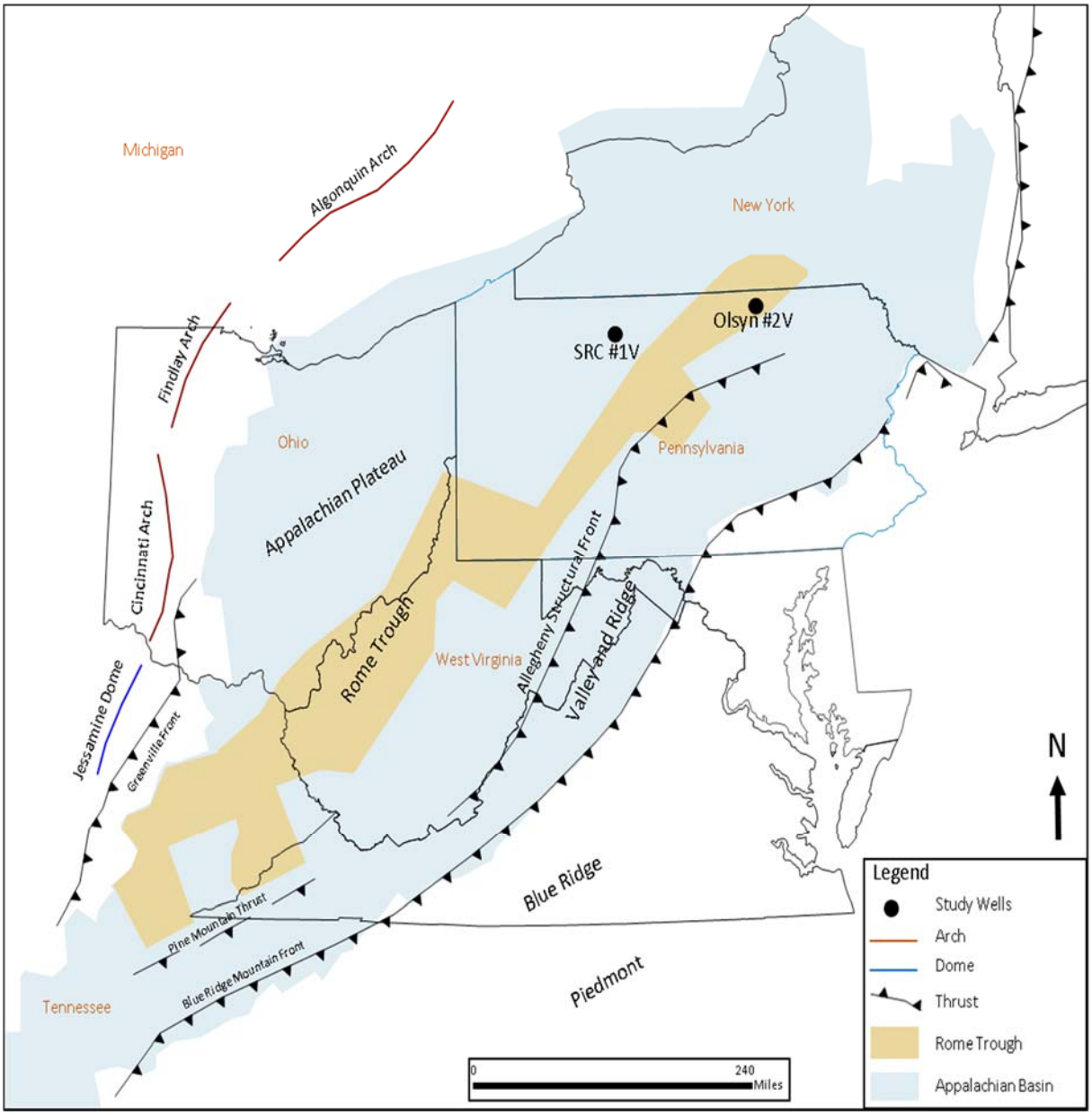

Figure 1.1 – The Appalachian Basin with major physiographic provinces and structural features. Olsyn #2V and SRC #1V wells used in study are also highlighted. Modified from Reed et al., 2007.

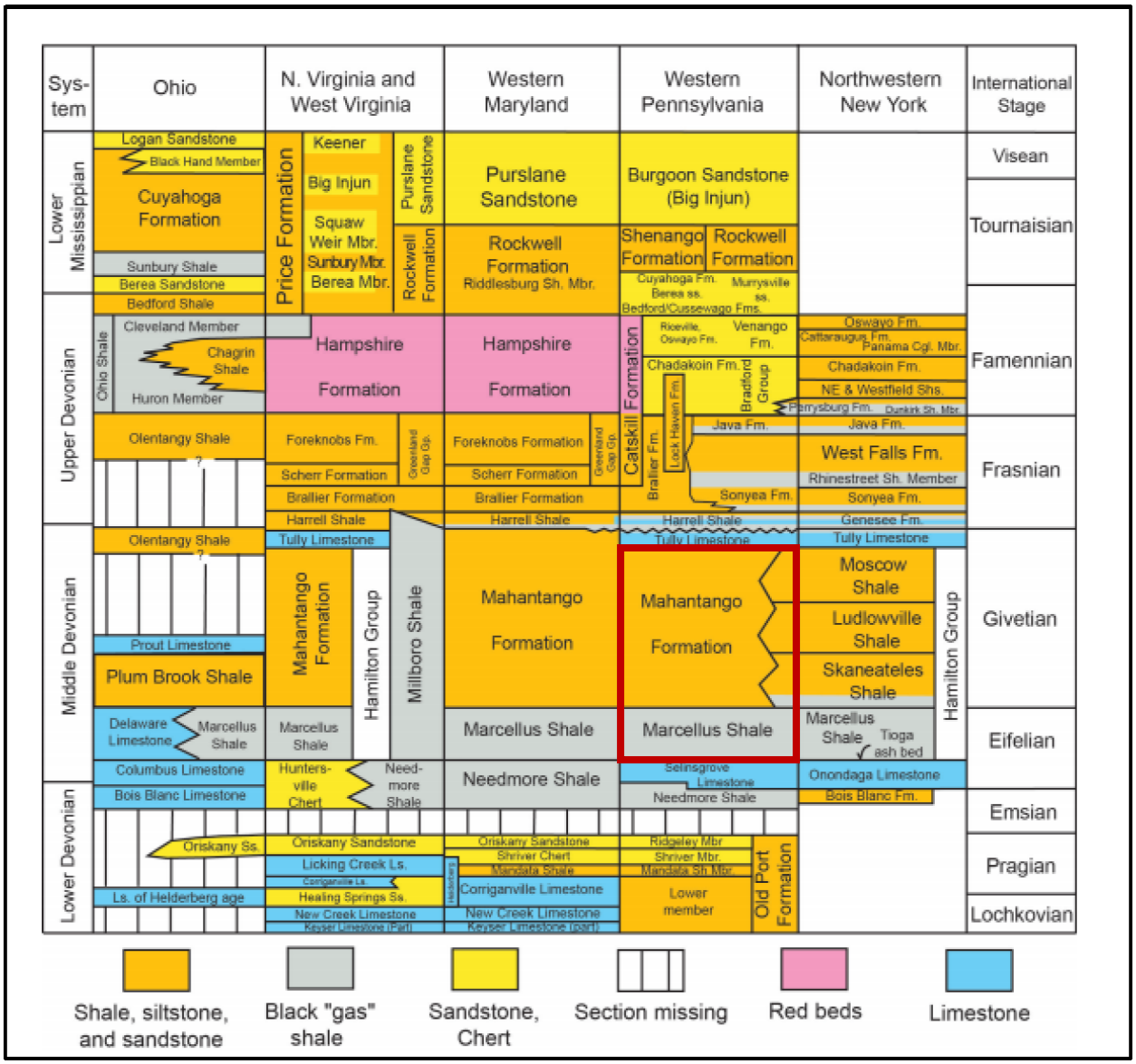

Figure 1.2 – Generalized Devonian and Lower Mississippian Stratigraphy of the Northern and central Appalachian basin. Mahantango and Marcellus Formations highlighted. Modified from Milici and Swezey (2006).

1.1: Geology of the Appalachian Basin

1.1.1: Tectonic Setting

The Appalachian basin formed as a result of the collision of eastern Laurentia (North American plate) with a volcanic island arc during the Taconic orogeny in the middle Ordovician (Ver Straeten et al., 2011). Subsequent orogenies included the Acadian orogeny, which was the

result of the collision of a series of Avalonian continental fragments with the Laurentian continent in the Middle Devonian, and the Alleghanian orogeny, which occurred as a result of Africa colliding with North America in Late Carboniferous to Permian. Both orogenies resulted in the reactivation and reorganization of the basin into an active foreland basin system (Ver Straeten et al., 2011). The orientation and spatial distribution of new and reactivated features have strongly influenced depositional settings in the Appalachian basin from Ordovician through Permian (Roen, 1984).

To the north, the Appalachian basin extends as far as the United States-Canada border and continues offshore into Lake Erie and Lake Ontario (Ryder, 2008). To the west, the basin gradually shallows against the Cincinnati arch (Fig. 1.1). The Cincinnati arch is a broad, elongate northwest to southeast trending structural uplift that separates the Michigan basin to the west from the Appalachian basin to the east. The arch developed in response to stresses generated during the Taconic orogeny and existed as a positive topographic feature from the Late Ordovician through the Devonian period. The Cincinnati arch branches to form the Findlay and Kankakee arches north of Cincinnati, Ohio. The Findlay arch plunges at the extent of the basin under Ontario and reappears as the Algonquin arch farther north (Ryder, 2008). The Nashville Dome and the Jessamine Dome are also structural uplifts that bound the basin to the southwest. The Adirondack Dome is a positive feature that bounds the Appalachian basin to the northeast. The Adirondack Dome was formed by the uplift of previously deeply buried 1.2 billion years old metamorphic and igneous rocks (Richard, 2007). The Blue Ridge thrust belt/ Acadian mountains defines the eastern limit of the basin (Fig. 1.1). It is approximately 932 miles (1,500 km) long and underlies parts of eight states from central Alabama to southern Pennsylvania (Milici, 1977; Rodgers, 1990). The thrust belt consist of allochthonous, Proterozoic igneous and metamorphic rocks that were derived

from the early Paleozoic Laurentian continental margin and thrust as much as 249 miles (400 km) westward into the craton (Ettensohn, 1985).

There are several major tectonic features in the Appalachian basin such as the Rome Trough, Kentucky River and Irvine-Paint Creek fault zones that have had significant effects on the evolution of the basin and depositional sequences (Roen, 1984). The Rome Trough is a linear north-east trending structure bounded by normal faults in Precambrian basement rocks of the basin (Fig. 1) (Roen, 1984). It formed during the early and middle Cambrian when the Iapetus-Rheic ocean opened and began spreading (Thomas, 1991). It is approximately 30-50 miles (50-80 km) wide by 600 mile (960 km) long and extends from central Kentucky into central Pennsylvania. Seismic data and subsurface mapping suggest that these features have undergone intermittent movement throughout the Paleozoic, with the most significant movement occurring during the Devonian to Pennsylvanian time. The reactivation of Rome Trough faults appears to have influenced depositional patterns of the Paleozoic sediments and played an important role in the development of fractures especially in the Devonian-aged Marcellus Formation (Harris, 1978; Roen, 1984). The Kentucky River and the Irvine-Paint Creek fault systems are the only known surface manifestations of the Rome Trough graben complex and intersect the Devonian Shales at the surface where the shales crop out around the Jessamine Dome (Roen, 1984).

1.1.2: Stratigraphy of the Appalachian Basin

The deposits of the Appalachian basin consist almost entirely of Paleozoic sediments. Nearly 9, 000 feet (2,700 meters) of Paleozoic strata are present adjacent to the thrust belt in the deepest part of the basin. The early Devonian-aged Onondaga Limestone occurs beneath the Hamilton Group and is made up of limestones and dolostones. The Marcellus Shale is the basal unit of the Hamilton Group, and is comprised of organic black and gray shale interbedded with

thin limestone beds (Fig. 1.3). The Mahantango Formation is the upper unit of the Hamilton Group. It consists of bioturbated, thickly laminated silty shale with minor amounts of limestone and very fine grained sandstones (Hasson and Dennison, 1988). The Tully Limestone is the upper bounding formation of the Hamilton Group and is made up of fossilliferous limestones.

1.1.3: Marcellus Shale Stratigraphy

The Marcellus Formation of the Hamilton Group is an organic-rich shale and has a thickness of up to 900 feet (275 meters) in places (Lash and Engelder, 2011). It thickens from west to east and generally grades eastwards into gray and greenish shales (Emmanuel, 2013). The unit is informally divided into three members: the lower Union Springs member, the middle Cherry Valley member, and the upper Oatka Creek member (Lash and Engelder, 2011).

The Union Springs member is the basal unit of the Marcellus Formation (Fig. 1.3), although it is absent along a northeast-southwest trending axis in western New York into western Pennsylvania (Emmanuel, 2013). It unconformably overlies the Onondaga Limestone and is especially thick in northeast Pennsylvania where it exceeds 160 feet (50 m). The member is mostly an organic-rich shale and includes numerous calcite-filled fractures (Lash and Engelder, 2011). A layer of volcanic ash beds called the Tioga bentonite, or K-bentonite, which is approximately 2 feet (0.6 m) thick and consists of several discrete, relatively thin volcanic ash layers, underlies the Union Spring member in eastern Pennsylvania (Fig 1.3). The Stony Hollow member is a sub-unit of the Union Springs member and is a fine- to medium grained siliciclastic unit with varying amounts of calcite and dolomite.

The Cherry Valley Limestone member overlies the Union Springs member. Where the Union Springs member is absent due to erosion or non-deposition, the Cherry Valley Limestone

directly overlies the Onondaga Limestone (Lash and Engelder, 2011). It increases in thickness from approximately 10 feet (3 m) in western New York and northwestern Pennsylvania to more than 140 feet (45 m) in northeastern Pennsylvania and southeastern New York (Emmanuel, 2013). The limestone is comprised of variable amounts of interlayered fossilliferous carbonate, shale and sandstone (Emmanuel, 2013).

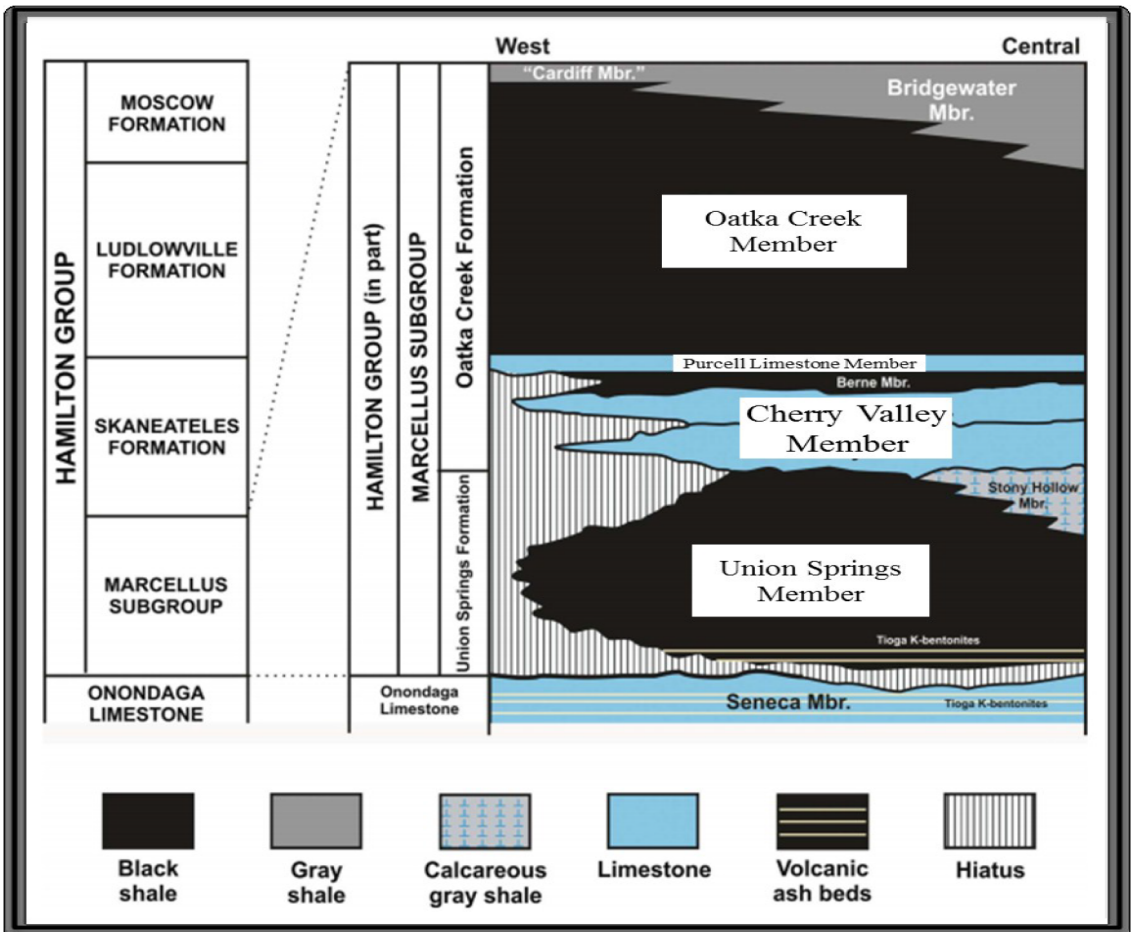

Figure 1.3 – Stratigraphy of the Marcellus Formation subdivided into the Oatka Creek member, Cherry Valley member and the Union Springs member. From Carter et al. (2011).

The Oatka Creek member overlies the Cherry Valley Limestone. It thickens from west to east and exceeds 550 feet (170 m) in eastern Wayne County, Pennsylvania and Sullivan County, New York (Lash and Engelder, 2011). The Oatka Creek member is composed of successions of

black and gray shales and minute amounts of siltstones and limestones (Lash and Engelder, 2011). The Berne member is a sub-unit of the Oatka Creek member and is a black organic-rich mudstone.

The Purcell Limestone separates the black shale succession of the Lower Oatka Creek member (Berne member) from the gray shale succession of the Upper Oatka Creek member in many parts of the basin, but it is thin to absent in some parts of the basin (Emmanuel, 2013). It extends into the subsurface of Pennsylvania, Maryland and West Virginia and is composed of carbonate mudstone, and grey silty shale, as well as scattered beds of siltstones, limestone nodules, and barite nodules about 1 to 2 inches (2 to 5 cm) in diameter (Cate, 1963; Emmanuel, 2013). The Purcell Limestone and the Cherry Valley Limestone appear to be thin to absent in different parts of New York, Pennsylvania and West Virginia. This may be a reason why different authors (e.g. Lash and Engelder, 2011; Ver Straeten et al., 2011) regard the two as being lateral equivalents.

1.2: Previous Work

The first known geologist to have worked on the Marcellus Formation was James Hall, an American paleontologist and stratigrapher, who had an influential role in the development of paleontology in the United States. In 1839, he published a report titled “Marcellus Shale in Seneca County” in which he argued in favor of location-based nomenclature where “the rock or group will receive its name from the place it is best developed” (Hall, 1839). Based on his persuasion, the location-based name for the Marcellus was adopted by the Pennsylvania survey. In 1843, Hall identified and described the volcanic ash beds at the base of the Marcellus without giving them a name (Collins, 1979). It was more than a 100 years later before they were given the name Tioga for the natural gas field in Tioga County in Pennsylvania.

Previous workers (Cate, 1963; De Witt et al., 1993; Lash and Engelder, 2011) have all differentiated the Marcellus Formation into upper and lower black shale intervals separated by a sequence of limestone, gray shale and siltstones of variable thicknesses. In the last few years, several students at West Virginia University have written a series of master's and doctoral dissertations that describe the lithostratigraphy, biostratigraphy, petrophysical properties, and depositional history of the Marcellus Formation interval (Yanni, 2010; Walker-Milani, 2011; Wang, 2012; VanMeter, 2013).

Several geochemical studies have been carried out on the Marcellus Formation. Benelli (2012) compared the concentrations of As, Cr, Mo, U, Zn and Ba between whole rock and fine sediments (< 2μm) in the Marcellus Shale using an Infrared Analyzer (Instrumental Neutron Activation Analyses), and X-ray Diffraction analyses, respectively. He found that the measured concentrations of some elements can be influenced by the size and mineral fraction used for the analyses. Fortson (2012) studied 14 core and 14 outcrop samples in West Virginia, New York, Virginia and Pennsylvania to determine the chemical and physical associations of uranium with the mineralogy of the Marcellus Formation and to also determine if these relationships differ between core and outcrop samples.

Lash and Blood (2011) undertook a preliminary chemostratigraphic study using x-ray fluorescence on cores obtained from the Marcellus Formation in eastern New York, southwestern Pennsylvania and northern West Virginia. They realized that molybdenum concentrations are significantly higher than uranium concentrations and suggested that there must have been an accelerated transport of molybdenum to the seafloor by a particulate manganese mechanism that would have required frequent fluctuations between suboxic and moderately sulfidic water column conditions. They also noticed regional occurrences of barium in the upper part of the Marcellus,

which may reflect an episode of enhanced paleoproductivity. Finally, elevated levels of chloride and strontium concentrations are identified in transgressive system tract deposits, which they relate to salinity excursions that could have enhanced preservations of organic matter in these intervals.

1.3: Objective and Scope of Study

The objective of this project is to provide a detailed lithological, chemical and mechanical characterization of the Marcellus Shale to better understand the variations in mineralogy, total organic carbon (TOC), and rock strength. The project will utilize two EOG Resources vertical cores (Olysn #2V and SRC #1V) for the study. The Olysn #2V is in Bradford County and is located in the basin depocenter and considered distal, whereas the SRC #1V is in Mckean County and is more proximal to the shelf. The study intervals are from 5803-5981 feet (1767-1823 m) and 5835-5941 feet (1779-1811 m) in the Olysn #2V and SRC #1V, respectively, for a total of 284 feet (87 m). Only the Olsyn #2V core covers the entire Marcellus Shale section.

The drill cores from the study area were analyzed using a hand-held x-ray fluorescence (ED-XRF) machine to determine the major and trace elemental composition in weight percent (wt. %) and parts per million (ppm), respectively. An Equotip Hardness Tester, which gives an indication of the strength of a rock surface was also used to analyze the drill cores. Several authors have considered the use of the Equotip hand-held rock strength values (L-values) to estimate unconfined compressive strength (UCS) (e.g., Aoki and Matsukura, 2008). Several of the hand-held rock strength to UCS relationships are investigated and utilized in this study. The drill core was sampled at 2-inch (5 cm) intervals for both analyses. A detailed core description was performed to complement the chemical and mechanical analyses. Thin sections for each of these cores were also available and were used to supplement the core description. Both well analyses also incorporate petrophysical logs and Leco TOC measurements.

This project has the capacity to enhance our understanding of the heterogeneity of the Marcellus Shale and to identify geological and geomechanical properties that are critical to the success of exploration and exploitation efforts in the Marcellus Shale.

CHAPTER 2
METHODS

An integrated geological approach that includes detailed core descriptions, thin section petrography, x-ray fluorescence (XRF) and hand-held rock strength tests (bambino) is used to understand the characteristics of the Marcellus Shale.

2.1: Core Descriptions

Cores from two wells (Olsyn #2V and SRC #1V) are described in detail documenting textural fabric, biota, depositional and structural features, fractures, and mineralogy. The Olsyn #2V core comprises a more complete representation of the Marcellus Shale succession since the cored section represents not just the Marcellus Shale, but also the underlying Onondaga transition zone, and a portion of the Onondaga Limestone. The top of the Olsyn #2V core is within the upper Marcellus Shale unit (Oatka Creek member), just a few feet away from the base of the Mahantango Formation.

Representative photographs were taken from both core slabs. Twenty-four standard-size thin sections were made from the cores and analyzed using a standard petrographic microscope. All the thin sections were roughly ground to 20 microns and impregnated with blue epoxy dye for porosity observation. Half of each thin section was also stained for calcite identification using alizarin red.

2.2: XRF Analyses

X-ray fluorescence is a useful tool for the quantitative and qualitative elemental analysis of rocks. Wavelength dispersive analysis (WD-XRF) and energy dispersive analysis (ED-XRF) are the two main techniques used in x-ray fluorescence analysis. A hand-held energy dispersive

XRF analyzer was utilized for this research. Specifically, the Bruker Tracer IV-SD XRF analyzer was used for this project because of its flexibility, accuracy, and reliability (Fig. 2.1). X-ray fluorescence tools measure the major and trace elemental concentration of a sample by simultaneously analyzing the different energies of fluorescence radiation emitted from the different sample elements after the sample has been bombarded by x-rays in a non-destructive manner.

Figure 2.1 – Bruker Tracer ED-XRF. From http://www.bruker.com/products/x-ray-diffraction-and-elemental-analysis/handheld-xrf/tracer-iii/applications.

The process of x-ray fluorescence begins by passing an electrical current through a tungsten filament to emit x-rays. When the emitted x-rays hit the sample, they interact with atoms in the sample by displacing electrons from the inner orbital shells of the atom (Fig 2.2). This displacement of electrons occurs due to the energy differences between the x-rays emitted from the analyzer and the binding energy holding the electrons in their proper orbits. Once the bombarding stops, an outer-shell electron replaces the electron displaced from the inner orbitals and loses energy in the process. The amount of energy lost is equivalent to the difference in energy

between the two electron shells and is unique to each element. The energy lost and the number of x-ray photons of that energy can be used to identify and quantify that element.

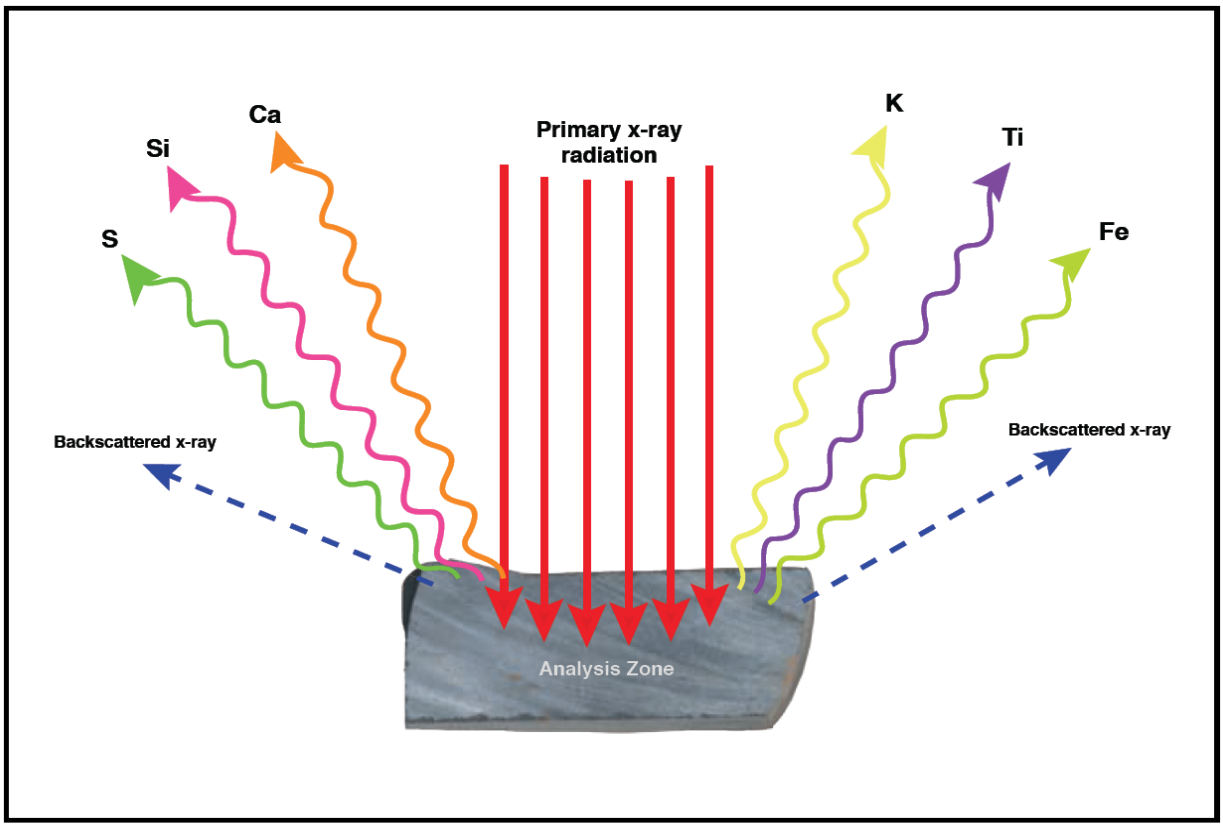

Figure 2.2 – When an emitted x-ray of sufficient energy strikes an atom, it dislodges an electron from one of its inner shells. An outer shell electron replaces the inner shell electron and the excess energy between the two electron shells is released. (Figure from Kiesel, 2013)

The Bruker Tracer IV-SD analyzer has 2 different modes: Soil and Test modes. These modes use different initial voltages to detect the following elements: Mo, Zr, Sr, U, Rb, Th, Pb, Zn, Cu, Ni, Co, Fe, Mn, Cr, V, Ti, Ca, K, S, Ba, Cd, Nb, Al, P, Si, and Mg. The readings from the analyzer are reported in elemental yields, which can be converted to weight percent for major elements and part per million (ppm) for trace elements.

Rowe et al. (2012) developed a methodology for calibrating the Bruker Tracer analyzer using a unique set of eighty-five reference materials from five internationally-accepted mudrock

standards. They found that a calibrated Bruker Tracer analyzer yields results comparable with wavelength-dispersive (WD-XRD) measurement and supports the use of the instrument for quantitative analysis of fine-grained sedimentary rocks.

XRF analysis was conducted at two inch (5 cm) intervals in order to provide high-resolution chemostratigraphy. The XRF analysis was performed at EOG core storage facility in San Antonio with the assistance of Mud Geochemicals and Harry Rowe at the Bureau of Economic Geology (BEG). All analyses were undertaken by laying the slabbed face of the core on top of the instrument, carefully balancing it on the nose of the instrument (Fig 2.3). Thorough care was taken to ensure that the sample lay directly on the instrument to prevent attenuation of the x-ray signal. Each sample was analyzed in duplicate at low energy (for major elements) and high energy (for trace elements). The major elements analyses were undertaken at 15KV under vacuum for 60 seconds, while the trace elements analyses were undertaken at a higher energy of 40 KV for 60 seconds. A copper filter was used in the trace element analysis to attenuate the major element x-ray photons.

2.3: Mechanical Strength Analyses

Unconfined compressive strength (UCS) is one of the most extensively used parameters for the classification and characterization of rock strength (Verwaal and Mulder, 1993). Commonly, the compressive strength of a rock is determined by performing a triaxial test on core samples in the laboratory. Several authors have considered an alternative indirect method in the estimation of unconfined compressive strength (UCS), which comprises the use of a rebound or micro-rebound hammer (Verwaal and Mulder, 1993; Aoki and Matsukura, 2008). For this research, a hand-held Equotip hardness index tester (Bambino) manufactured by Proceq was used.

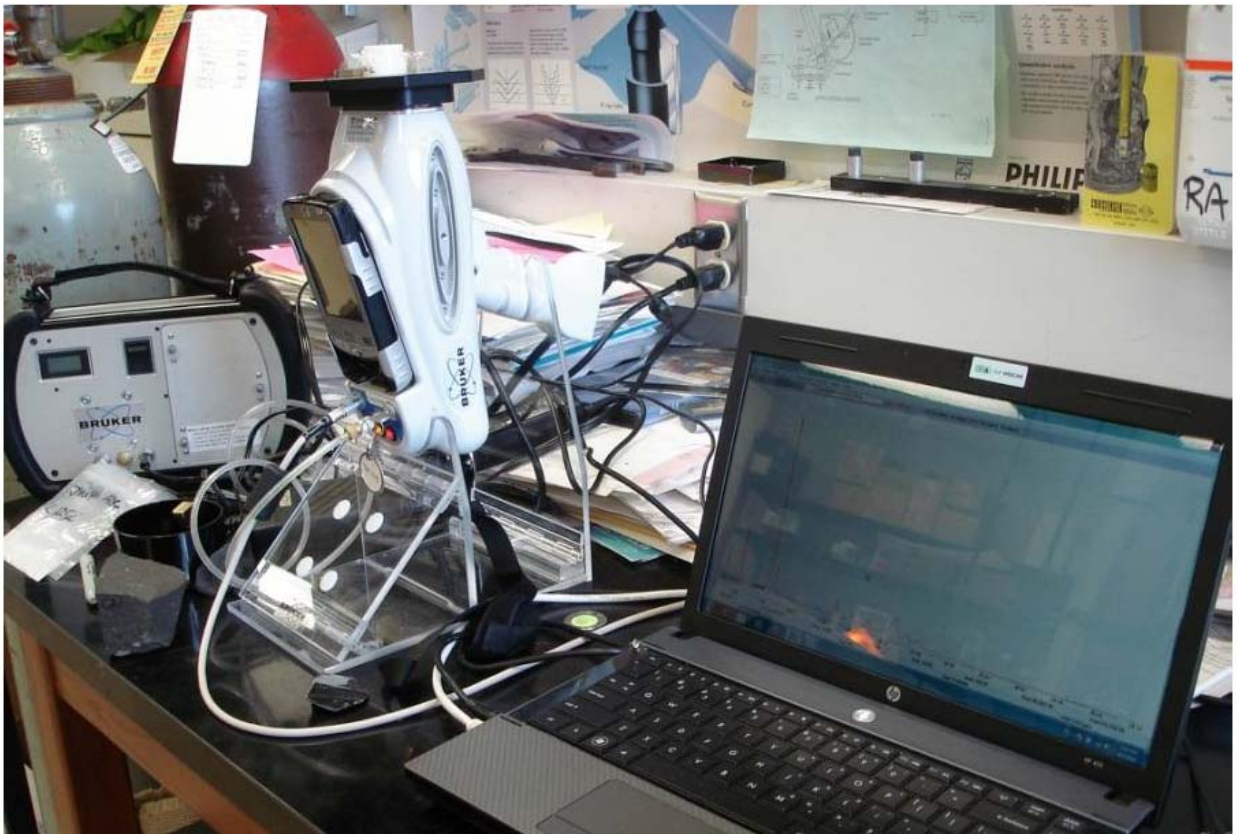

Figure 2.3 – Bruker handheld Tracer IV benchtop setup. From Conrey and Wolff (2011).

The Bambino (Fig. 2.4) is a digital, battery-operated micro rebound hammer that provides an indirect method to predict rock strength.

Figure 2.4 – Equotip Hardness Index Tester. From Daniels et al., (2012).

The light weight and low impact velocity of the tool allows for the gathering of high-resolution data in an efficient manner without any significant destruction to the core sample. The

tool works by comparing the impact and rebound velocities (vi and vr) of a small steel ball after its collision with a rock surface (Fig. 2.5). The impact steel ball will rebound faster from harder rocks than from softer ones resulting in a higher energy quotient, which in turn reflects the relative strength of the rock (Daniels et al., 2012). The Bambino records the rebound data in Leeb hardness units (L).

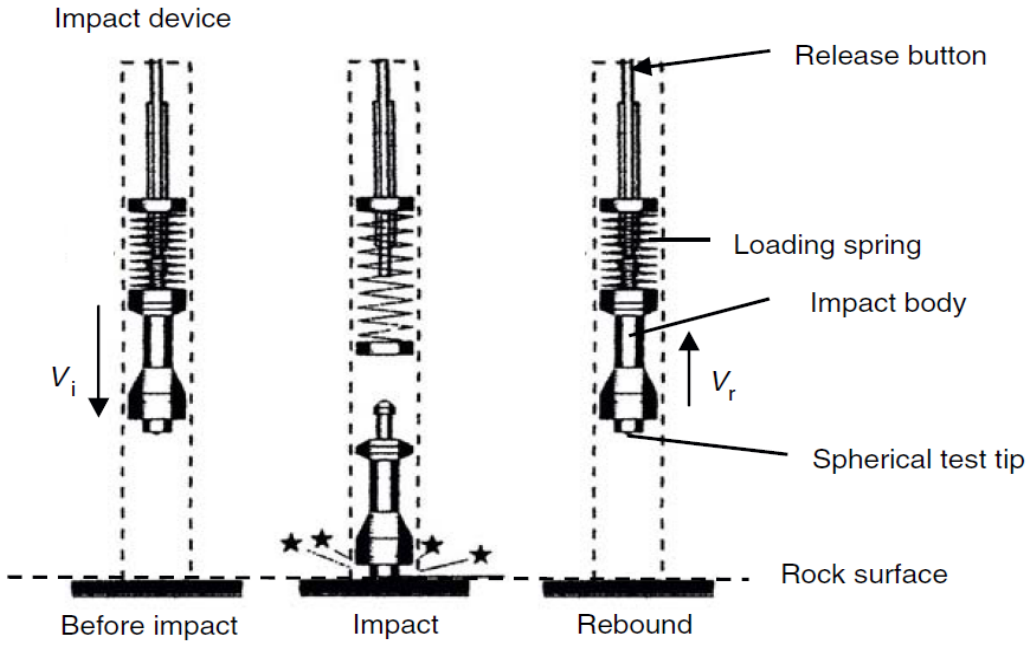

Figure 2.5 – Equotip Hardness Index Tester mode of operation. From Aoki and Matsukura (2008).

The Bambino analyses were also conducted at two inch (5 cm) intervals in order to provide high-resolution mechanical stratigraphy. Testing was conducted on the slabbed cores for both wells. For each two inch (5 cm) interval tested, the slabbed cores were laid on a flat, hard surface and seven hardness measurements were taken. Measurements were exported from the Bambino instrument to an excel spreadsheet. Minimum and maximum values of the seven measurements were removed and the remaining five values were averaged to get the final Leeb hardness value.

This procedure was done to remove any anomalously low or high values, which might not be a true representation of that interval.

CHAPTER 3
LITHOLOGY AND PETROLOGY

The Marcellus Shale often appears to be homogenous at first glance, but detailed analysis confirms that the Marcellus Shale can be subdivided into several distinct lithological facies. Core and petrographic analysis were carried out on the Olsyn # 2V and SRC #1V to enhance the understanding of the heterogeneity of the Marcellus Shale Formation. Six major lithofacies are identified in the Marcellus Shale and underlying Onondaga using textural fabric, grain type, size and abundance, biota and sedimentary structures (Fig. 3.1 & 3.2). XRD analyses were also utilized to estimate mineralogical abundances of the fine-grained mudrock matrix. The six major lithological facies identified (Table 1) are listed below:

1) Massive Fossiliferous Wackestone/Packstone
2) Calcareous Argillaceous Mudstone
3) Silty Mudstone
4) Pyritic Silty Argillaceous Mudstone
5) Fossiliferous Packstone/Grainstone
    a) Spiculitic Packstone
    b) Byrozoa, Pelecypod Grainstone
6) Argillaceous Silty Mudstone

Table 1: Types and characteristics of dominant depositional facies in the Marcellus Formation.

Facies Name	Sub-Facies Name	Color	Dominant Mineralogy	Description	Primary Allochem/ Grain Type	Occurrence (by abundance)	Depositional Setting
1. Massive Fossiliferous Wackestone/Packstone		Light and medium grey	Calcite	Massive bedded, fossiliferous, highly bioturbated	Brachiopod	Onondaga	Shelf
2. Calcareous Argillaceous Mudstone	a) Calcareous Mudstone b) Calcareous Argillaceous Mudstone	Medium grey to dark grey	Calcite, Clay	Skeletal argillaceous mudstone with interbeded calcareous mudstone/wackestone	Quartz, Algal cysts	Onondaga Transition Zone, Lower Marcellus	Shelf to Basin
3. Silty Mudstone		Dark grey to black	Quartz	Organic rich, faintly laminated silty mudstone	Quartz, Algal cysts	Lower Marcellus	Basin
4. Pyritic Silty Argillaceous Mudstone		Dark grey to black	Clay, Quartz	Pyrite and organic rich, faintly planar laminated argillaceous mudstone	Pyrite, Quartz	Lower Marcellus, Upper Marcellus	Basin
5. Fossiliferous Packstone/Grainstone	a) Spiculitic Packstone b) Bryozoan Pelecypod Grainstone	Light grey to medium grey	Calcite	Bioturbated, massive bedded fossiliferous packstone/grainstone	Spicules, Bryozoan, Pelecypod	Cherry Valley, Lower Marcellus, Upper Marcellus	Shelf
6. Argillaceous Silty Mudstone		Dark Brown to Black	Quartz, Clay	Faintly laminated argillaceous silty mudstone	Quartz, Algal Cysts	Upper Marcellus, Lower Marcellus	Basin

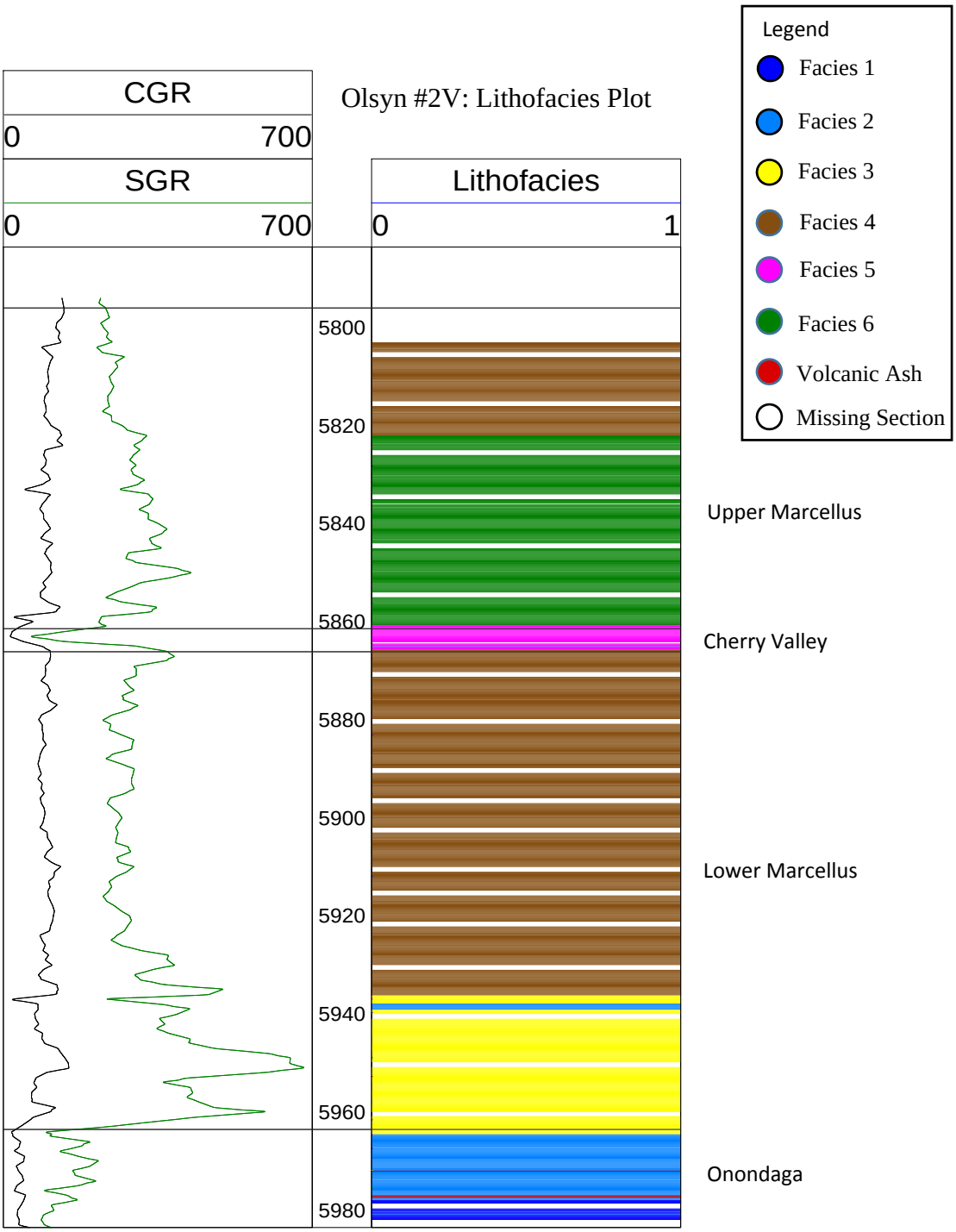

Figure 3.1: Lithofacies plot from the Olsyn #2V well showing the six lithofacies and volcanic ash bed layers. Standard gamma ray (SGR) in green and computed gamma ray (SGR minus uranium contribution) are plotted in first track.

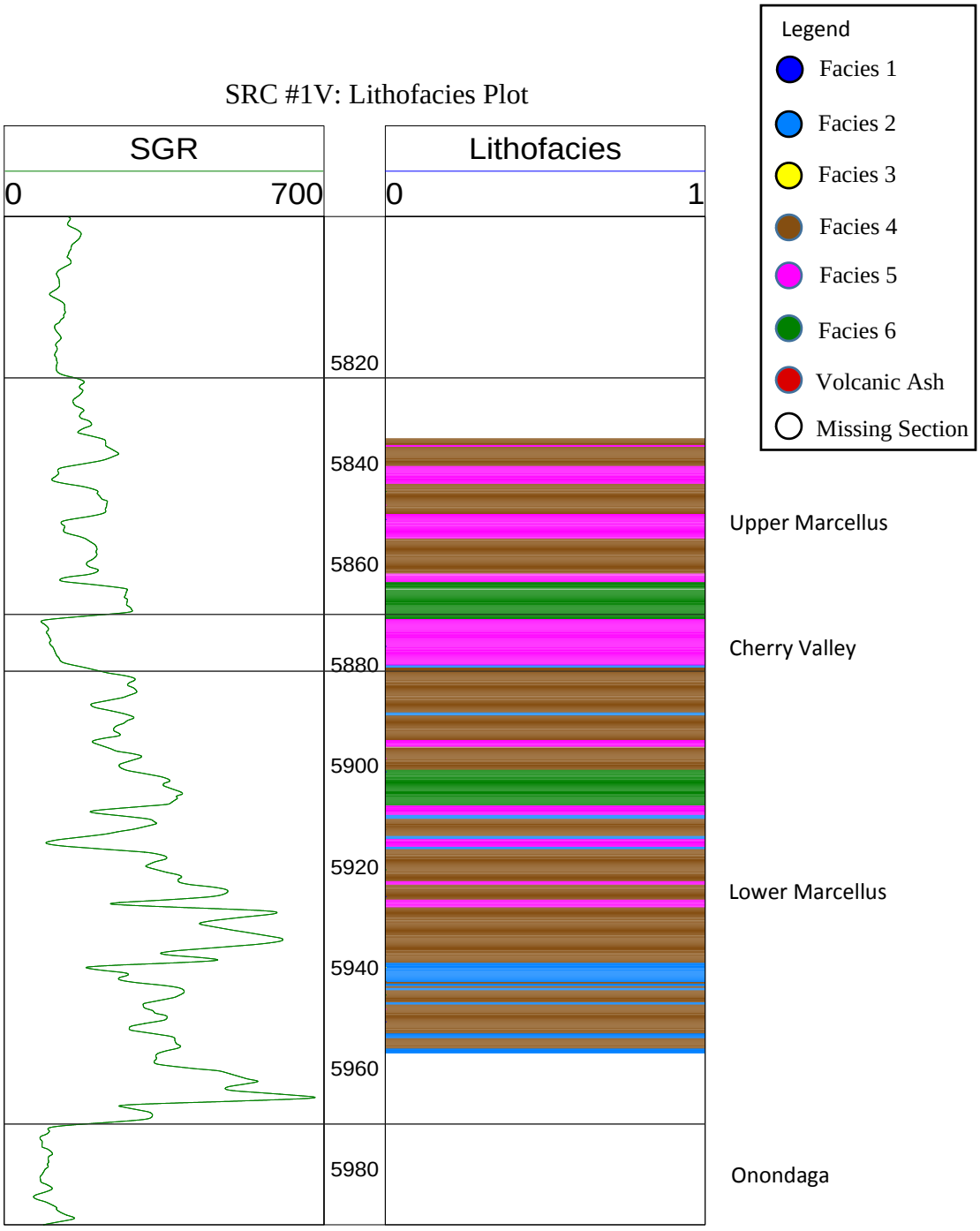

Figure 3.2: Lithofacies plot from the SRC #1V well. Standard gamma ray (SGR) in green is plotted in first track.

3.1: Facies 1 (Massive Fossiliferous Wackestone/Packstone)

Facies 1 consists of light gray to medium gray, bioturbated, massive fossiliferous wackestone/packstone (Fig 3.3a). The facies occurs predominantly in the Onondaga Limestone, which underlies the Marcellus Shale. Based on XRD analysis, this facies contains less than 10 wt. % clays or clastics, over 90 wt. % calcite and low to no organic content. Biodiversity and abundance of fauna are both moderate in this facies. The major allochems in the facies are predominantly brachiopods and styliolinids (Fig 3.3b). Calcite recrystallization of algal cysts can be observed in this facies. Several silt-sized quartz grains and algal cysts that have been replaced by silica can also be observed in thin section. A volcanic ash bed, 5.5 inches (14 cm) in thickness is present within this wackestone/packstone facies. Two vertical to sub-vertical calcite cemented fractures can also be observed within the facies. The fractures are 0.4 inches (1 cm) wide and 2.3-3.5 inches (6-9 cm) in length.

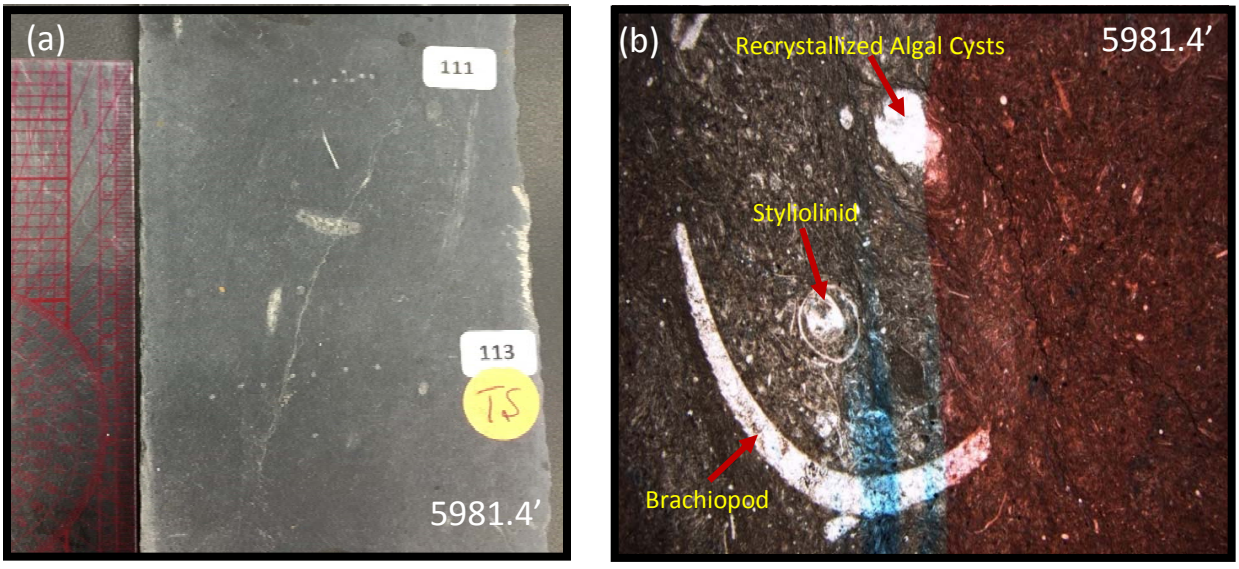

Figure 3.3: Facies 1 (fossiliferous wackestone/packstone) in the Olsyn #2V core. (a) Core photograph of light grey to medium grey wackestone/packstone from depth 5981ft. TS indicates depth thin section was taken. Numbers indicate XRF and bambino locations. Core is 7.6 cm wide. (b) Facies 1 thin section photomicrograph in plane-polarized light from Olsyn # 2V core showing recrystallized algal cysts, brachiopod and styliolinid fragments. Field of view is 20 mm across.

3.2: Facies 2 (Calcareous Argillaceous Mudstone with interbedded Calcareous Mudstone)

The calcareous argillaceous mudstone is characterized by medium grey to dark grey, mixed calcite and clay mineral matrix (Fig 3.4a). This facies occurs within the Onondaga transition zone and in the basal section of the Lower Marcellus. A volcanic ash bed, 2 inches (5 cm) in thickness is present in the Onondaga transition zone. Two vertical to sub-vertical calcite cemented fractures are also observed. The fractures are 0.4 inches (1 cm) wide and 3.5-6.3 inches (9-16 cm) in length. Two interbeded sub-facies are identifiable in core and thin section.

2a. Calcareous Mudstone: Facies 2a consists of medium grey, slightly bioturbated calcareous mudstone/wackestone. This facies appears homogenous in core and thin section, but shows a scattered occurrence of a few algal cysts, which have been replaced by calcite (Fig 3.4b). Accessory grains that can be observed in thin section include silt-sized quartz grains and authigenic pyrite replacing algal cysts. The calcareous mudstone intervals exhibit variable thickness between 1 and 16 inches (2.5-40 cm) and strongly react with HCl.

2b. Calcareous Argillaceous Mudstone: Facies 2b is a dark grey, weakly laminated skeletal argillaceous mudstone. This facies contains algal cysts grains that have been replaced by silica and calcite. Laminae within the argillaceous mudstone are generally discontinuous across the core, wavy and parallel, but may be continuous, planar and parallel. Skeletal fragments are common within the facies, showing evidence of compaction and exist as bedding parallel, flattened shell pieces (Fig 3.4c). Silt-sized quartz grains can also be observed within the facies. The argillaceous mudstone facies reacts less strongly with HCl and are consistently thicker (> 3 inches; > 7.5 cm) compared to the variable thickness of the calcareous mudstone sub-facies.

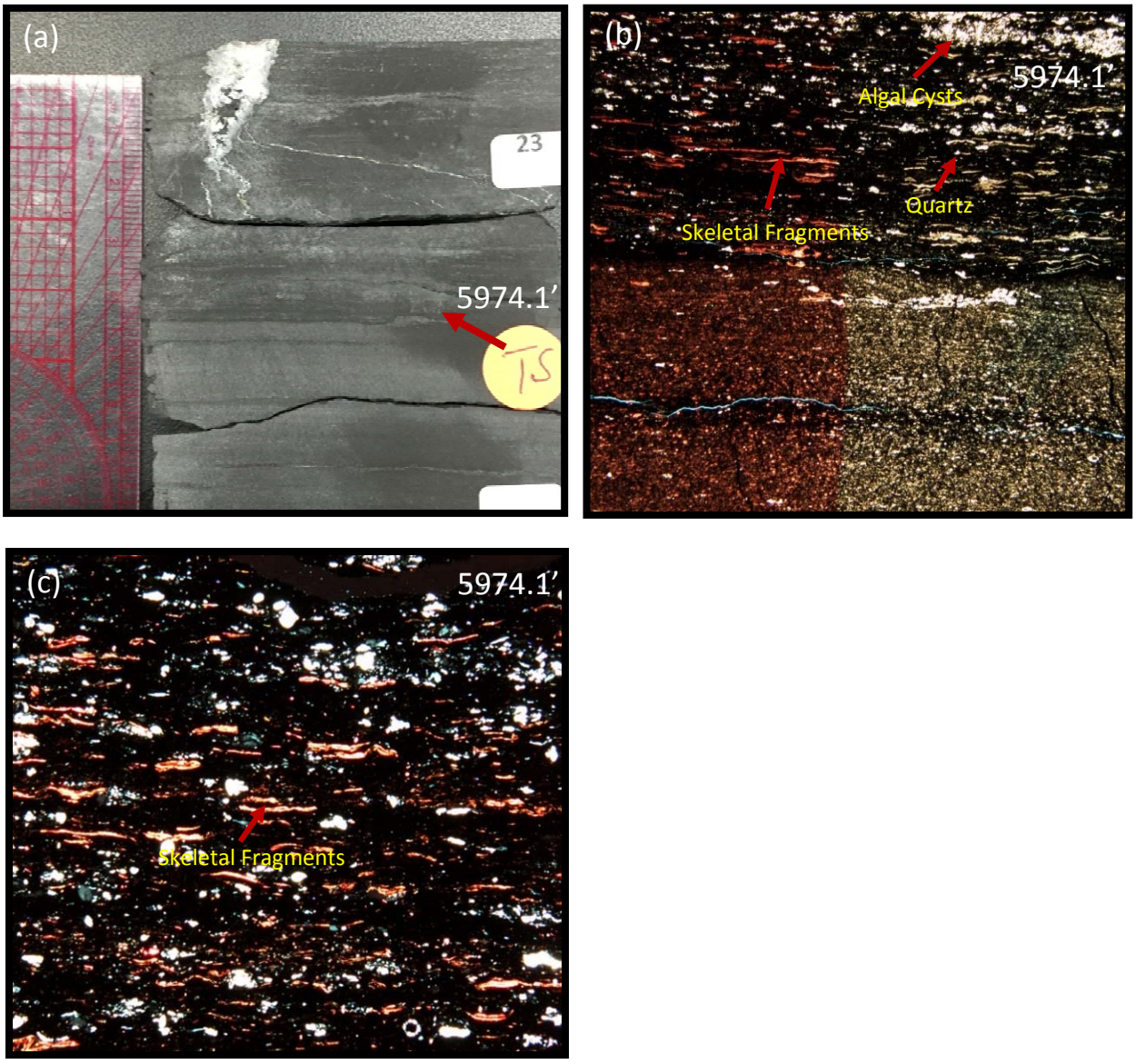

Figure 3.4: Facies 2 in the Olsyn #2V core. (a) Core photograph of medium grey to dark grey calcareous argillaceous mudstone with interbedded calcareous mudstone facies from depth 5974.1 ft. Core is 7.6 cm wide. (b) Thin section photomicrograph in plane-polarized light from the Olsyn #2V core showing the calcareous mudstone below and calcareous argillaceous mudstone above. Field of view is 14 mm across. (c) Thin section photomicrograph from the Olsyn # 2V core showing the calcareous argillaceous mudstone sub-facies. Note flattened skeletal fragments and algal cysts. Cross-polarized light. Field of view is 8 mm across.

3.3: Facies 3 (Silty Mudstone)

Facies 3 is a dark grey to black, organic-rich, faintly laminated silty mudstone (Table 1). XRD analysis shows that this facies is composed of less than 20 wt. % calcite, less than 35 wt. % clay and over 40 wt. % quartz. This facies also has 6-8 wt. % TOC based on Leco TOC analysis. The silty mudstone facies is faintly planar laminated to massively bedded (Fig 3.5a). Laminae within the silty mudstone facies can also be discontinuous, planar and wavy. The facies also does not react strongly to HCl indicating a low calcite content. Silt-sized quartz grains are the predominant grains that can be identified in thin section (Fig 3.5b). The main biotic component present in this facies are algal cysts that have been significantly replaced by silica. A few horizontal, vertical to sub-vertical calcite cemented fractures can also be observed within the facies. Facies 3 occurs only in the basal section of the Lower Marcellus interval in the Olsyn #2V well (Fig. 3.1).

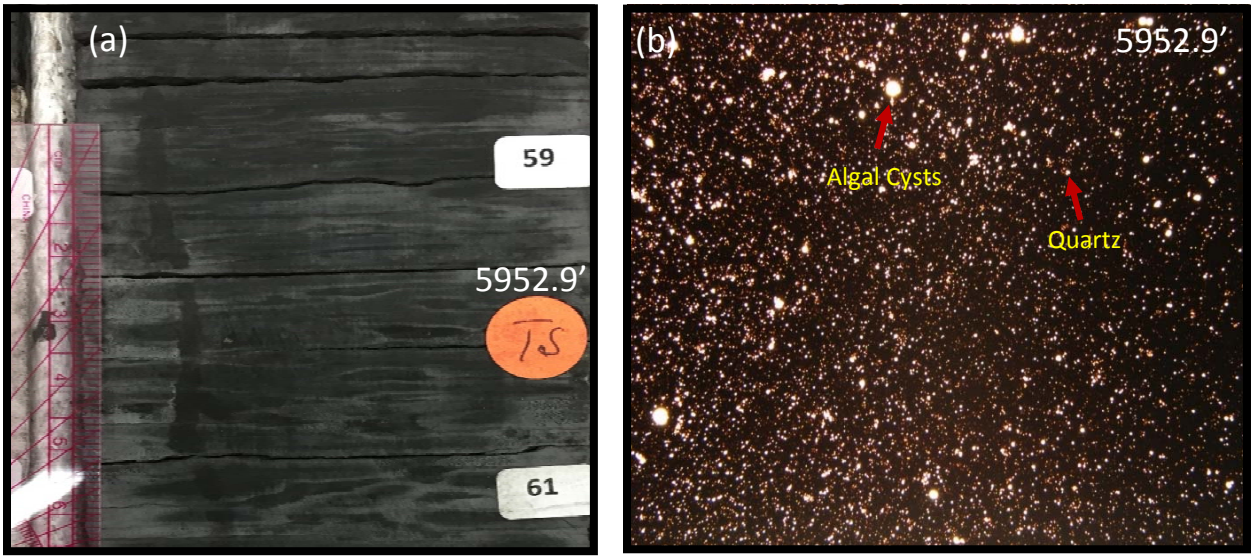

Figure 3.5: Facies 3 (silty mudstone) in the Olsyn #2V core. (a) Core photograph of dark grey to black silty mudstone facies from depth 5952.9 ft. TS indicates depth thin section was taken. Core is 7.6 cm wide (b) Thin section photomicrograph in plane-polarized light from the Olsyn #2V core showing silt-size quartz grains and algal cysts. Field of view is 14 mm across.

3.4: Facies 4 (Pyritic Silty Argillaceous Mudstone)

The pyritic silty argillaceous mudstone facies is dark grey to black in appearance and is faintly planar laminated (Fig 3.6a). This facies exhibits higher clay content, reaching up to 40 wt. %, lower quartz content (15-30 wt. %) and over 10 wt. % pyrite as compared to the silty mudstone facies. Algal cysts are also less abundant in this facies as compared to facies 3 and a significant proportion of the algal cysts seem to be replaced by pyrite as opposed to silica (Fig 3.6b). Silt-sized quartz grains can be observed to be disseminated throughout the matrix in thin section. A volcanic ash bed, 0.35 inches (1 cm) in thickness is present within this facies in the Olsyn #2V core. Facies 4 occurs in both the Lower and Upper Marcellus intervals.

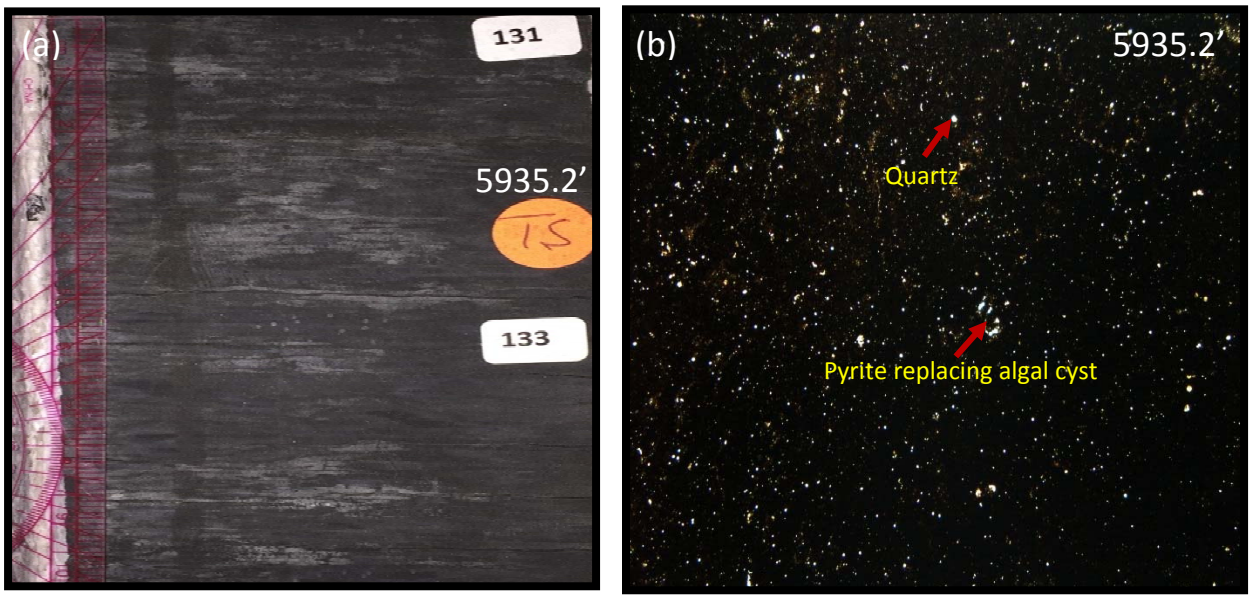

Figure 3.6: Facies 4 in the Olsyn #2V core. (a) Core photograph of dark grey to black pyritc silty argillaceous mudstone facies from depth 5935.2 ft. TS indicates depth thin section was taken. Core is 7.6 cm wide (b) Thin section photomicrograph in plane-polarized light from the Olsyn #2V core showing clay matrix, silt-sized quartz grains, and algal cysts. Pyrite can be observed replacing some algal cysts. Field of view is 14 mm across.

3.5: Facies 5 (Fossiliferous Packstone/Grainstone)

Facies 5 consists of light grey to medium grey, bioturbated massive fossiliferous packstone/grainstone (Fig 3.7a). The facies occurs predominantly in the Cherry Valley in both Olsyn #2V and SRC #1V cores. It also occurs at several intervals in the Lower and Upper Marcellus in the SRC #1V. This facies contains less than 20 wt. % clays or clastics, over 80 wt. % calcite based on XRD analysis and low to no organic content according to Leco TOC analysis. The major allochems in the facies are sponge spicules, bryozoa, pelecypod, and algal cysts. Two sub-facies are identifiable in thin section:

5a. Spiculitic Packstone: Facies 5a consists of medium grey, bioturbated, fosiliferous spiculitic packstone. Sponge spicules are the dominant allochems in this facies and are randomly dispersed throughout the matrix in thin section (Fig 3.7b).This facies also contains recrystallized algal cysts and silt-sized quartz grains. Burrows are present and appear as color differences in thin section. This facies occurs in both Olsyn #2V and SRC #1V cores in the Cherry Valley Formation and Lower Marcellus intervals.

5b. Bryozoa-Pelecypod Grainstone: Facies 5b consists of light grey to medium grey, bioturbated, fossiliferous grainstone. This facies is characterized by a higher allochem diversity and abundance than facies 5a. The dominant allochems are bryozoa, and pelecypod. This facies contains lower amounts of algal cysts and silt-sized quartz grains as compared to the spiculitic packstone facies. This facies is found only in the SRC #1V in the Lower Marcellus, Upper Marcellus and Cherry Valley.

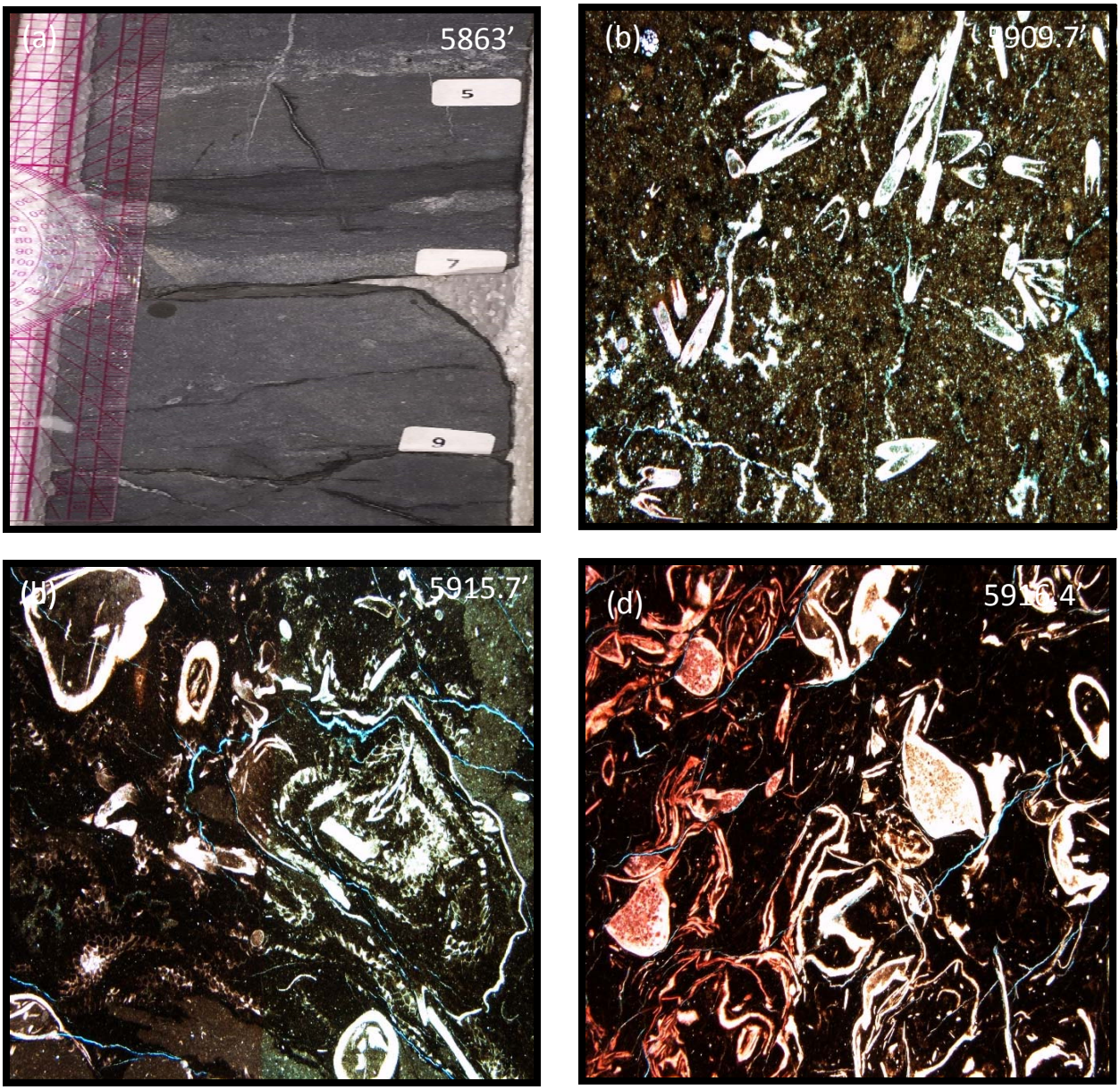

Figure 3.7: Facies 5 in the Olsyn #2V and SRC #1V cores. (a) Core photograph of light grey to medium grey fosiliferous packstone/grainstone facies from depth 5863 ft in the Olsyn #2V core. Core is 7.6 cm wide (b) Thin section photomicrograph in plane-polarized light from the Olsyn #2V core showing sponge spicules, silt-sized quartz grains, and algal cysts. Field of view is 14 mm across. (c) Thin section photomicrograph in plane-polarized light from the SRC # 1V core showing bryozoan, and pelecypod fragments. Field of view is 14 mm across. (d) Thin section photomicrograph in plane-polarized light from the SRC #1V core showing pelecypod fragments. Depth is 5916.4’ Field of view is 14 mm across.

3.6: Facies 6 (Argillaceous Silty Mudstone)

Facies 6 is a dark grey to black, organic-rich, faintly laminated argillaceous silty mudstone (Fig 3.8a). XRD analysis shows that this facies is composed of more than 40 wt. % clay, over 30 wt. % quartz, and less than 5 wt. % calcite. Clay mineral composition are predominantly illite, with trace quantities of chlorite and kaolinite (Fig 3.8b). The facies reacts weakly to HCl indicating a low calcite content. The argillaceous silty mudstone facies is poorly to faintly planar to wavy/irregular laminated. Localized soft sediment deformation can also be observed. Silt-sized quartz grains are disseminated throughout the matrix and are easily identified in thin section (Fig 3.8b). The main biotic component present in this facies are algal cysts that have been replaced by silica and authigenic pyrite. Facies 6 occurs in the Upper Marcellus in the Olsyn #2V core and both Upper and Lower Marcellus intervals in the SRC #1V core.

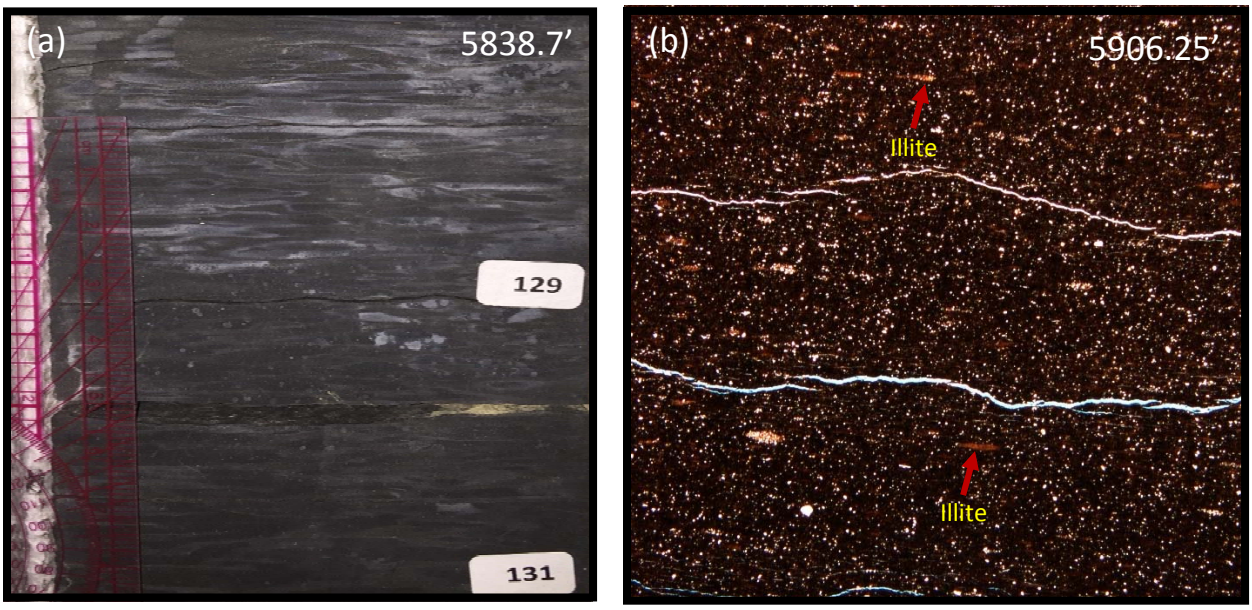

Figure 3.8: Facies 6 (argillaceous silty mudstone) in the Olsyn #2V and SRC #1V core. (a) Core photograph of dark grey to black argillaceous silty mudstone from depth 5838.7 ft in the Olsyn #2V core. Numbers indicate XRF and bambino locations. Core is 7.6 cm wide. (b) Thin section photomicrograph in plane-polarized light from SRC #1V core showing quartz grains and clay mineral matrix. Field of view is 14 mm across.

CHAPTER 4

ELEMENTAL CHEMOSTRATIGRAPHY AND GEOCHEMISTRY

The evaluation of major and trace elements can provide valuable insights into the vertical and lateral variations of fine-grained sedimentary rocks and the chemical state of the environment of deposition. The combination of elemental chemostratigraphy with core description and TOC pyrolysis data provides a powerful tool in determining the depositional and diagenetic characteristics of fine-grained rocks like the Marcellus Formation (O'Neal, 2015). This chapter introduces the concept of elemental chemostratigraphy, sedimentary provenance, and environmental redox proxies. It also introduces the use of hierarchical cluster analysis and elemental cross-plots in defining various chemostratigraphic subgroups, and helps constraining the depositional and diagenetic characteristics of the Marcellus Formation.

The distribution of chemical elements in sedimentary rocks are controlled by three major inputs: 1) terrigenous detritus from weathering of continental rocks, 2) biogenic components derived from primary biological production, and 3) authigenic materials precipitated at or near the sediment-water interface. The chemical state of the environment of deposition can also play a role in the final distribution of the elements in the sediments because certain elements can have distinctly different behaviors under oxic and anoxic depositional conditions (Calvert and Pedersen, 1993).

Several elements can be used as proxies to infer the geologic processes or mechanisms that resulted in the generation and deposition of sediments and also the redox condition of the environment during sediment deposition. A few of those elemental proxies are discussed below.

4.1: Terrestrial and Detrital Elements

The major and trace elements most widely used as proxies for terrestrially-derived sediments are Al, K, Rb, Zr, and Ti. Aluminum is the most abundant metallic element in the crust and is the intrinsic element in several minerals including kaolinite $Al_2Si_2O_5(OH)_4$, corundum Al_2O_3 and sillimanite Al_2SiO_5 (Salminen et al., 2005). Al has low solubility and high diagenetic stability under most environmental conditions and is regarded as the main proxy for clay minerals in hemipelagic rocks (Arthur and Dean, 1991). Correlating Al with other major and trace elements can show if those other elements are associated with terrigenous or detrital sediment input or not. A positive correlation indicates that the element is most likely detrital and a negative correlation indicates that the element is most likely authigenic or biogenic in origin (Tribovillard et al., 2006). Most of the cross-plots shown hereafter are from the Olsyn #2V core, which is the more complete core of the Marcellus interval compared to the SRC #1V. Only selected cross-plots from the SRC #1V are shown in this section and the remaining cross-plots for both wells are presented in Appendix 1.

Potassium and rubidium are both lithophile elements and are derived from the weathering of felsic igneous rocks. The mobility of K under various environmental conditions is limited by the following processes: 1) adsorption on the surfaces of clay minerals and organic matter, 2) incorporation into clay-mineral lattices because of its large size, and 3) utilization by growing plants and organisms (Salminen et al., 2005). Rb has a positive relationship with K and commonly substitutes for K in micas and K-feldspars due to their similarity in ionic radius and ionic charge (Salminen et al., 2005).

Titanium is also a lithophile element and is found as the main constituent element in several minerals, including rutile, ilmenite, and sphene. Ti has high diagenitic stability under most

environmental conditions, due to the non-reactivity of its insoluble oxide TiO_2 and this makes it extremely useful as a detrital proxy (Brookins, 1988). Likewise, Zr is also a lithophile element and is mostly found in zircon ($ZrSiO_4$). Zr is also derived from felsic igneous rocks, can substitute for Ti in rutile and ilmenite and is present in trace levels in a few other minerals such as, amphibole, mica, garnet, and clinopyroxene (Salminen et al., 2005).

Cross-plotting K, Zr and Ti with Al shows the relationship of these elements to Al (Fig. 4.1 a, b & c). These cross-plots show high positive covariance of K, Zr and Ti to Al, which suggests that K, Zr and Ti originates from detrital sediments and are most likely in clay minerals. Also, cross-plots of K to Rb show high positive covariation indicating the substitution of K by Rb (Fig. 4.1 d).

The biogenic or detrital origin of silica in the system can be determined from a cross-plot of Si to Al. A strong positive correlation between Si and Al indicates the silica is most likely detrital in origin, whereas a negative correlation between Si and Al likely indicates Si is of authigenic or biogenic origin (Sageman and Lyons, 2009). Negative covariance of Si to Al can be observed in certain intervals in the Olsyn #2V indicating the presence of authigenic or biogenic silica, whereas the SRC #1V well shows only strong positive covariance between Si to Al (Fig. 4.1 e & f). The negative covariance between Si and Al in the Olsyn #2V is more pronounced in the basal section of the Lower Marcellus and upper part of the Onondaga formation. The upper Marcellus and Cherry Valley show strong positive covariance.

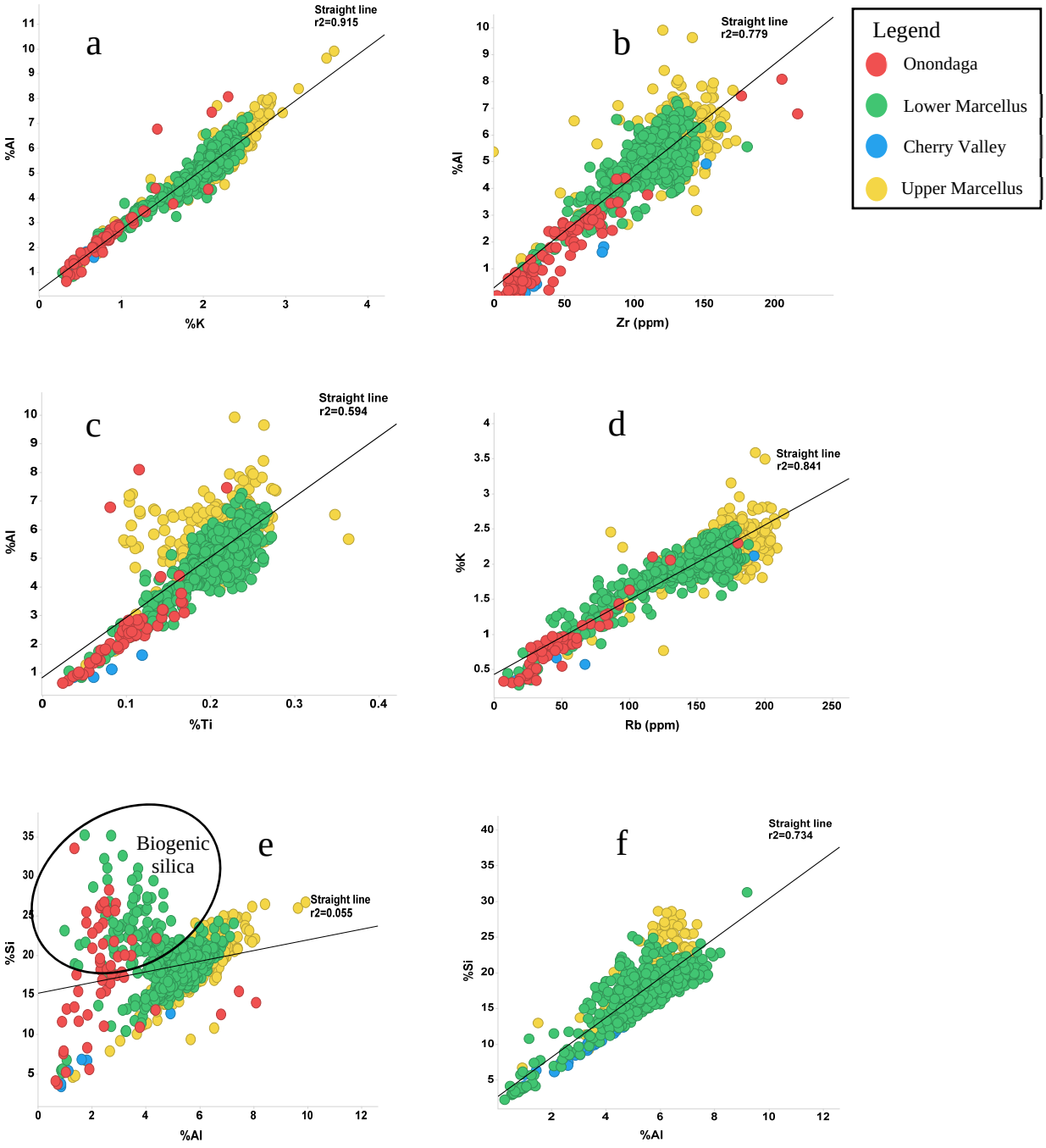

Figure 4.1: Cross plots of XRF-derived data for the Olsyn #2V (a through e) and SRC #1V (f) cores. a) Geochemical cross plot of Al against K showing positive covariance (R^2 = 0.92) suggesting that K is a detrital element; b) cross plot of Al versus Zr showing similar positive covariance (R^2 = 0.78) suggesting Zr is being delivered into the system with other detrital elements; c) cross plot of Al versus Ti showing moderate positive covariance; d) cross plot of K versus Rb also shows strong positive covariance (R^2 = 0.84); e) geochemical cross plot of Si versus Al showing an increase in Si to Al ratio in the Onondaga and Lower Marcellus samples, which could indicate that some of the Si component is not related to detrital input, but enriched by authigenic or biogenic processes; f) Cross plot of Si versus Al well showing strong correlation between Si and Al and no evidence of authigenic or biogenic silica production in the cored interval. The basal section of the lower Marcellus and Onondaga was not cored in the SRC #1V well.

4.2: Carbonate Elements

Several major and trace elements, specifically calcium, strontium, magnesium, and manganese are the main constituents of carbonate minerals such as calcite, aragonite, dolomite, and rhodochrosite. The enrichment or depletion of several of these elements in hemipelagic to pelagic systems can be used to identify differing carbonate depositional and diagenetic processes.

4.2.1: Calcium

Calcium is the fifth most abundant element in the crust and is an important element in several common minerals including calcite, dolomite, anhydrite and gypsum (McLennan and Taylor, 1995). Calcium can also be found in other minerals such as plagioclase feldspars, amphibole, and pyroxene. Some clay minerals can also have minute quantities of calcite, but plagioclase feldspars are usually the principal host for Ca in detrital sediments (Salminen et al., 2005). In the XRF data from the two cores, Ca negatively covaries with Al, suggesting Ca is of biogenic or authigenic origin instead of detrital (Fig. 4.2a & b). Analysis of both cores and several thin sections support this interpretation with intact skeletal fragments of brachiopods, styliolinids and ostracods observed especially in the SRC #1V well.

4.2.2: Strontium

Strontium is a lithophile element with an ionic charge of (+2) similar to that of Ca and an ionic radius between that of Ca and K. The similar ionic charge and ionic radius makes it possible for Sr to substitute for Ca in carbonate minerals (Salminen et al., 2005). The substitution of Sr for Ca is more prevalent in orthorhombic carbonate minerals like aragonite than rhombohedral minerals like calcite due to the crystal lattice orientation restraints of rhombohedral minerals (Katz et al., 1972; O'Neal, 2015). A large increase in Sr concentration versus Ca could indicate a

predominant increase in aragonite precipitation or skeletal fragment deposition. Sr and Ca show good positive covariance in both wells indicating substitution of Ca by Sr (Fig. 4.2c). A slight increase in Sr to Ca ratio can be seen in the SRC #1V well, which may indicate an increase in aragonitic allochems (Fig. 4.2d).

4.2.3: Manganese

Manganese is a common lithophile element that forms several minerals including manganite, rhodochrosite and pyrolusite. Mn tends to substitute for Ca in rhombohedral carbonate species like calcite (O'Neal, 2015). Mn is delivered by fluvial or eolian processes to the ocean as oxide coatings on particulate material and by diffusion out of shelf sediments (Tribovillard et al., 2006). Mn (II) and $MnCl_2$ are the dominant manganese species found in seawater, but Mn (II) is eventually oxidized due to its geochemical instability in oxygenated waters to Mn (IV). Mn (IV) is also referred to as Mn-oxyhydroxides solid phase or precipitate. Mn-oxyhydroxides are important geochemically due to the fact that several trace elements such as V, Mo, Cu, and Zn adsorb onto them and are transported to the sediment-water interface. These trace elements are then released in less oxygenated environments by reductive dissolution of the hydroxides at or below the sediment-water interface (Tribovillard et al., 2006). The Mn (IV) oxyhydroxides, which are very mobile in reducing environments, tend to escape back to the water column or be trapped in authigenic Mn-carbonates or as oxides. Because of the varied solubility of Mn, it cannot be used as a biogenic or redox proxy, but its main role is in the facilitation of trace element transfer from the water column to the sediment-water interface (Tribovillard et al., 2006). Mn shows no covariation with Ca in Olsyn #2V and SRC #1V wells (Fig. 4.2 e & f). Mn also shows no covariance with TOC in the Olsyn #2V well and slight negative covariance with TOC in the SRC #1V well (Fig. 4.2 g & h).

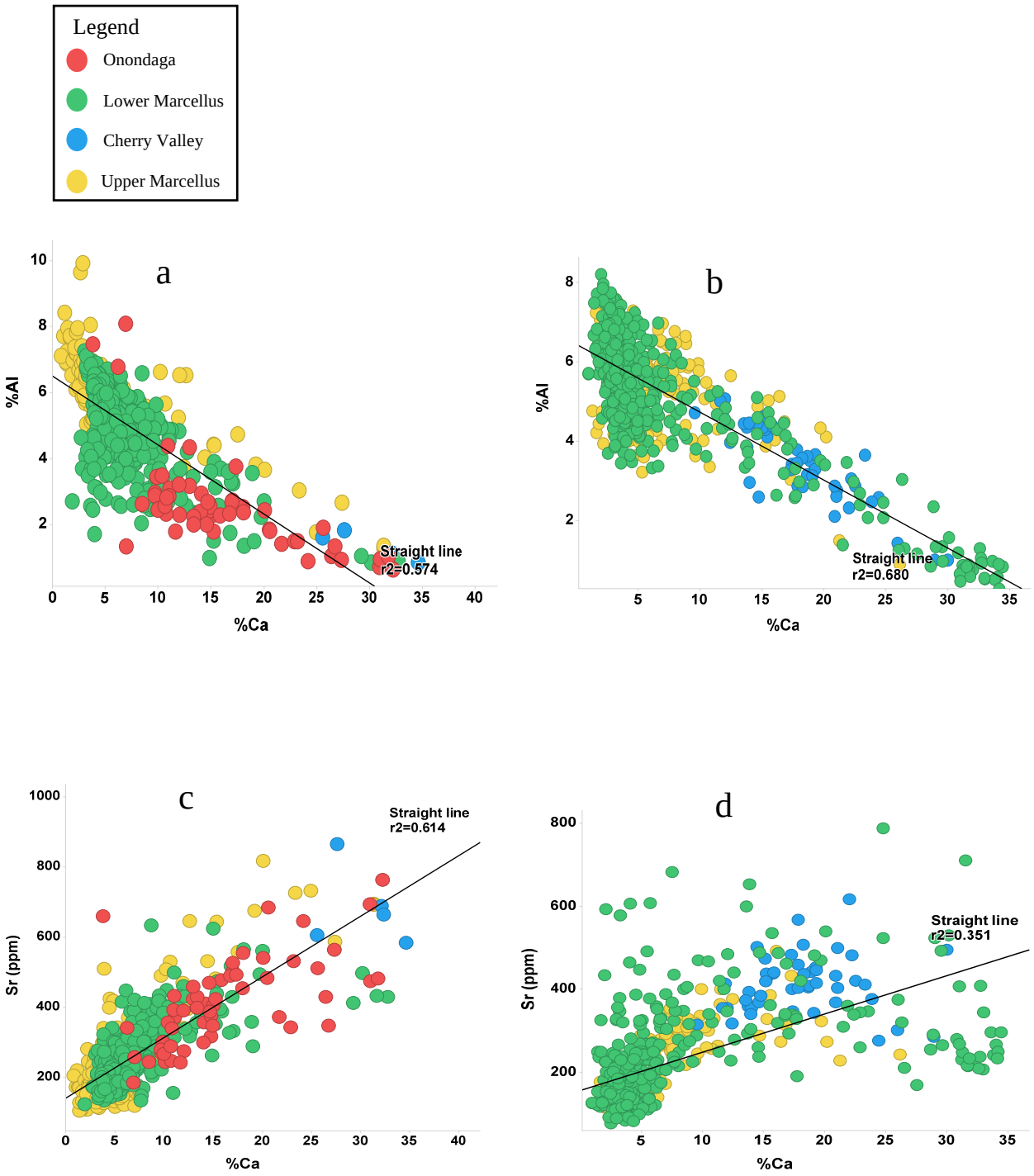

Figure 4.2: a) Geochemical cross plot of Al against Ca from XRF data in Olsyn #2V well, showing negative covariance (R^2 = 0.57) suggesting that the Ca component is not related to detrital influxes; b) cross plot of Al versus Ca from the SRC #1V, showing similar negative covariance (R^2 = 0.68) as in a); c) cross plot of Ca versus Sr from Olsyn #2V XRF data showing strong positive covariance indicating good substitution of Ca by Sr; d) cross plot of Ca versus Sr from SRC #1V showing weaker positive covariance (R^2 = 0.35).

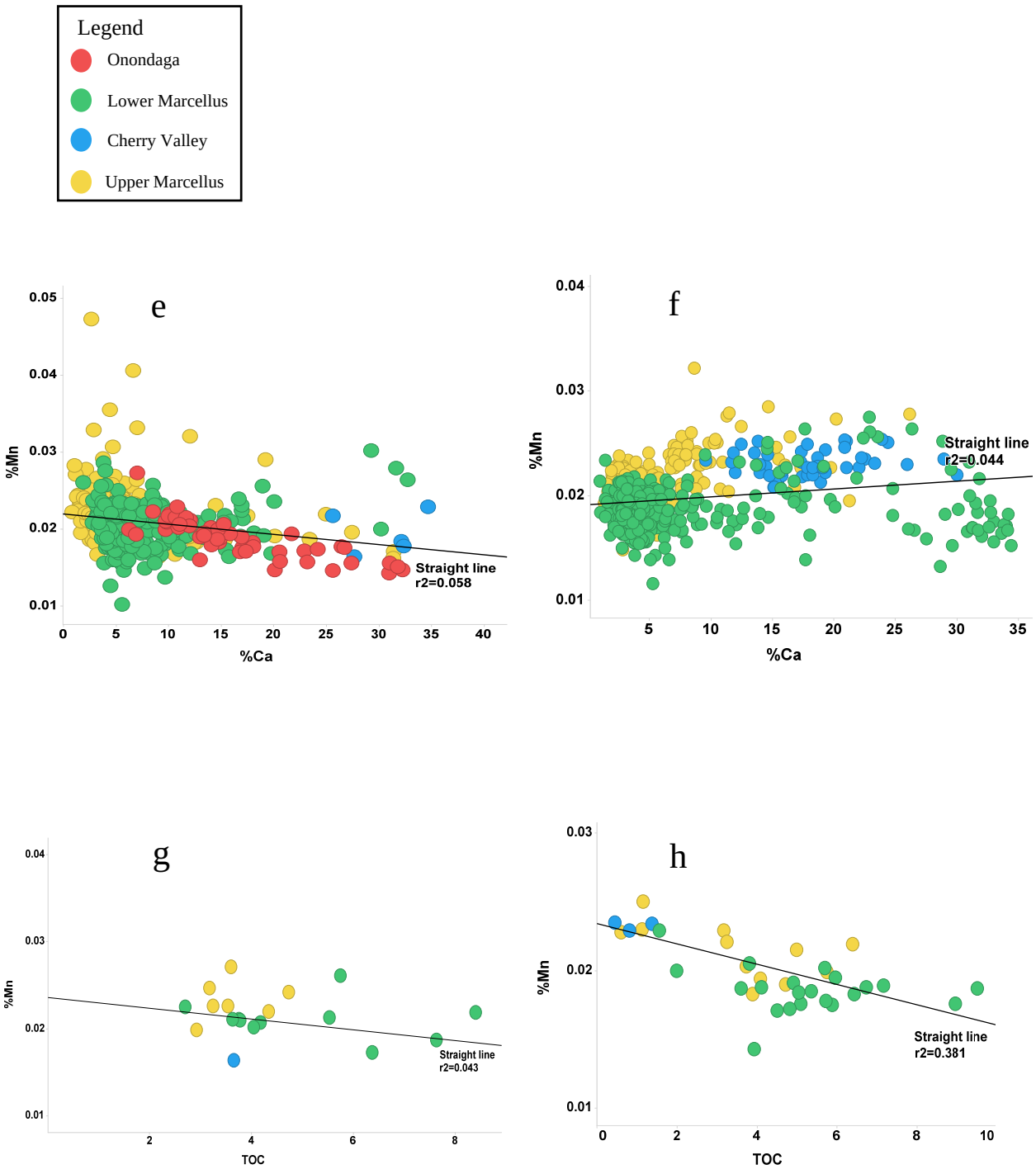

Figure 4.2: e) Geochemical cross plot of Mn versus Ca from Olsyn #2V showing no correlation between both elements; f) cross plot of Mn versus Ca from SRC #1V showing no correlation between both elements; g) cross plot of Mn versus TOC from the Olsyn #2V well showing no correlation between Mn and TOC; h) cross plot of Mn versus TOC from SRC #1V showing weak negative correlation between Mn and TOC likely suggesting lower Mn enrichment in less oxygenated environments.

4.3: Redox-sensitive Trace Elements

The enrichment or depletion of several trace elements such as Mo, U, and V can be used as a tool to infer the paleo-oxygen content of the Appalachian basin during Marcellus deposition and thus the redox potential. The determination of redox potential or conditions of an environment distinctively means discerning whether conditions were oxidizing or reducing. Organic matter preservation is usually prevalent in reducing conditions because these conditions prohibit macrofaunal and bacteria scavenging. Chromium is another element that can also be used to infer redox conditions, but may be transported to the sediment with land-derived clastic fractions, which limits its use as reliable redox proxies (Tribovillard et al., 2006). Cr shows weak positive covariance with TOC (Fig. 4.3a).

4.3.1: Molybdenum

In natural oxygenated water, molybdenum forms two main molybdate oxyanions, which include $HMoO_4^-$ and MoO_4^{2-} (Brookins, 1988). Mo displays almost no affinity for clay surfaces and most natural particles in the marine environment, but is easily captured by Mn-oxyhydroxides generally at the surface environment (Calvert and Pedersen, 1993). Mo is then released at the sediment-water interface through the reductive dissolution of the Mn-oxyhroxide complexes. This process can lead to a subsequent concentration of Mo in the sediment. Also, reduction of molybdate anions especially in anoxic to euxinic environments can lead to the formation of organic thiomolybdates (Mo-S organic compounds) and Mo-Fe-S complexes. These organic compounds and Mo-Fe-S complexes are prone to scavenging by authigenic pyrite or by sulphur-rich organic compounds in euxinic environments leading to an enrichment of Mo below the sediment-water interface (Tribovillard et al., 2006). Therefore, Mo is an excellent indicator of both anoxic and euxinic (H_2S rich) environments. Mo displays a strong positive covariance with TOC, but displays

a weak positive correlation with S (Fig. 4.3b & c). The strong relationship with TOC, but weak relationship with S suggest that the study area was probably anoxic, but not euxinic during Marcellus deposition (Algeo and Maynard, 2004).

4.3.2: Uranium

Uranium is a radioactive element that is found as U (VI) cation bounded to carbonate ions in normal oxygenated seawaters (Tribovillard et al., 2006). The enrichment of U is considered to take place primarily in the sediment because the U (VI) compounds are not affected by the reducing conditions in the water column itself, but within the sediment. The enrichment process involves the diffusion of U (VI) compounds across the sediment-water interface, forming U (IV) if the sediment exhibits reducing conditions and subsequently precipitating uraninite (UO_2) (Tribovillard et al., 2006, O'Neal, 2015). Redox conditions of the water are therefore not important to the enrichment of U. To complicate things further, the element can be mobilized within the sediment if oxygen penetrates deep into the sediment (Tribovillard et al., 2006). Despite this shortcoming, U still shows strong positive covariance with TOC ($r^2 = 0.54$ and 0.55) in both Olsyn #2V and SRC #1V wells (Fig. 4.3d & e), respectively. U also shows a good positive covariance with Mo, but no relationship with S (Fig 4.3 f & g).

4.3.3: Vanadium

In natural oxygenated waters, vanadium is present as V(V) and forms two vanadate oxyanions, which include HVO_4^{2-} and $H_2VO_4^-$ (Tribovillard et al., 2006). Similar to Mo, V normally adsorbs onto both Mn and Fe-oxyhydroxides, which facilitates its transportation to the sediment-water interface. If mildly reducing conditions exist at the sediment-water interface, V (V) is reduced to V (IV) forming vanadyl ions (VO^{2-}) and insoluble hydroxide compounds VO

$(OH)_2$ that precipitate out to the bottom sediments in the presence of humic acids. Under more strongly reducing conditions approaching euxinic conditions, V (IV) is further reduced to V (III) forming geoporphyrins or solid oxide (V_2O_3) and hydroxides ($V(OH)_3$) in the presence of free H_2S (Tribovillard et al., 2006). However, unlike Mo the presence of euxinic conditions does not necessarily increase V enrichment compared to anoxia probably due to the fact that the V (III) compound is not taken up in solid solution by Fe-sulfides (Algeo and Maynard, 2004). Because of these processes, V is an excellent indicator of anoxia, but not a reliable indicator of euxinia. Accordingly, V displays good positive covariance with TOC ($r^2 = 0.66$) (Fig. 4.3h).

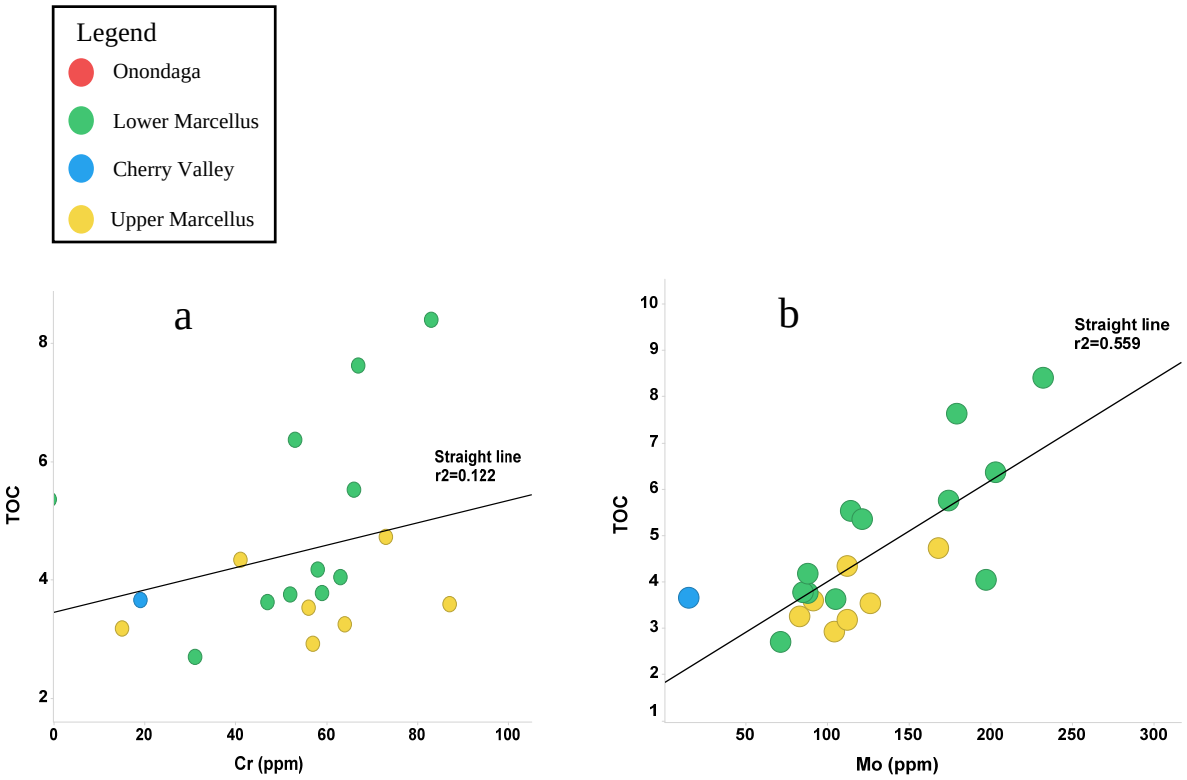

Figure 4.3: a) Geochemical cross plot of Cr against TOC in wt. % from XRF data in Olsyn #2V well, showing weak positive covariance; b) cross plot of Mo versus TOC in wt. % from Olsyn #2V showing moderate positive covariance ($R^2 = 0.56$).

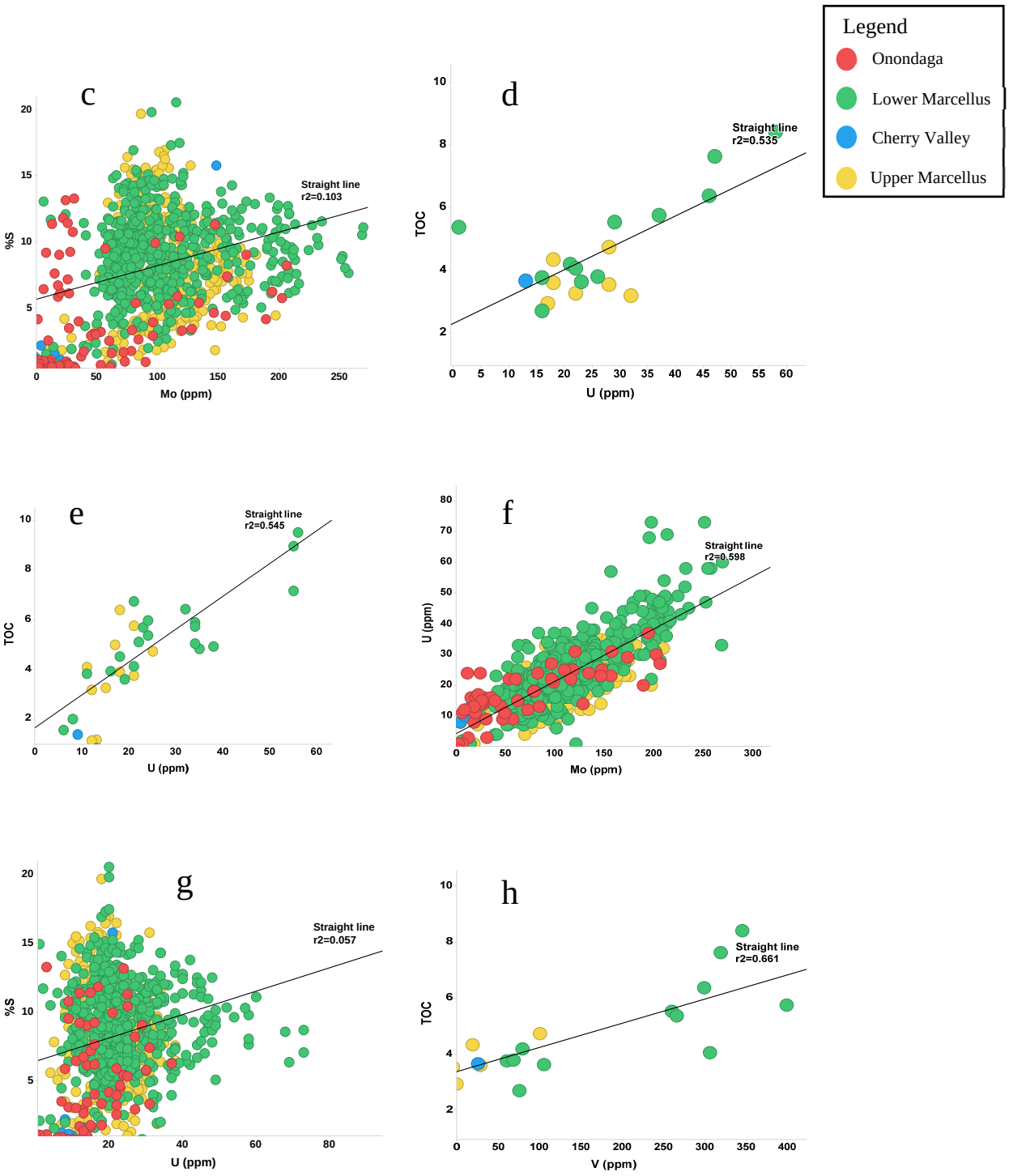

Figure 4.3: c) Cross plot of Mo versus S from Olsyn #2V showing no correlation suggesting that bottom waters were probably not euxinic; d) cross plot of U versus TOC from Olsyn #2V showing moderate positive covariance (R^2 = 0.54); e) geochemical cross plot of U against TOC from SRC #1V well, showing moderate positive covariance; f) cross plot of Mo versus U from Olsyn #2V showing moderate positive covariance (R^2 = 0.60) suggesting Mo and U follow similar authigenic enrichment mechanisms; g) cross plot of U versus S from Olsyn #2V showing no correlation suggesting that bottom waters were probably not euxinic; h) cross plot of V against TOC from Olsyn #2V showing strong positive covariance (R^2 = 0.66).

4.4: Organophillic Trace Elements

Several elements including Ni, Cu, and Zn behave as micronutrients in the water column and are preferentially enriched in organic matter, which makes them good geochemical proxies for various levels of paleoproductivity, which represents the degree to which biological productivity occurred in the surface waters of the ocean (Tribovillard et al., 2006, O'Neal, 2015). High concentrations of Ni, Cu, and Zn in sediments or sedimentary rocks can indicate periods of high biological productivity where a significant fraction of the organic matter left the surface waters and reached the bottom sediments.

4.4.1: Nickel

In oxygenated environments, Ni is present as a micronutrient for marine organisms in the water column and is mainly found as Ni carbonate ($NiCO_3$) or adsorbed onto organic acids (Tribovillard et al., 2006). Removal of Ni from the water column may be accelerated by the formation of organometallic complexes or ligands between Ni compounds and organic matter, which settle to the sediment-water interface. Ni is released to sediment pore waters by the remineralization or decay of the organic matter at or below the sediment-water interface. Under reducing conditions, the released Ni binds with any available S to form an insoluble sulfide (NiS) that can be taken up in solid solution by authigenic pyrite (Tribovillard et al., 2006). Ni displays a weak positive covariance with TOC in the Marcellus Formation, but has no relationship with S (Fig. 4.4a & b) suggesting Ni is related to TOC, but not to S.

4.4.2: Copper

In oxygenated environments, Cu is found in organometallic ligands and serves as micronutrients for marine organisms in the water column just like Ni (Algeo and Maynard, 2004).

Copper removal from surface waters and enrichment in sediments may occur via two different processes: 1) formation and settling of Cu-organometallic ligands, and 2) adsorption onto Mn- and Fe-oxyhydroxides and settling to the sediment-water interface. Like Ni, Cu may be released within the sediment or at the sediment-water interface upon the decay of organic matter and reductive dissolution of the oxyhydroxides. Also, under reducing conditions, Cu within the organic complexes or oxyhydroxides may be reduced from Cu(II) to Cu(I) and the reduced Cu may be incorporated into a solid solution with pyrite or even form its own sulfide phase, CuS or CuS_2 (Tribovillard et al., 2006). Cu displays a good positive covariance with TOC for the Marcellus Formation (Fig. 4.4c). It displays no relationship with S, suggesting that Cu is probably not related to pyrite content. (Fig. 4.4d).

4.4.3: Zinc

Similar to Ni and Cu, Zn serves as a micronutrient for marine organisms in oxygenated marine conditions (Tribovillard et al., 2006). It is found adsorbed onto organic acids and Mn- and Fe-oxyhydroxides and becomes enriched in sediments through processes similar to those of Ni and Cu, which involves settling of organic complexes and oxyhydroxides to the sediment-water interface, and subsequent release of Zn through the decay of organic matter and reductive dissolution of oxyhydroxides. Finally, Zn may be incorporated into a solid solution with pyrite or to a lesser extent form its own sulfides under reducing conditions (Tribovillard et al., 2006). In the existing dataset Zn has a moderate positive correlation with TOC (Fig. 4.4 e).

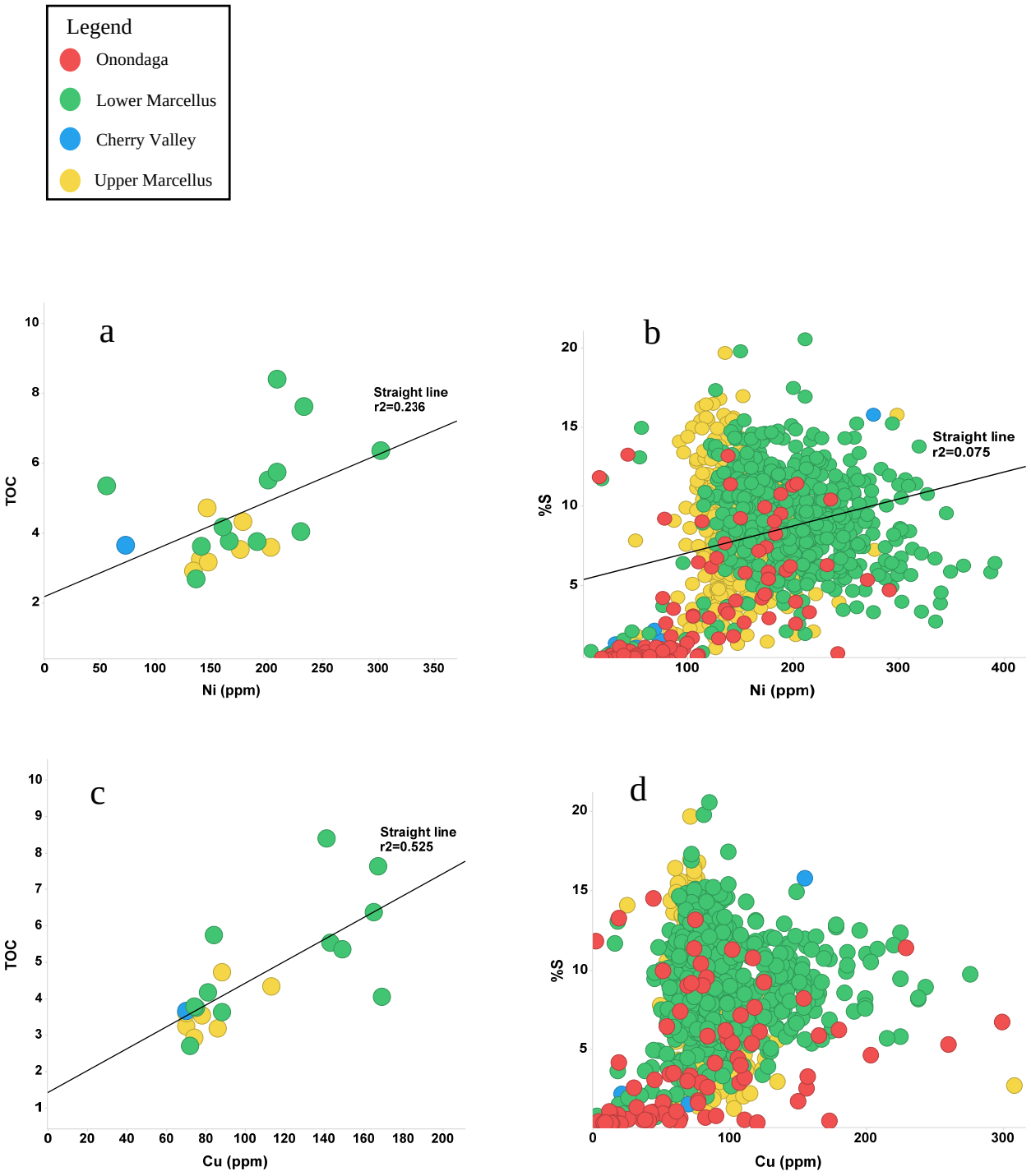

Figure 4.4: a) Geochemical cross plot of Ni from XRF data against TOC in Olsyn #2V well, showing weak positive covariance (R^2 = 0.24); b) cross plot of Ni versus S from Olsyn #2V showing no correlation; c) cross plot of Cu against TOC from Olsyn #2V showing moderate positive correlation (R^2 = 0.53); d) cross plot of Cu versus S from Olsyn #2V showing no correlation.

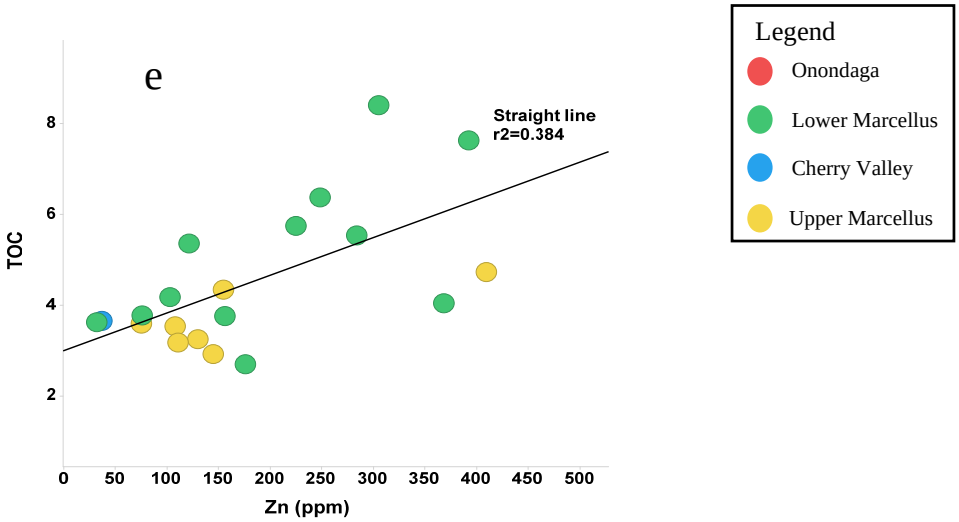

Figure 4.4: e) Geochemical cross plot of Zn versus TOC from Olsyn #2V showing weak positive covariance (R^2 = 0.38).

4.5: Hierarchical Cluster Analysis

Hierarchical cluster analysis (HCA) was performed on the XRF samples from the Olsyn #2V and SRC #1V wells. Hierarchical cluster analysis is a statistical technique that can be used to classify samples into groups, such that all the samples within a group are similar to each other. The traditional approach of XRF analysis has involved treating each sample data as 29 one-dimensional characterizations or plots, whereas hierarchical cluster analysis is a unique way of visualizing or analyzing each sample as an assemblage of the elements (Phillips, 1991). In hierarchical cluster analysis, the samples are joined together in a hierarchical manner based on how each sample compares to the next sample based on the covariance of all the elements from one sample to the other. A correlation based grouping method was selected in this study from a plethora of several other methods in the HCA process to characterize a sample's similarity to another sample. The correlation method considers two samples to be similar if all the elements in both samples are highly correlated. The unweighted pair group method with arithmetic mean (UPGMA) was then used to derive the distance between the groups of similar samples to form the

clusters. These clusters can also be considered to be chemically distinct units or chemofacies. Twenty-five of the twenty-nine elements were utilized in the clustering. Vanadium, titanium, chromium and barium were not utilized in the clustering because of extremely high barium concentrations observed at certain depths, which led to negative values for V, Ti, and Cr. High Ba concentrations can affect the ability to resolve Ti, V and Cr because the XRF K-shell energy peaks for Ti, V and Cr, and XRF L-shell energy peaks for Ba overlap (Rowe, pers. comm. 2016). This overlap makes it difficult to accurately estimate V, Ti and Cr concentrations when high Ba concentrations exist. A brief overview of the clusters generated for both wells is discussed below followed by a more detailed discussion in the chemostratigraphic interpretation section (4.6).

4.5.1: Olsyn #2V

Six general chemofacies are identified in the Olsyn #2V core using the hierarchical cluster analysis technique: limestone (LS), siliceous organic mudstone (SOM), pyrite-rich organic mudstone (POM), organic mudstone (OM), calcareous mudstone (CM), and mudstone (M). As discussed in the previous section, the correlation and UPGMA distance method was used to group the various samples into chemofacies (Fig 4.5). To determine the chemofacies type or nomenclature, average concentrations of the elements in the clusters/chemofacies are compared to the average concentration of the sum of that element in both wells using the following equation (Eq. 5.1; Phillips, pers. comm. 2015):

Enrichment ratio (ER) = Avg. conc. of element X in cluster / Avg. conc. of element X from all 1690 samples in project (5.1)

The enrichment or depletion of certain elements in the clusters are then used to identify the chemofacies type (Table 2).

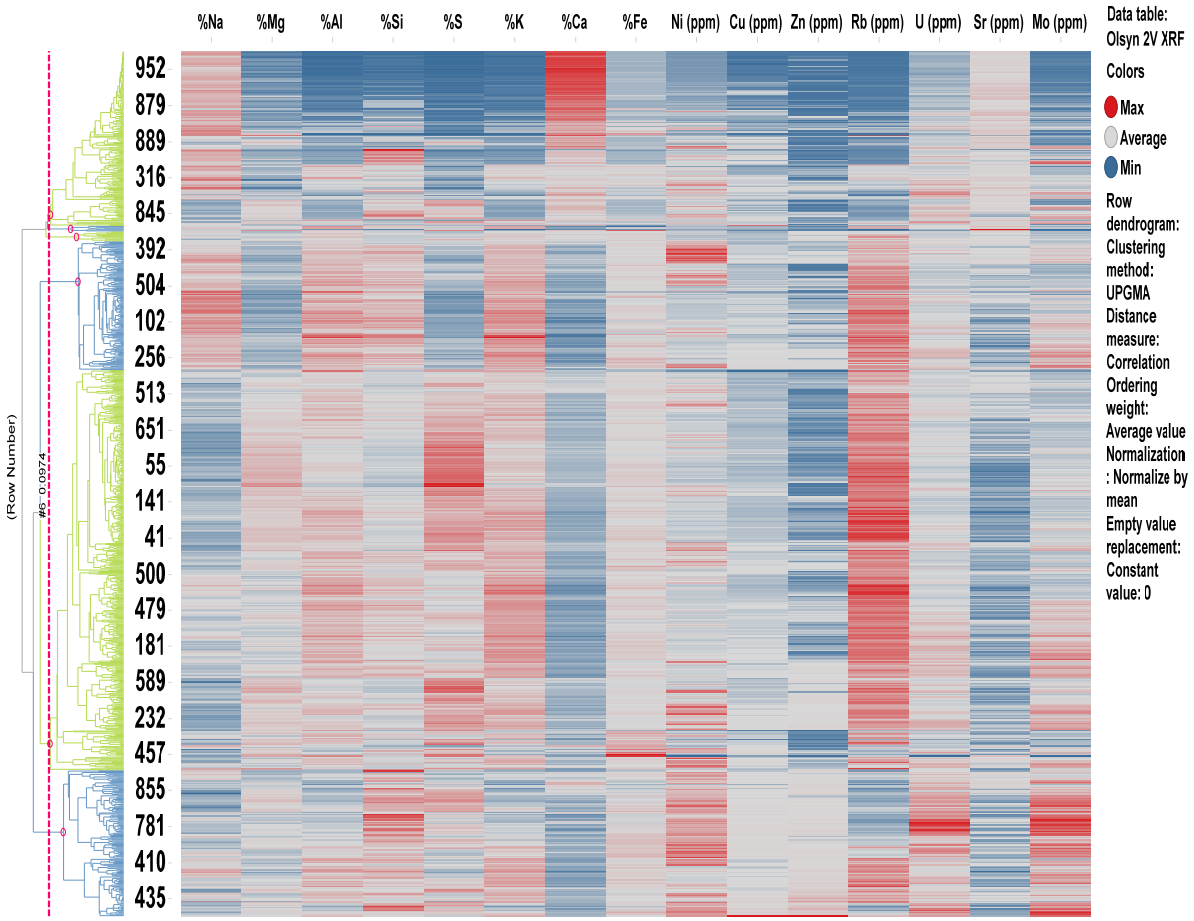

Figure 4.5: Dendogram and heat map of the Olsyn #2V hierarchical cluster analysis data. The red line on the left indicates the pruning line used to subdivide the data into six chemofacies. The numbers in the column next to the dendogram indicate different sample depths which the heat map is referenced to. Only 15 of the 25 elements utilized in the clustering are shown in the heat map. The red colors on the heat map indicate high values for each elements, whereas the blue colors indicate lower values for the various elements.

The first row in table 2 indicates the number of samples in each cluster/chemofacies. The second row indicates the cluster identificaton number (ID) for each cluster given by the spotfire software. The first four columns in table 2 indicate the element number, element, mean value for element in dataset (Olsyn #2V & SRC # 1V), and total numbers of XRF sample points from dataset. For each cluster (i.e cluster 6), the mean value for each element in that cluster, enrichment ratio for the element in that cluster and the range of the element in the cluster is shown in table 2.

Table 2: Olsyn #2V spreadsheet showing the various initial spotfire clusters and number of samples for each cluster. Shown below are the elements enriched in the various clusters, which are used to identify the chemofacies type. The elements are colored based on their use as proxies for minerals, redox conditions or paleoproductivity (i.e detrital elements colored grey and carbonate elements colored blue).

		# of Samples		444			194			162			6			11			143		
		Spotfire Cluster ID ->		6	6	6	7	7	7	12	12	12	18	18	18	26	26	26	30	30	30
Order	Element	[Sample Mean]	Total #	[Mean]	E.R	Range	[Mean]	E.R	Range	[Mean]	E.R	Range	[Mean]	E.R	Range	[Mean]	E.R	Range	[Mean]	E.R	Range
1	%Al	4.95	1690	5.48	1.11	5.49	2.31	0.47	6.60	4.64	0.94	5.58	5.32	1.07	5.33	5.15	1.04	0.92	6.15	1.24	6.43
2	%K	1.97	1690	2.15	1.09	2.03	0.84	0.43	2.47	1.78	0.90	2.09	1.54	0.78	2.22	1.91	0.97	0.29	2.31	1.17	1.85
3	%Rb	141.18	1690	167.96	1.19	160.00	54.52	0.39	196.00	116.00	0.82	173.00	95.00	0.67	168.00	142.36	1.01	37.00	162.75	1.15	112.00
4	%Si	17.45	1690	17.70	1.02	14.74	13.38	0.77	33.52	21.48	1.23	24.71	15.70	0.90	14.39	16.55	0.95	3.85	20.55	1.18	12.15
5	Zr (ppm)	105.4	1690	127.04	1.21	139.00	52.90	0.50	142.00	103.07	0.98	119.00	53.67	0.51	202.00	107.45	1.02	18.00	126.97	1.20	159.00
6	%Na	0.12	1690	0.07	0.58	0.25	0.19	1.58	0.42	0.10	0.83	0.29	0.13	1.08	0.12	0.11	0.92	0.13	0.22	1.83	0.47
7	Th (ppm)	12.12	1690	14.03	1.16	10.00	5.51	0.45	15.00	10.67	0.88	13.00	9.67	0.80	11.00	12.18	1.00	3.00	13.65	1.13	9.00
8	%Ca	7.99	1690	5.36	0.67	13.60	20.29	2.54	38.43	5.83	0.73	14.40	4.99	0.62	10.80	8.79	1.11	3.15	4.58	0.57	9.00
9	%Mn	0.02	1690	0.02	1.00	0.04	0.02	1.00	0.04	0.02	1.00	0.01	0.03	1.50	0.02	0.02	1.00	0.00	0.02	1.00	0.03
10	Sr (ppm)	266.78	1690	217.92	0.82	552.00	423.17	1.59	709.00	243.59	0.91	363.00	1074.17	4.03	2957.00	306.27	1.15	112.00	249.38	0.93	402.00
11	%Mg	2.12	1690	2.65	1.25	4.50	1.42	0.67	10.44	2.10	0.99	2.88	2.67	1.26	3.50	1.98	0.93	1.14	1.38	0.65	2.42
12	%Fe	2.12	1690	2.24	1.06	5.93	1.34	0.63	2.90	2.16	1.02	2.20	0.94	0.44	6.10	2.21	1.04	0.55	2.18	1.03	3.06
13	%S	8.25	1690	10.83	1.31	16.34	3.82	0.46	14.36	8.76	1.06	10.68	9.15	1.11	7.48	7.67	0.95	4.63	5.31	0.64	8.40
14	As (ppm)	33.5	1690	32.19	0.96	121.00	23.89	0.71	55.00	44.71	1.33	136.00	29.33	0.88	17.00	22.00	0.66	20.00	33.03	0.99	54.00
15	Pb (ppm)	19.03	1690	20.05	1.05	62.00	15.32	0.81	17.00	21.12	1.11	14.00	20.67	1.09	6.00	17.90	0.94	5.00	20.79	1.08	13.00
16	Co (ppm)	26.13	1690	31.57	1.21	596.00	11.24	0.43	86.00	24.93	0.95	55.00	36.67	1.40	69.00	23.54	0.90	15.00	28.29	1.08	62.00
17	Nb (ppm)	11.7	1690	13.00	1.11	13.00	7.62	0.65	27.00	12.30	1.09	21.00	9.33	0.80	8.00	14.54	1.24	7.00	12.65	1.08	13.00
18	Ga (ppm)	17.74	1690	19.99	1.13	30.00	9.07	0.51	20.00	18.89	1.06	83.00	20.50	1.16	15.00	17.72	1.00	2.00	19.76	1.11	12.00
19	Y (ppm)	24.98	1690	22.10	0.88	33.00	31.18	1.25	123.00	26.32	1.05	52.00	23.17	0.93	35.00	32.36	1.26	8.00	22.65	0.91	24.00
20	%P	0.21	1690	0.27	1.29	0.54	0.15	0.71	3.88	0.24	1.14	0.38	0.25	1.19	0.48	0.20	0.95	0.14	0.11	0.52	0.18
21	Mo (ppm)	97.39	1690	98.57	1.01	225.00	54.62	0.56	206.00	154.11	1.58	240.00	44.17	0.45	112.00	77.55	0.80	38.00	101.11	1.04	179.00
22	Cu (ppm)	103.22	1690	82.21	0.80	201.00	81.45	0.79	2967.00	152.45	1.48	2885.00	58.33	0.57	57.00	69.81	0.68	27.00	87.43	0.85	157.00
23	Ni (ppm)	155.49	1690	164.91	1.06	273.00	122.08	0.79	285.00	218.57	1.41	292.00	97.17	0.62	98.00	138.81	0.89	84.00	182.97	1.18	383.00
24	Zn (ppm)	171.16	1690	128.01	0.75	530.00	73.84	0.43	384.00	489.78	2.86	6735.00	65.67	0.38	96.00	240.90	1.41	237.00	148.22	0.87	296.00
25	U (ppm)	20.95	1690	19.86	0.95	77.00	14.57	0.70	59.00	33.00	1.58	62.00	12.50	0.60	37.00	17.18	0.82	15.00	19.85	0.95	28.00

Enriched in...		Enriched in...		Enriched in...		Enriched in...		Enriched in...		Enriched in...	
%Al	1.11	%Na	1.58	%Si	1.23	%Al	1.07	%Al	1.04	%Al	1.24
%K	1.09	%Ca	2.54	%Fe	1.02	%Na	1.08	%Ca	1.11	%K	1.17
%Rb	1.19	Sr (ppm)	1.59	%Si	1.06	%Mn	1.50	Sr (ppm)	1.15	%Rb	1.15
Zr (ppm)	1.21	Y (ppm)	1.25	AS (ppm)	1.33	Sr (ppm)	4.03	Nb (ppm)	1.24	%Si	1.18
Th (ppm)	1.16			Pb (ppm)	1.11	%Mg	1.26	Zn (ppm)	1.41	Zr (ppm)	1.20
%Mg	1.25			%P	1.14	%S	1.11			%Na	1.83
%Fe	1.06			Mo (ppm)	1.58	Pb (ppm)	1.09			Th (ppm)	1.13
%S	1.31			Cu (ppm)	1.48	Co (ppm)	1.40			Pb (ppm)	1.08
Co (ppm)	1.21			Ni (ppm)	1.41	%P	1.19			Co (ppm)	1.08
%P	1.29			Zn (ppm)	2.86					Mo (ppm)	1.04
Zn (ppm)	1.06			U (ppm)	1.58					Ni (ppm)	1.18
Chemofacies 3.0		Chemofacies 1.0		Chemofacies 2.0		Chemofacies 4.0		Chemofacies 5.0		Chemofacies 6.0	
Pyrite rich Org. Mudstone (POM)		Limestone (LS)		Siliceous Organic Mudstone (SOM)		Mudstone (M)		Calcareous Mudstone (CM)		Organic Mudstone (OM)	

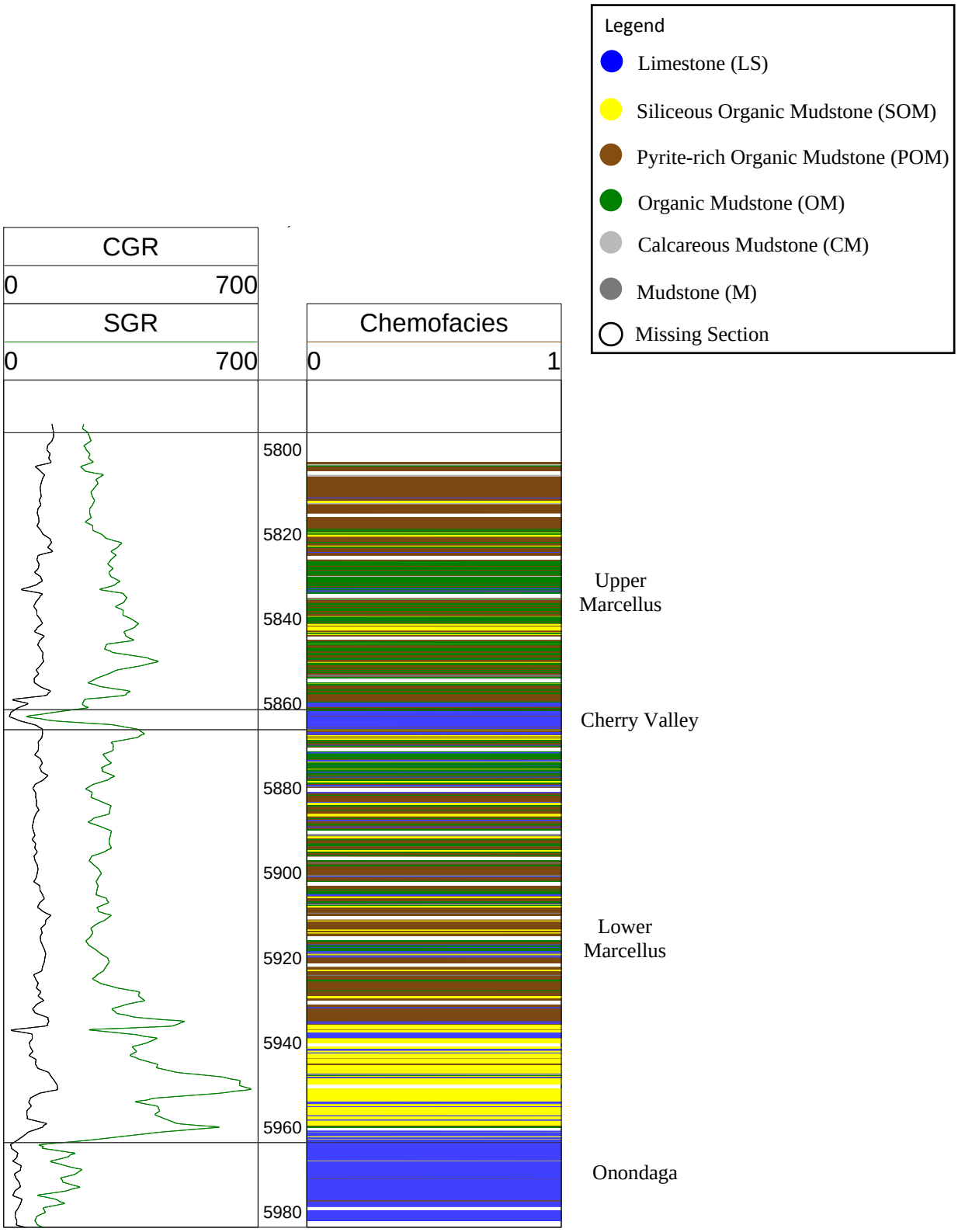

Figure 4.6: Chemofacies plot from the Olsyn #2V well showing the six chemofacies obtained from the hierarchical cluster analysis. Standard gamma ray (SGR) in green and computed gamma ray (SGR minus uranium contribution) are plotted in first track.

The Limestone (LS) chemofacies comprises most of the Onondaga and Cherry Valley formations (Fig 4.6). The Siliceous organic mudstone chemofacies (SOM) predominantly occurs in the basal section of the lower Marcellus. The pyrite-rich organic mudstone (POM) and the organic mudstone (OM) chemofacies are disseminated all across the lower Marcellus and upper Marcellus. The calcareous mudstone chemofacies (CM) is mostly in the lower Marcellus, whereas the mudstone chemofacies (M) is in the upper Marcellus.

4.5.2: SRC #1V

Four general chemofacies are identified in the SRC #1V core using the hierarchical cluster analysis technique: limestone (LS), pyrite-rich organic mudstone (POM), organic mudstone (OM), and Sr-rich organic mudstone (COM). The correlation and UPGMA distance hierarchical clustering method was also used to group the various samples into chemofacies (Fig 4.7). Just as in the Olsyn #2V well, average concentrations of the elements in the clusters/chemofacies were compared to the average concentration of the sum of that element in both wells to determine the chemofacies type (Table 3).

The first row in table 3 indicates the number of samples in each cluster/chemofacies. The second row indicates the cluster identificaton number (ID) for each cluster given by the spotfire software. The first four columns in table 3 indicate the element number, element, mean value for element in dataset (Olsyn #2V & SRC # 1V), and total numbers of XRF sample points from dataset. For each cluster (e.g., cluster 4), the mean value for each element in that cluster, enrichment ratio for the element in that cluster and the range of the element in the cluster is shown in table 3. Shown at the bottom of the table are the elements each cluster is enriched in which is used to name the chemofacies.

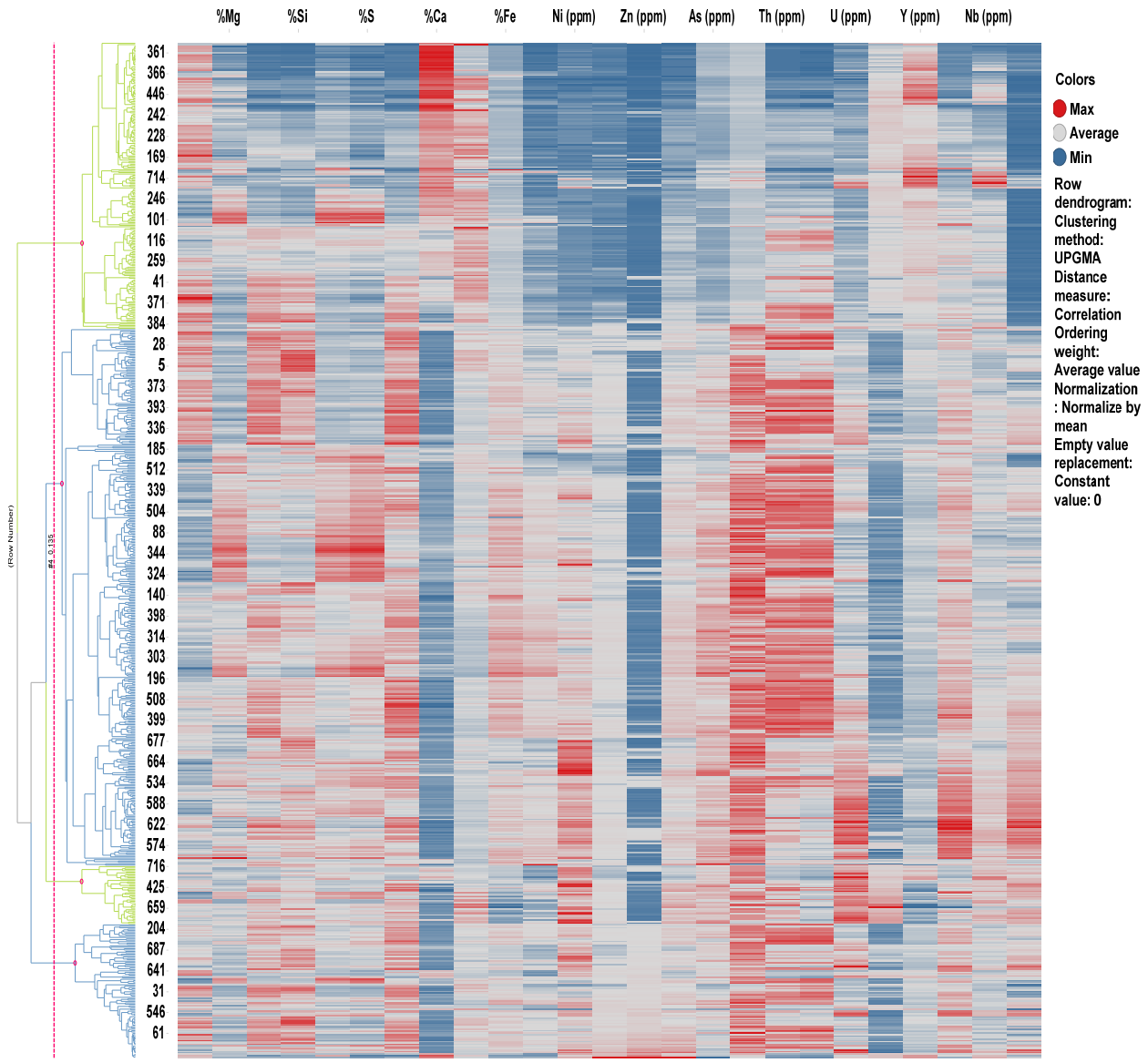

Figure 4.7: Dendogram and heat map of the SRC#1V hierarchical cluster analysis data. The red line on the left indicates the pruning line used to subdivide the data into 4 chemofacies. The numbers in the column next to the dendogram indicate different sample depths which the heat map is referenced to. Only 12 of the 25 elements utilized in the clustering are shown in the heat map. The red colors on the heat map indicate high values for each elements, while the blue colors indicate lower values for the various elements.

Table 3: SRC #1V spreadsheet showing the various initial spotfire clusters and number of samples for each cluster. Shown below are the elements enriched in the various clusters, which are used to identify the chemofacies type. The elements are colored based on their use as proxies for minerals, redox conditions or paleoproductivity (i.e detrital elements colored grey and carbonate elements colored blue).

			# of Samples	386			96			42			206		
			Spotfire Cluster ID ->	4	4	4	9	9	9	11	11	11	12	12	12
Order	Element	[Sample Mean]	Total #	[Mean]	E.R	Range	[Mean]	E.R	Range	[Mean]	E.R	Range	[Mean]	E.R	Range
1	%Al	4.95	1690	5.65	1.14	5.98	5.77	1.17	5.63	5.27	1.06	3.74	3.91	0.79	7.07
2	%K	1.97	1690	2.42	1.23	1.81	2.39	1.21	2.46	2.24	1.14	1.30	1.50	0.76	2.66
3	%Rb	141.18	1690	170.60	1.21	128.00	161.79	1.15	165.00	127.14	0.90	116.00	109.31	0.77	179.00
4	%Si	17.45	1690	18.47	1.06	21.55	19.66	1.13	18.55	17.55	1.01	10.74	12.58	0.72	24.53
5	Zr (ppm)	105.4	1690	115.63	1.10	103.00	111.57	1.06	81.00	91.69	0.87	147.00	77.28	0.73	127.00
6	%Na	0.12	1690	0.11	0.92	0.27	0.14	1.17	0.29	0.11	0.92	0.20	0.16	1.33	0.35
7	Th (ppm)	12.12	1690	14.39	1.19	8.00	13.55	1.12	11.00	12.71	1.05	7.00	9.31	0.77	14.00
8	%Ca	7.99	1690	3.72	0.47	11.02	4.77	0.60	24.64	5.29	0.66	12.43	16.21	2.03	31.96
9	%Mn	0.02	1690	0.02	1.00	0.01	0.02	1.00	0.01	0.02	1.00	0.01	0.02	1.00	0.03
10	Sr (ppm)	266.78	1690	170.85	0.64	599.00	197.86	0.74	576.00	780.00	2.92	2403.00	336.69	1.26	642.00
11	%Mg	2.12	1690	2.35	1.11	5.43	1.85	0.87	2.82	1.98	0.93	1.85	1.85	0.87	5.23
12	%Fe	2.12	1690	2.64	1.25	3.69	2.31	1.09	2.46	1.37	0.65	2.65	1.68	0.79	5.38
13	%S	8.25	1690	9.71	1.18	15.35	7.81	0.95	14.70	8.52	1.03	7.97	5.92	0.72	19.28
14	As (ppm)	33.5	1690	45.57	1.36	104.00	33.67	1.01	90.00	46.48	1.39	45.00	12.28	0.37	44.00
15	Pb (ppm)	19.03	1690	21.13	1.11	43.00	20.65	1.09	16.00	20.31	1.07	11.00	12.50	0.66	16.00
16	Co (ppm)	26.13	1690	34.54	1.32	176.00	26.17	1.00	52.00	22.55	0.86	49.00	12.62	0.48	52.00
17	Nb (ppm)	11.7	1690	11.63	0.99	16.00	11.17	0.95	12.00	15.67	1.34	18.00	10.67	0.91	43.00
18	Ga (ppm)	17.74	1690	20.19	1.14	18.00	21.11	1.19	45.00	22.21	1.25	20.00	11.59	0.65	16.00
19	Y (ppm)	24.98	1690	18.67	0.75	48.00	21.71	0.87	48.00	15.10	0.60	68.00	40.94	1.64	107.00
20	%P	0.21	1690	0.22	1.05	0.50	0.18	0.86	0.39	0.20	0.95	0.24	0.15	0.71	0.57
21	Mo (ppm)	97.39	1690	127.27	1.31	439.00	115.08	1.18	332.00	158.10	1.62	194.00	13.96	0.14	134.00
22	Cu (ppm)	103.22	1690	130.88	1.27	198.00	201.24	1.95	2162.00	134.33	1.30	131.00	40.45	0.39	130.00
23	Ni (ppm)	155.49	1690	166.43	1.07	298.00	164.38	1.06	227.00	228.24	1.47	207.00	61.06	0.39	178.00
24	Zn (ppm)	171.16	1690	64.29	0.38	266.00	829.20	4.84	9043.00	62.02	0.36	196.00	36.39	0.21	339.00
25	U (ppm)	20.95	1690	24.41	1.17	60.00	23.16	1.11	56.00	41.88	2.00	38.00	9.28	0.44	53.00

Enriched in...	
%Al	1.14
%K	1.23
%Rb	1.21
%Si	1.06
Zr (ppm)	1.10
Th (ppm)	1.19
%Mg	1.11
%Fe	1.25
%S	1.18
As (ppm)	1.36
Pb (ppm)	1.11
Co (ppm)	1.32
Mo (ppm)	1.31
Cu (ppm)	1.27
U (ppm)	1.17

Chemofacies 3.0
Pyrite rich Org. Mudstone (POM)

Enriched in...	
%Al	1.17
%K	1.21
%Rb	1.15
%Si	1.13
Zr (ppm)	1.06
%Na	1.17
Th (ppm)	1.12
%Fe	1.09
Pb (ppm)	1.09
Mo (ppm)	1.18
Cu (ppm)	1.95
Ni (ppm)	1.06
Zn (ppm)	4.84
U (ppm)	1.11

Chemofacies 6.0
Organic Mudstone (OM)

Enriched in...	
%Al	1.06
%K	1.14
Th (ppm)	1.05
Sr (ppm)	2.92
As (ppm)	1.39
Pb (ppm)	1.07
Nb (ppm)	1.34
Ga (ppm)	1.25
Mo (ppm)	1.62
Cu (ppm)	1.30
Ni (ppm)	1.47
U (ppm)	2

Chemofacies 6.1
Sr rich Organic Mudstone (COM)

Enriched in...	
%Na	1.33
%Ca	2.03
Sr (ppm)	1.26
Y (ppm)	1.64

Chemofacies 1.0
Limestone (LS)

The Limestone (LS) chemofacies in the SRC #1V comprises most of the Cherry Valley Limestone just as the Olsyn #2V well, but shows more variability across the Lower and Upper Marcellus (Fig. 4.8). A significant portion of the cored interval is made up of the pyrite-rich organic mudstone chemofacies (POM), whereas the organic mudstone (OM) chemofacies is thinly disseminated across the Lower and Upper Marcellus. The Sr-rich mudstone chemofacies (COM) is mostly confined to the Lower Marcellus and is not as abundant as the other chemofacies.

4.6: Chemostratigraphic Analysis and Interpretation

The following section will thoroughly describe the Olsyn #2V and SRC #1V XRF data with notable emphasis on carbonate elements, detrital indicators, redox-sensitive elements and organophillic elements. This section also relates the major and trace element indicators to the chemofacies obtained from the hierarchical cluster analysis.

4.6.1: Olsyn #2V Chemostratigraphy

The Olsyn #2V core contains 18 ft (~ 6m) of the Onondaga Formation consisting predominantly of the limestone chemofacies (LS) derived from hierarchical cluster analysis (Fig. 4.6). The limestone chemofacies contain high Ca (> 30 wt. %), and Sr (> 600 ppm) concentrations and low concentrations of Si and Al (2-6 wt. % and 1-3 wt. %, respectively). It also has low concentrations of redox-sensitive trace elements. A few intervals of the limestone chemofacies between 5965 and 5975 ft exhibit high Si values (20-30 wt. %), moderate Ca and Sr values (10-25 wt. % and 200-500 ppm, respectively), and low Al, K, and Zr values. These intervals also have high concentrations of V, Mo, and U. The V, Mo, and U values range from 150-350 ppm, 50-150 ppm, and 10-30 ppm, respectively.

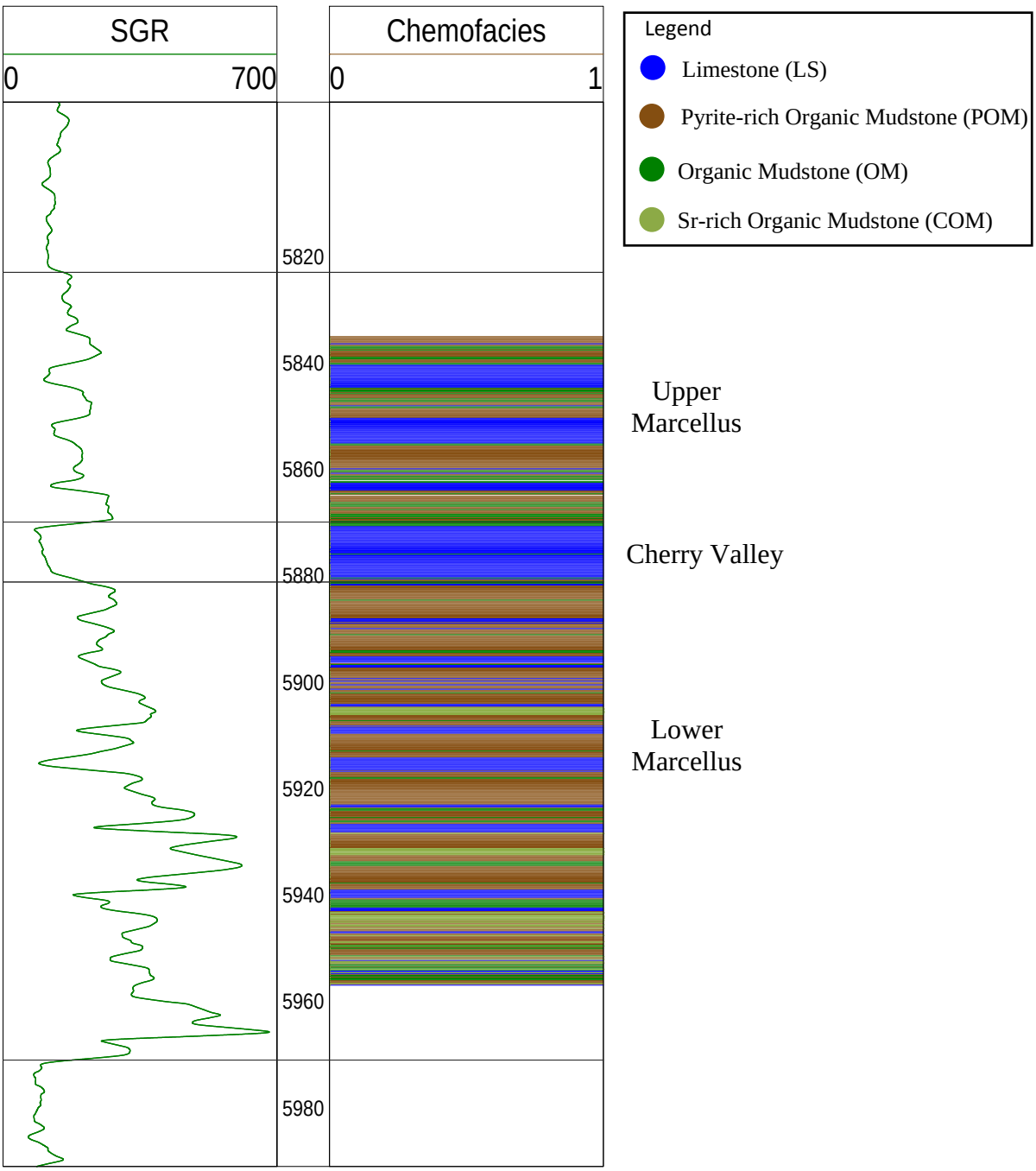

Figure 4.8: Chemofacies plot from the SRC #1V well showing the four chemofacies obtained from the hierarchical cluster analysis. Standard gamma ray (SGR) in green is plotted in first track.

The Lower Marcellus Formation, which directly overlies the Onondaga Formation has a thickness of 97 ft (30 m) in the Olsyn #2V well. The lowermost 27 ft (8 m) of the Lower Marcellus contains high concentrations of Si (25-35 wt. %), moderate concentrations of Ca and Sr (10-20 wt. % and 150-500 ppm, respectively) and low concentrations of Al, K, Zr and Ti (Fig. 4.9). This 27 ft (8 m) interval is defined from hierarchical cluster analysis as predominantly siliceous organic mudstone (SOM) chemofacies with interbedded limestone chemofacies. Redox-sensitive and organophillic trace elements are high in this interval. The highest TOC values in this well from geochemical analysis are also measured in this interval (8 wt. %). A gradual increase in Al, K, and Zr and decrease in Si, and Ca can be identified from the base to the top of the interval. There is a pronounced spike in Ca and Sr at 5938 ft with significant depletion in Al, K, Zr, and Si that briefly reverses the increasing detrital trend.

Above the siliceous organic mudstone chemofacies from 5936 ft to the top of the Lower Marcellus, is a high concentration of Al, K, Zr, and Si (>5 wt. %, >2 wt. %, >100 ppm, and >20 wt. %, respectively). Ca and Sr are depleted in this interval and have values that are less than 10 wt. % and 250 ppm, respectively (Fig. 4.9). Redox-sensitive and organophillic elements such as Mo, U, Cr, Cu, and Ni show slightly lower values as compared to the siliceous organic mudstone chemofacies interval below (Figs. 4.10 and 4.11). V only shows high concentrations from 5890 ft to the top of the Lower Marcellus. Ni also shows high values at the top of the Lower Marcellus (Fig. 4.11). From hierarchical cluster analysis, this interval predominantly consist of the pyrite-rich organic mudstone (POM) and organic mudstone (OM) chemofacies (Fig. 4.6).

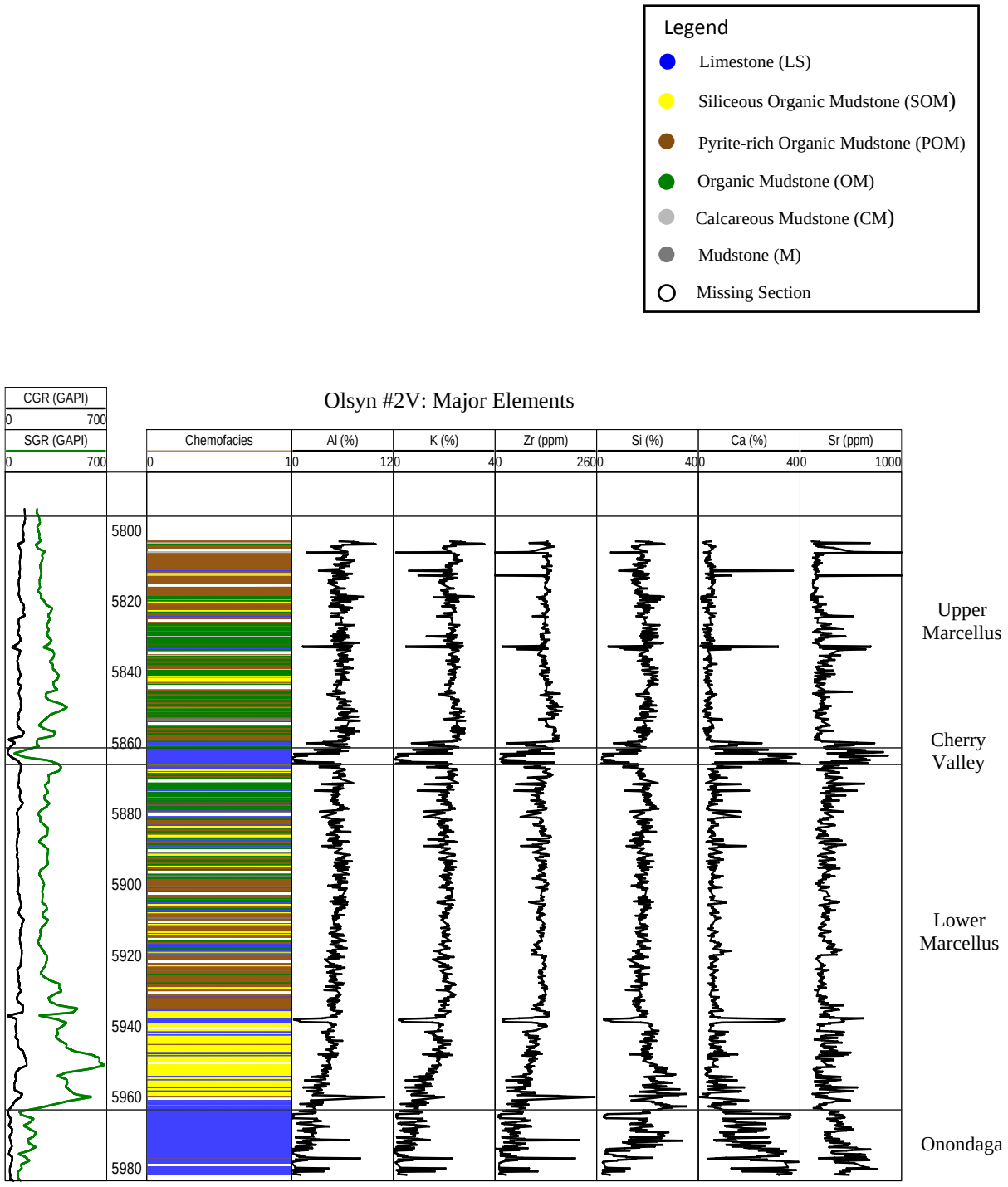

Figure 4.9: Major element chemostratigraphy for Olsyn #2V including corrected gamma ray (CGR), standard gamma ray (SGR), chemofacies, Al, K, Zr, Si, Ca, and Sr. Note inverse trends between Ca, and Al, K, Zr, and Si. Standard gamma ray (SGR) in green and computed gamma ray (SGR minus uranium contribution) are plotted in first track. Both gamma ray curves are presented in gamma ray, American Petroleum Institute units (GAPI).

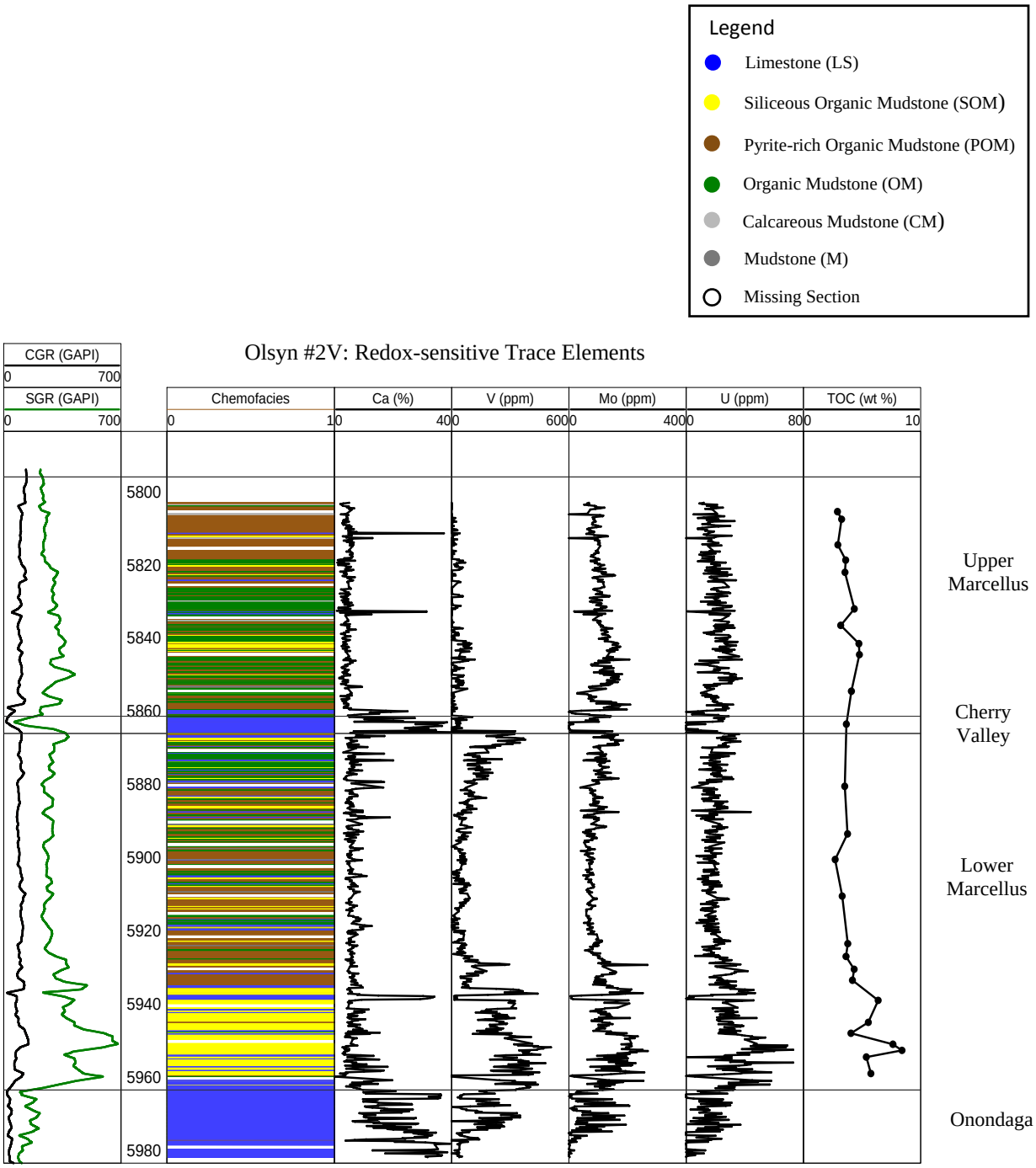

Figure 4.10: Redox-sensitive trace element chemostratigraphy for Olsyn #2V including corrected gamma ray (CGR), standard gamma ray (SGR), chemofacies, Ca, V, Mo, U, and TOC. Note high concentrations of V, Mo, and U at the base of the lower Marcellus. Standard gamma ray (SGR) in green and computed gamma ray (SGR minus uranium contribution) are plotted in first track. Both gamma ray curves are presented in gamma ray, American Petroleum Institute units (GAPI).

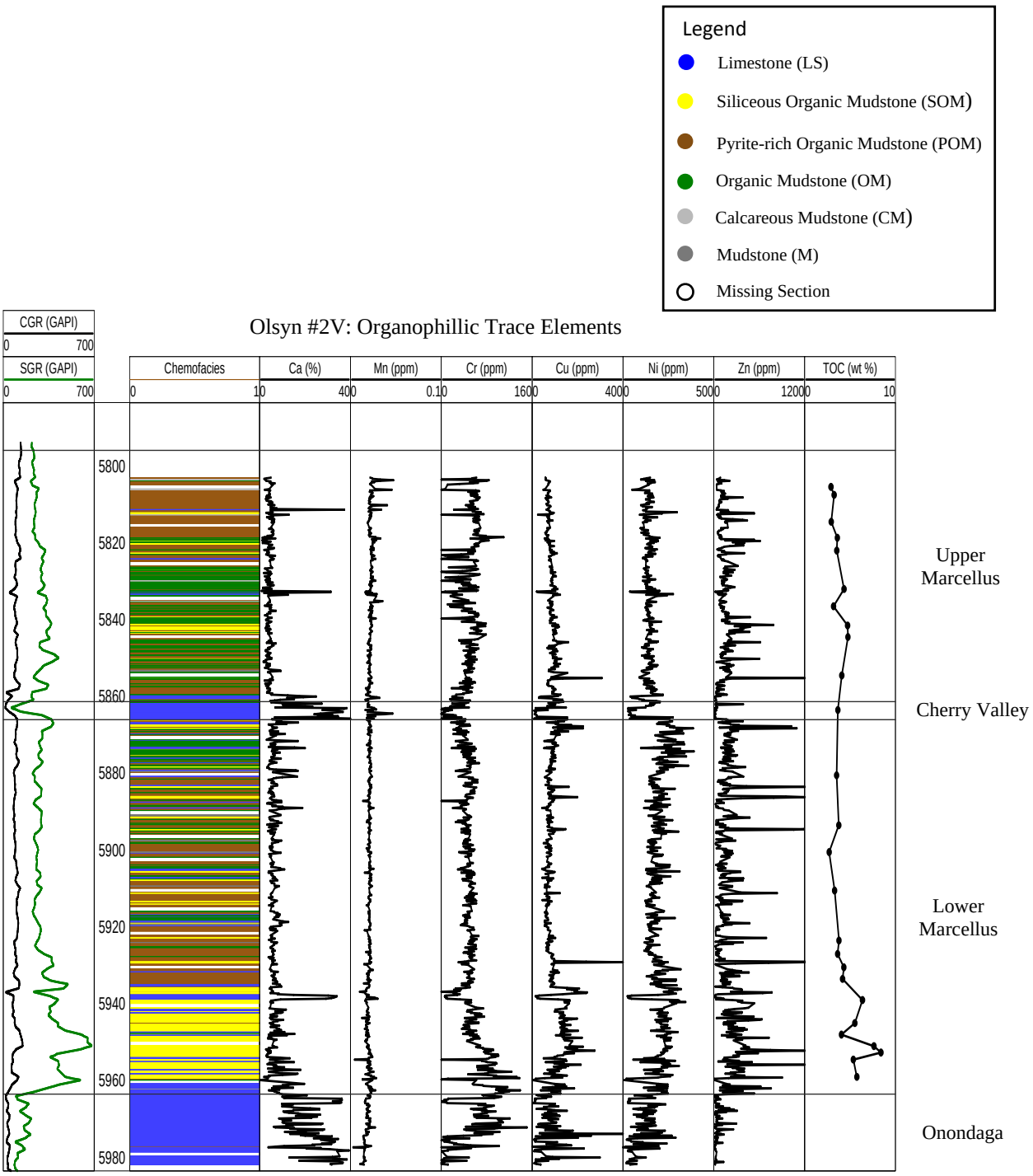

Figure 4.11: Organophillic trace element chemostratigraphy for Olsyn #2V (Cr, Cu, Ni, and Zn) with accompanying TOC data. Standard gamma ray (SGR) in green and computed gamma ray (SGR minus uranium contribution) are plotted in first track.

The Cherry Valley Limestone is 6 ft (2m) thick in the Olsyn # 2V well and has high Ca and Sr concentrations with low Al, K, Zr, and Si concentrations (Fig. 4.9). Redox-sensitive and organophillic elements are also low in the Cherry Valley (Figs. 4.10 and 4.11). Mn shows a high concentration in the lower section of the Cherry Valley (Fig. 4.11). The Cherry Valley Limestone falls into the limestone chemofacies (LS).

Major element, redox-sensitive and organophillic element geochemistry in the Upper Marcellus is similar to the upper section of the Lower Marcellus. High concentrations of Al, K, Zr, and Si can be identified throughout the Upper Marcellus (Fig. 4.9). The upper Marcellus also exhibits the same inverse relationship between Ca and Al, K, Zr, and Si. A unique occurrence is an extremely high concentration of barium from 5853 to 5821 ft (Fig. 4.12). The pyrite-rich organic mudstone (POM) and organic mudstone (OM) chemofacies make up most of the Upper Marcellus in this well.

4.6.2: Olsyn #2V Chemostratigraphic Interpretation

The high Ca and Sr concentrations (> 30% and > 600ppm) in the Onondaga represent times of high carbonate deposition and limited detrital input. Also enhanced Si values towards the top of the Onondaga and in the lowermost 27 ft (8 m) of the lower Marcellus most likely suggest biogenic silica production due to the very limited detrital input (Figs. 4.9 and 4.13). The siliceous organic mudstone (SOM) chemofacies has the highest concentration of U, V, and Mo and also correlates to the section with the highest amount of TOC of 8 wt. % (Fig. 4.10).

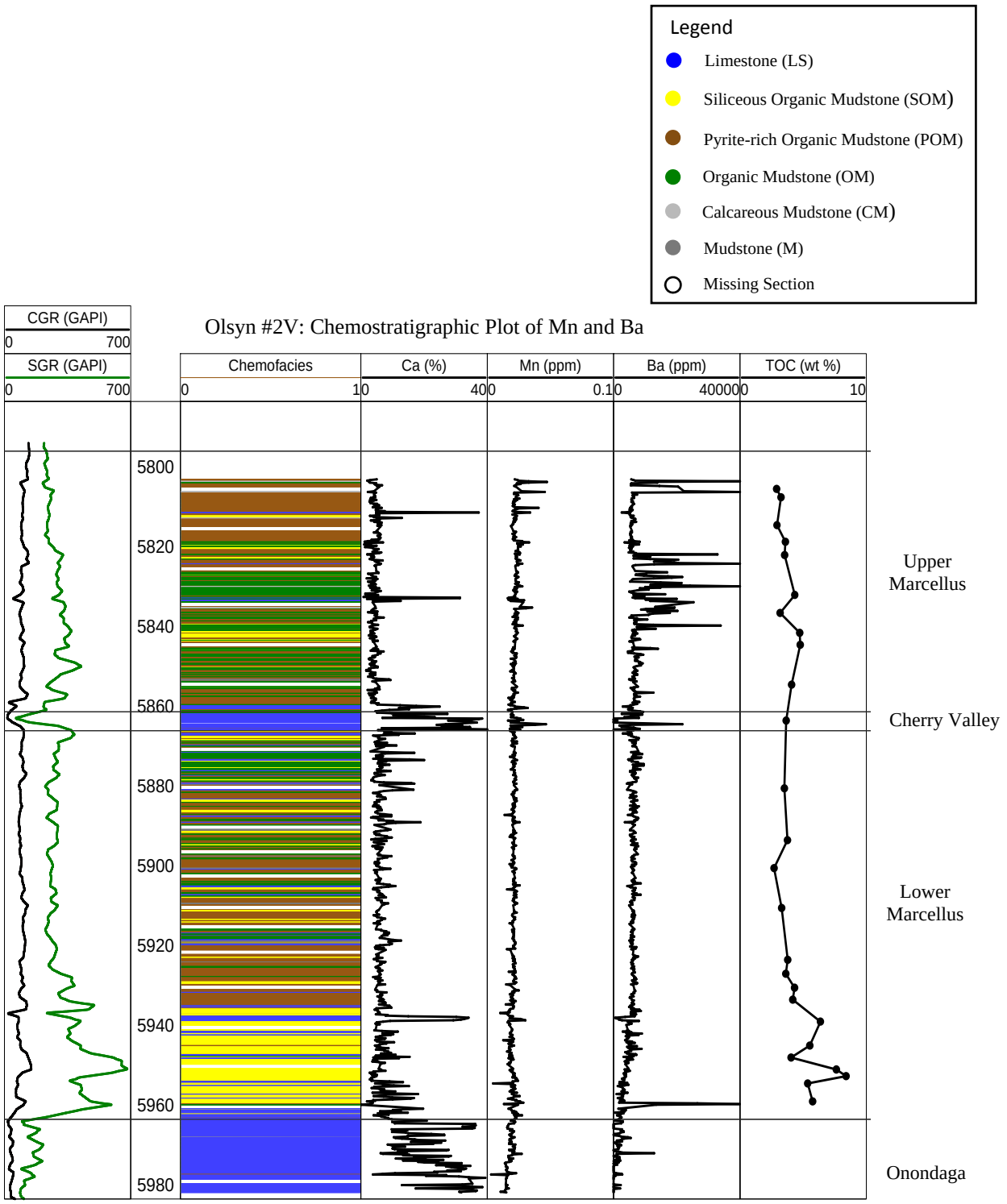

Figure 4.12: Chemostratigraphic plot for Olsyn #2V showing Mn and Ba concentrations in the Marcellus. Note extremely high concentrations of Ba in the upper Marcellus. Standard gamma ray (SGR) in green and computed gamma ray (SGR minus uranium contribution) are plotted in first track.

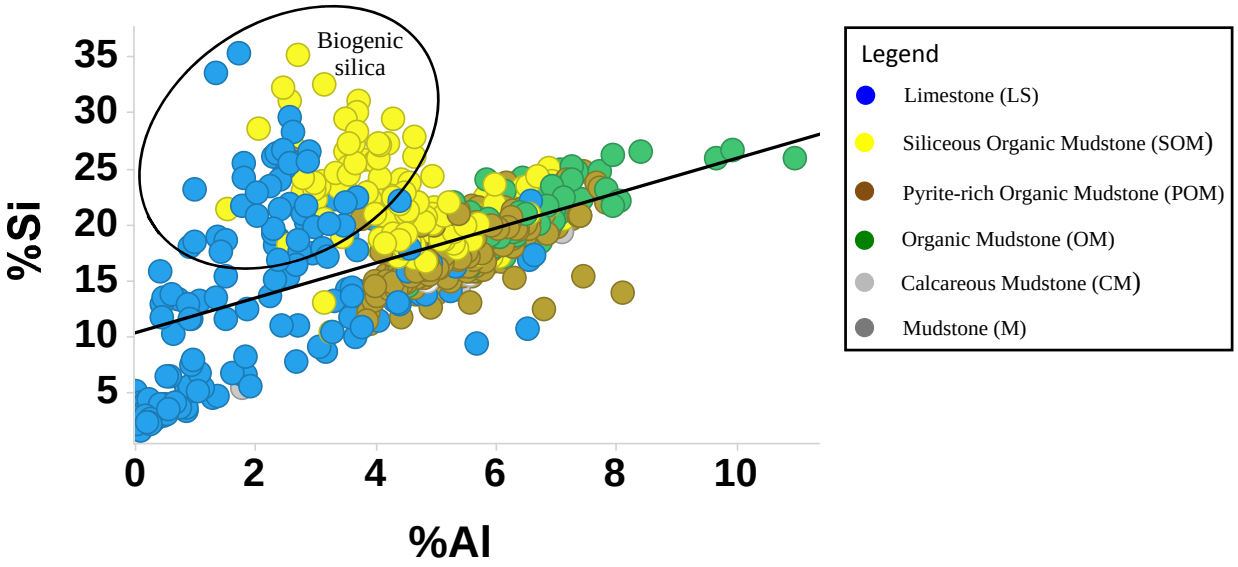

Figure 4.13: Geochemical cross plot of Si versus Al from Olsyn #2V showing an increase in Si to Al ratio in the Limestone (LS) and Siliceous Organic Mudstone (SOM) chemofacies samples, which most likely indicates that some of the Si component is not related to detrital input, but enriched by authigenic or biogenic processes.

Low concentrations of detrital elements can be observed in the basal section of the Lower Marcellus (5962-5945 ft) to much higher values in the upper section of the Lower Marcellus as well as in the Upper Marcellus. Increased detrital elements in these intervals correspond to dilution effects from clay and silt deposition most likely from the Acadian highlands in the southeast. This varying detrital input into the basin caused the inverse relationship observed between Ca and detrital indicators (Al, K, Zr, and Ti).

High values of Mo and U in the Lower Marcellus and Upper Marcellus as compared to the average concentration in the dataset likely indicates that anoxic conditions were present in the water column during the deposition of these intervals. The anoxic conditions probably facilitated the preservation of TOC greater than 4 wt. % as measured from Leco TOC analysis in these intervals (Fig. 4.10). The Onondaga Formation and Cherry Valley Limestone have much lower to null values of Mo, and U, which indicates deposition in oxic to suboxic conditions. Also, higher

concentrations of Cu, and Ni in the Lower Marcellus and Upper Marcellus as compared to the Onondaga Formation and Cherry Valley Limestone likely indicates higher organic productivity (Tribovillard et al., 2006) (Fig. 4.11).

4.6.3: SRC #1V Chemostratigraphy

SRC #1V major element chemostratigraphy has similar patterns to that of Olsyn #2V for most of the cored interval, which does not include the lowermost section of the lower Marcellus and the Onondaga. Just as in the Olsyn #2V, Ca in the SRC #1V is inversely proportional to detrital indicators such as Al, K, and Zr (Fig 4.14). Several cycles of high Ca concentrations (> 35 wt. %) can be observed across the Lower Marcellus, Cherry Valley, and the Upper Marcellus. Within the Cherry Valley, Ca and Sr concentrations are in the 20-35 wt. % and 300-500 ppm range, respectively. Al, K, Zr, and Si maintain fairly consistent concentrations throughout the cored interval with the exception of the high concentration Ca intervals. The high concentration Ca intervals have fairly low concentrations in detrital elements especially in the Lower Marcellus and Cherry Valley.

Redox-sensitive trace element geochemistry show that the detrital-rich sections are more enriched with respect to V, Mo, and U than the calcareous sections (Fig 4.15), which are generally depleted in redox-sensitive elements. The redox-sensitive trace element-rich sections correspond to the pyrite-rich organic mudstone (POM) and organic-rich mudstone (OM) chemofacies, whereas the calcareous-rich sections correspond to the limestone (LS) chemofacies. The highest concentrations of Mo and U (> 200 ppm and > 40 ppm, respectively) occurs between 5920 and 5945 ft. This interval also corresponds to the highest TOC values of 8-10 wt. %.

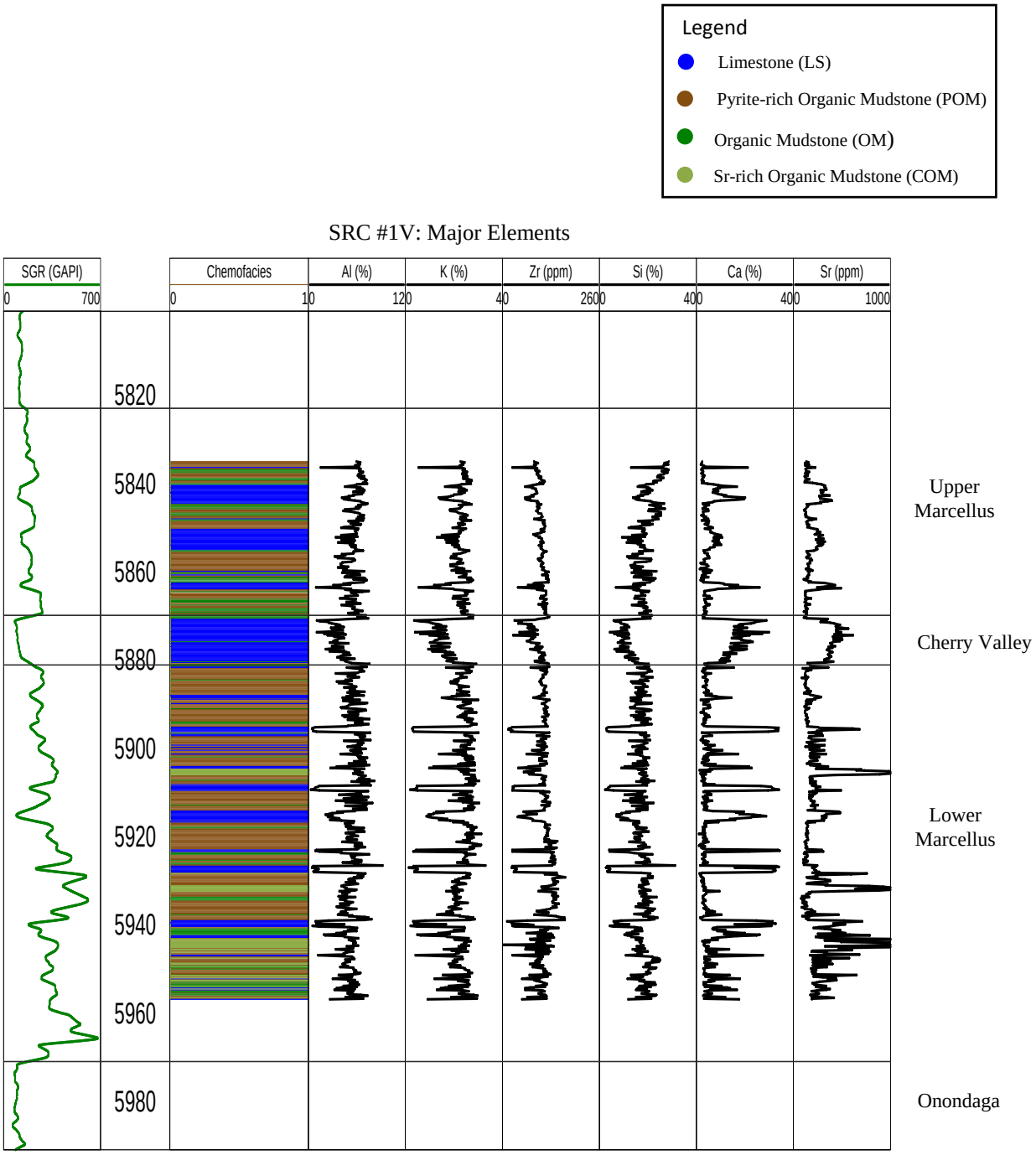

Figure 4.14: Major element chemostratigraphy for SRC #1V including standard gamma ray (SGR), chemofacies, Al, K, Zr, Si, Ca, and Sr. Note inverse trends between Ca, and Al, K, Zr, and Si.

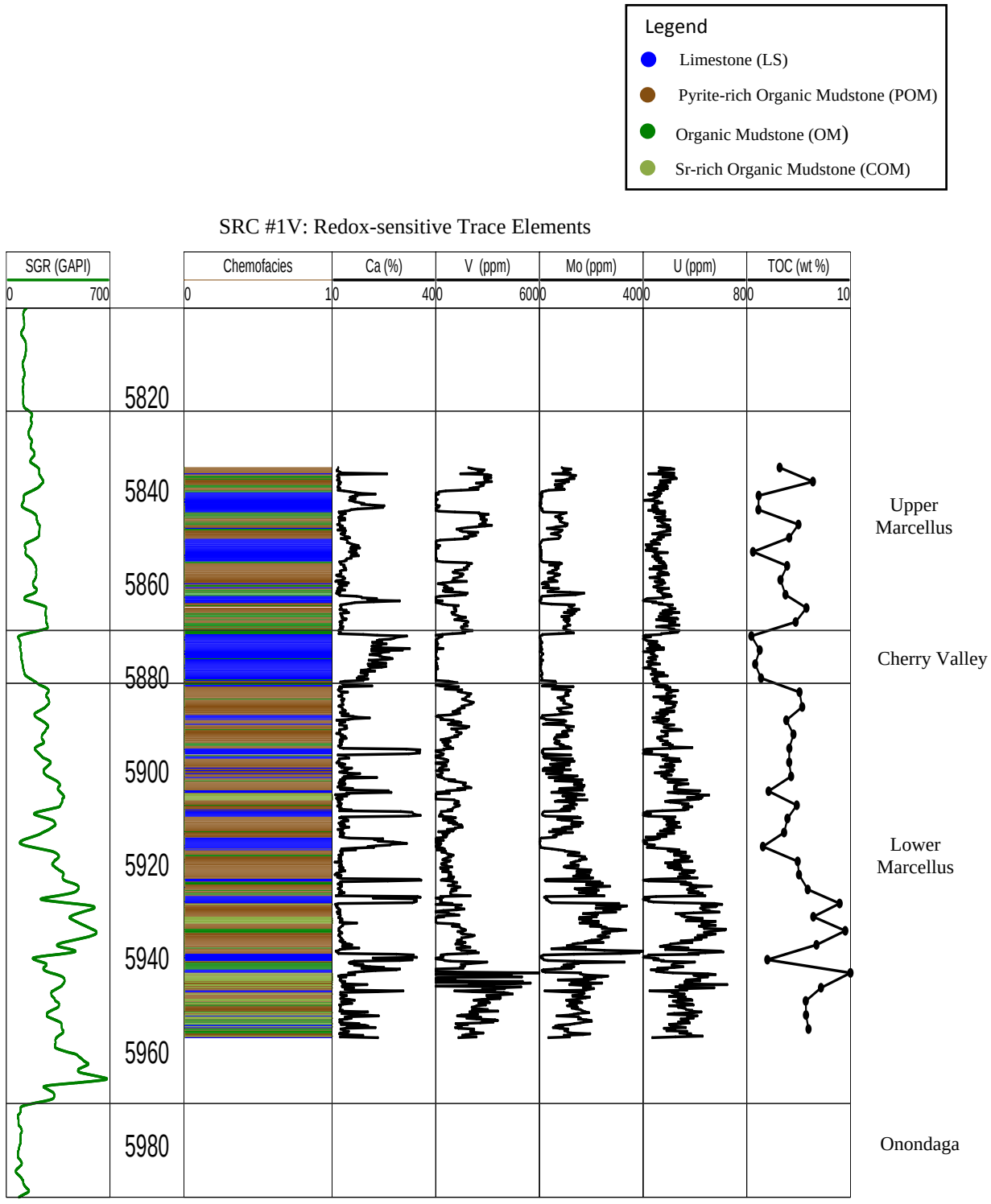

Figure 4.15: Redox-sensitive trace element chemostratigraphy for SRC #1V including standard gamma ray (SGR), chemofacies, Ca, V, Mo, U, and TOC. Note high concentrations of Mo, and U between 5920-5945 ft.

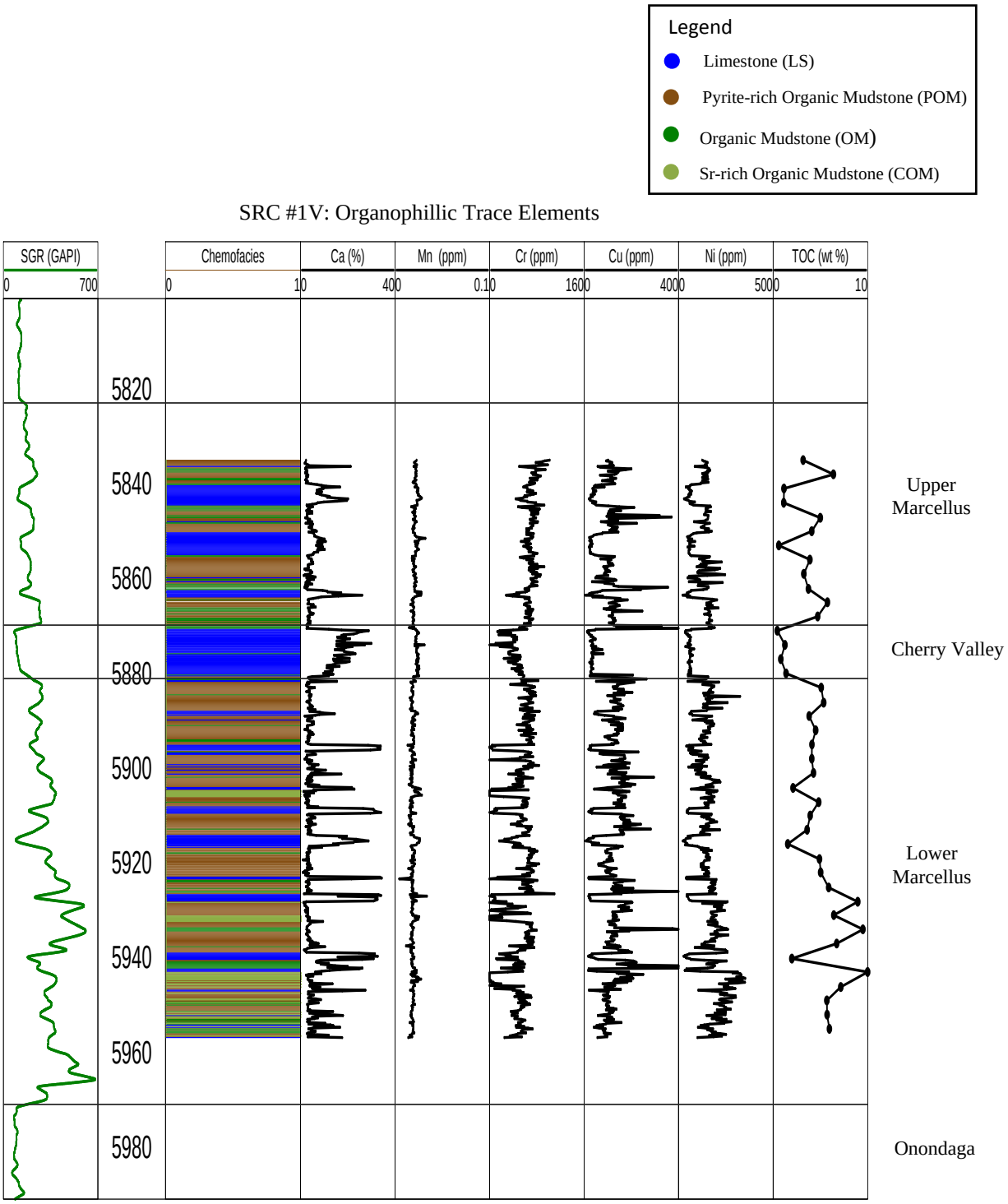

Figure 4.16: Organophillic trace element chemostratigraphy for SRC #1V (Cr, Cu, and Ni) with accompanying TOC data.

Organophillic trace elements are also higher in the detrital-rich sections and higher TOC intervals (Fig 4.16). Ni, Zn, and Cr show significantly lower values in the Ca-rich intervals in the Lower Marcellus, Cherry Valley, and Upper Marcellus.

4.6.4: SRC #1V Chemostratigraphic Interpretation

The Ca or carbonate-rich intervals occur more frequently and are thicker in the SRC #1V well than in the Olsyn #2V well. The frequent alternation between detrital-rich and carbonate-rich sediments could be due to the fact that the SRC #1V was closer to the basin edge and likely in shallower water. In this location sediment deposition may have been more strongly affected by sea level fluctuations.

Redox-sensitive and organophillic trace elements all suggest periodic episodes of anoxic to oxic bottom water conditions during deposition of the Marcellus. High concentrations of Cr, Cu, Ni, V, Mo, and U can be observed in the detrital-rich intervals, which likely suggest periods of anoxia with higher organic productivity. The highest concentrations of U and Mo occur in the detrital-rich sections of the Lower Marcellus interval, which corresponds with TOC values greater than 5 wt. %. Anoxic conditions most likely transitioned to oxic conditions during carbonate deposition, which can be related to sea level fall and mixing of surface and bottom waters.

4.7: Correlation of Chemostratigraphy to Storage Potential

The Marcellus Formation represents a good example of a formation in which porosity can be observed or is associated with organic material (Milliken et al., 2013). As mentioned previously, Mo, V and U show good correlations with total organic carbon (TOC), which is a measure of the amount of organic material present in the rock. This section will briefly discuss the relationship of

various elements and chemofacies with the storage potential/porosity in both the Olsyn #2V and SRC #1Vwells.

Total porosity was computed from neutron and density wireline logs. The neutron and density logs were initially corrected for mineralogical effects and calibrated to core porosity before being used for log porosity computation. The total porosity was then cross plotted against the various major and trace elements to identify any possible geochemical relationships of the elements to the storage potential of the rock.

Several detrital elements show slight covariance to total porosity in both the Olsyn #2V and SRC #1V wells (Figs. 4.17 and 4.18) with Ca being the most notable. Ca shows weak to moderate inverse relationship to total porosity in both wells (Figs. 4.17b and 4.18b). Ca values are the highest in the Limestone (LS) chemofacies, which makes up most of the Onondaga Formation and Cherry Valley Limestone. As mentioned previously, zones with high Ca concentrations most likely represent periods of increased carbonate sedimentation with low detrital input and bottom water oxygenation, which led to low organic matter preservation. Si shows slight positive correlation to total porosity in both the Olsyn #2V and SRC #1V wells (Figs. 4.17c and 4.18c).

Some redox-sensitive and organophillic trace elements also show positive relationships with total porosity with Mo and Ni being the most notable. Mo and Ni show a weak positive covariance to total porosity in both wells (Figs. 4.17d and 4.18e). Cross plots of TOC and total porosity also show that both rock properties have a weak positive covariance (Figs. 4.17f and 4.18f).

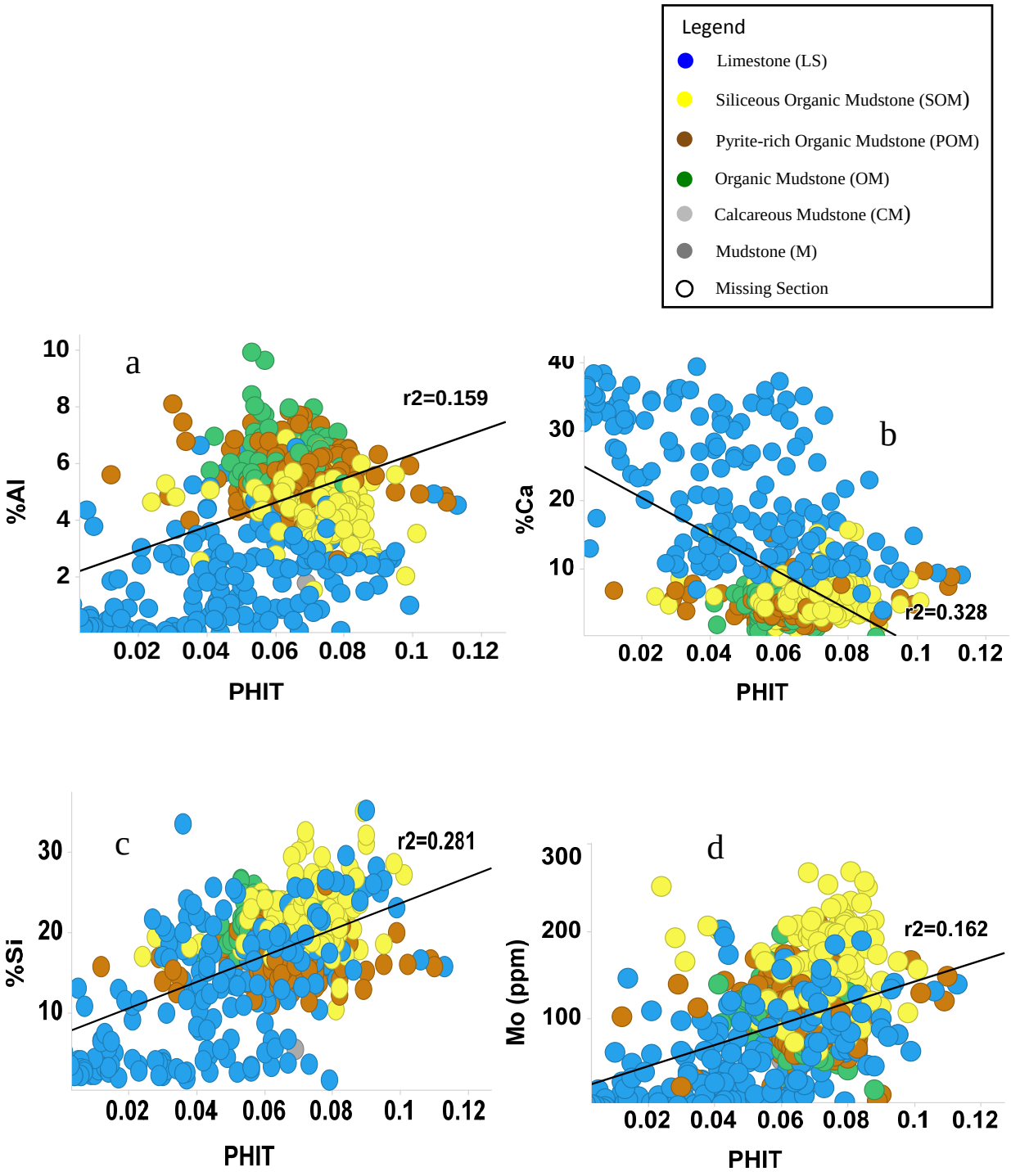

Figure 4.17: Cross plots of elemental data and total porosity (PHIT) for the Olsyn #2V well. a) Cross plot of Al versus total porosity showing a weak positive covariance (R^2 = 0.16); b) cross plot of Ca versus total porosity showing negative covariance; c) cross plot of Si against total porosity showing weak positive covariance; d) cross plot of Mo versus total porosity showing weak positive covariance.

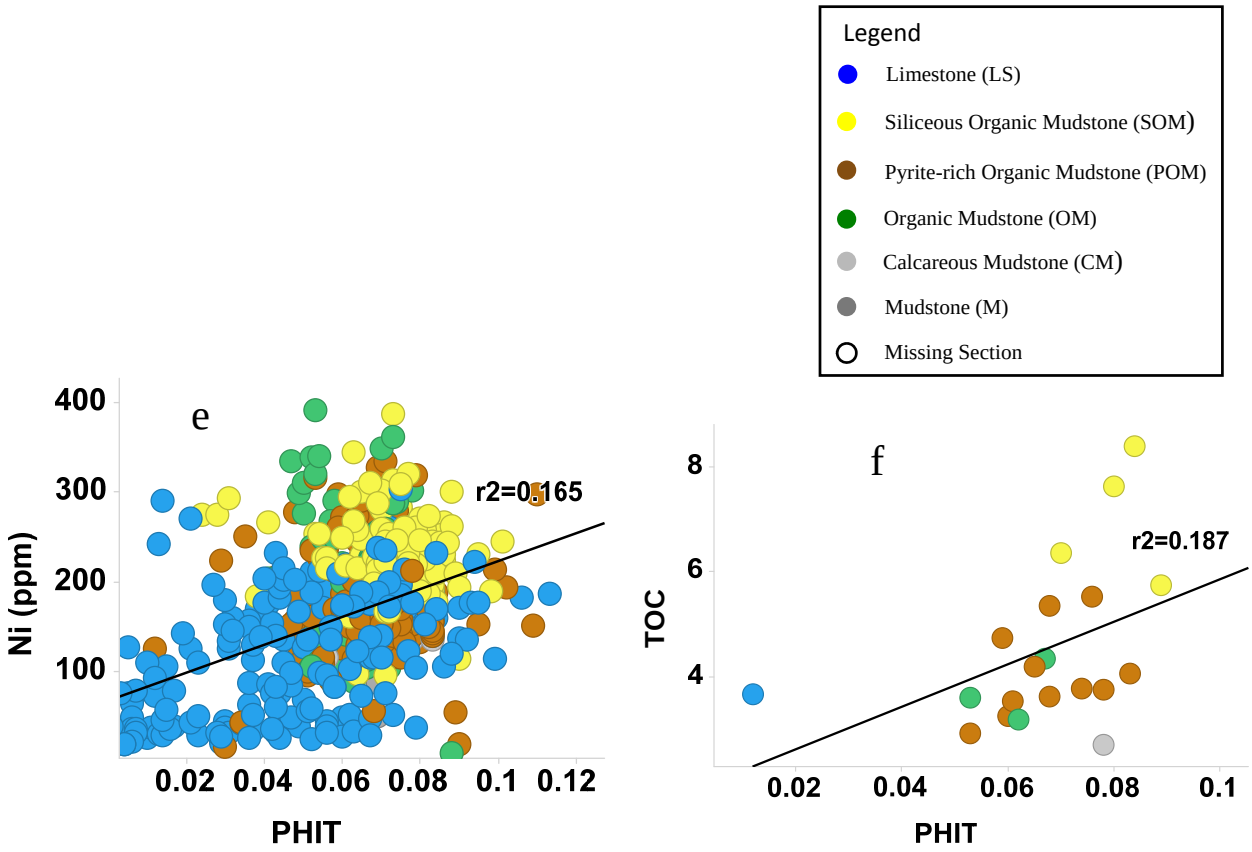

Figure 4.17: e) Cross plot of Ni versus total porosity showing weak positive covariance; f) cross plot of TOC against total porosity showing weak positive covariance (R^2 = 0.19).

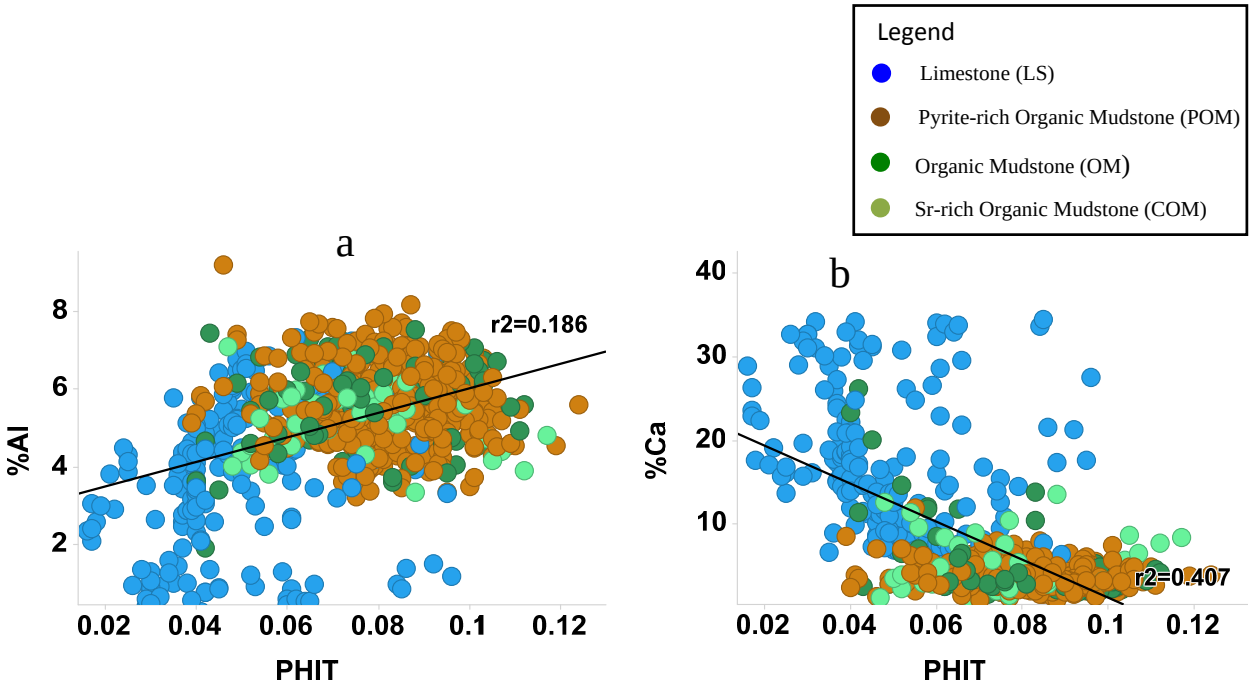

Figure 4.18: Cross plots of elemental data and total porosity (PHIT) for the SRC #1V well. a) Cross plot of Al versus total porosity showing a weak positive covariance (R^2 = 0.19); b) cross plot of Ca versus total porosity showing moderate negative covariance (R^2 = 0.41).

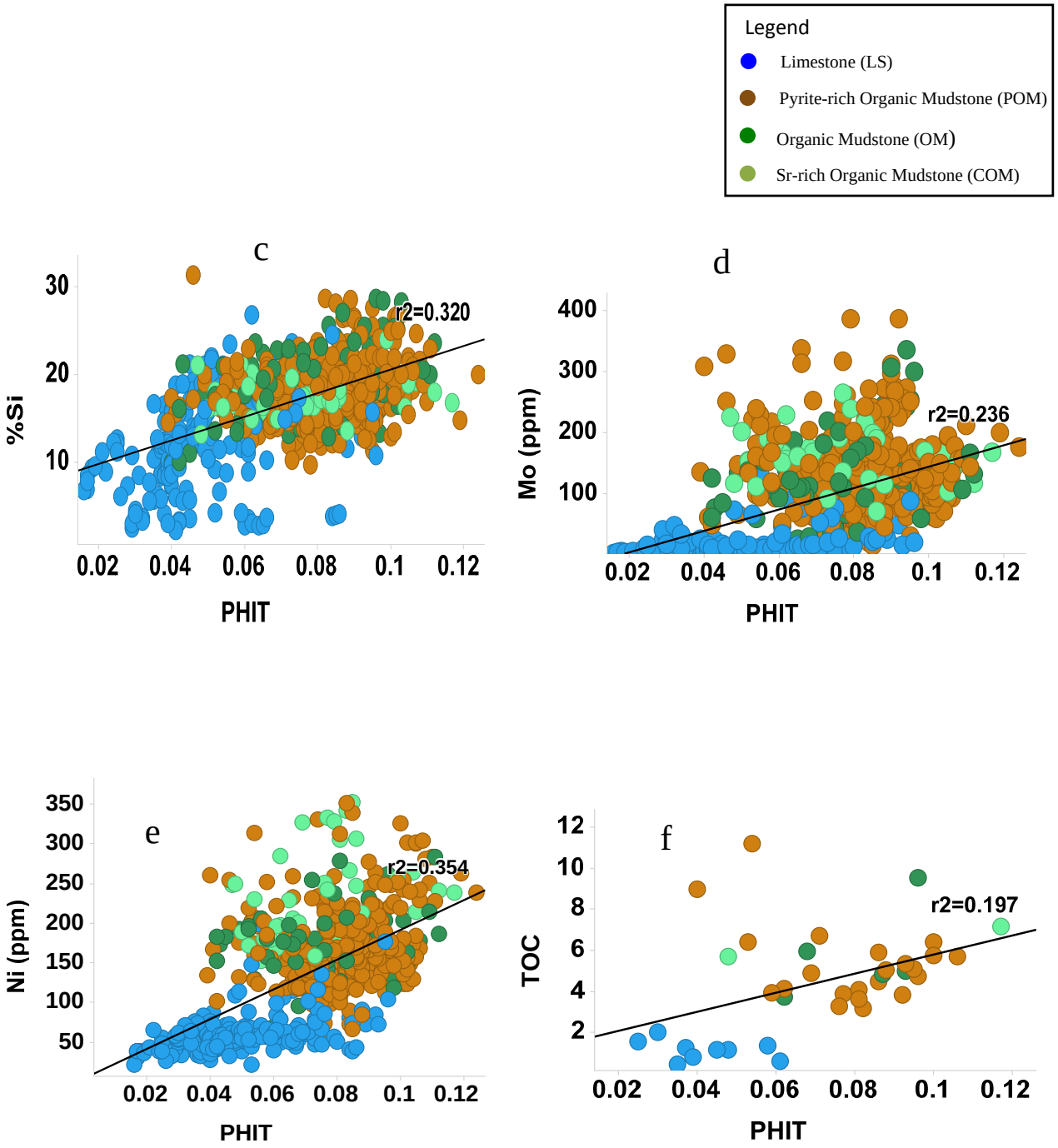

Figure 4.18: c) cross plot of Si against total porosity; d) cross plot of Mo versus total porosity; e) Cross plot of Ni versus total porosity showing weak positive covariance; f) cross plot of TOC against total porosity showing weak positive covariance ($R^2 = 0.20$).

4.8: Conclusions

1) Major element detrital indicators (Al, Zr, K, Si, and Ti) have an inverse relationship with Ca and Sr elements, which indicates that Ca and Sr elements are most likely biogenic or authigenic in origin. Si concentrations are elevated with respect to the detrital elements at the base of the Lower Marcellus in the Olsyn #2V well, which suggest that the Si at that interval might also be of biogenic or authigenic origin (Fig. 4.13).

2) Redox-sensitive and organophillic trace elements (Mo, U, V, Cr, Ni, Cu, and Zn) all show higher values throughout the Lower and Upper Marcellus as compared to the Onondaga and Cherry Valley that suggest that anoxic conditions most likely persisted during the deposition of these intervals. No evidence of euxinia during the deposition of these interval was identified.

3) The 27 ft (8m) interval at the base of the lower Marcellus observed in the Olsyn core with the highest Si, Mo, V, U, and gamma ray values is likely a regionally extensive anoxic unit with limited detrital input and high silica content. This unit corresponds to the siliceous organic mudstone (SOM) chemofacies and has the highest values of TOC and porosity (Figs. 4.17f).

4) Variations in major/trace element concentrations and chemofacies in both wells indicate vertical and likely lateral heterogeneity in the Marcellus Shale (Figs. 4.9, 4.10, 4.14 and 4.15).

CHAPTER 5

MECHANICAL STRATIGRAPHY AND GEOMECHANICS

The evaluation of the mechanical properties of a rock using a hand-held equotip hardness index tester (bambino) on a high resolution scale can provide valuable insights into the vertical and lateral variations in rock strength not easily identified from logs or basic core analysis (Zahm and Enderlin, 2010). Notably, the high resolution hand-held equotip hardness testing makes it possible to identify and characterize the mechanical properties of thinly-bedded layers interspersed within thicker bedded layers. Characterizing these thin or highly variable layers is difficult using traditional core or log analysis methods. Geomechanical properties are important in unconventional exploration and development because the effectiveness or failure of a hydraulic fracture stimulation operation can significantly depend on the mechanical properties of a rock, pore pressure and in situ stress (Daniels et al., 2012). The combination of high resolution mechanical stratigraphy from the hand-held strength tester with core description and log-based analysis using dipole sonic logs can provide a comprehensive view for understanding variations in mechanical properties of the Marcellus Formation. This chapter will introduce the concept of mechanical stratigraphy, elastic mechanical properties, and empirical relationships for unconfined compressive strength (UCS) determination from Leeb hardness values.

5.1: Mechanical Stratigraphic Analysis and Interpretation

Hand-held rock strength testing (Bambino) was performed at the same sample interval of two inches (5 cm) as the XRF analysis on the Olsyn # 2V and SRC #1V cores. The Bambino is a digital, battery-operated micro rebound hammer that provides an indirect method to predict rock strength. The unit of measurement of the Bambino is in Leeb hardness unit (L). The strength of a rock is defined by its stress/strain relationships, and is an important property, which can have an

effect on drilling, completion and production processes such as wellbore stability, hydraulic fracture effectiveness, sand production, and changes in porosity and permeability due to compaction during hydrocarbon production (Zoback et al., 2006). A clustering based approach was used in the Olsyn #2V and SRC #1V wells to create a mechanical stratigraphic profile by grouping intervals with similar hardness values into distinct units or facies. Three general mechanical facies are identified from the cluster analysis: weak, medium, and strong. The weak mechanical facies has a Leeb hardness value range of 150-300, medium facies has a value range of 301-500, and the strong facies has a Leeb hardness value range of 501-750. The following section will describe the different mechanical facies obtained from both Olsyn #2V and SRC #1V cores.

5.1.1: Olsyn #2V Mechanical Stratigraphy

The hand-held rock strength values from the Olsyn core are the highest in the Onondaga and Cherry Valley (Fig 5.1). These intervals correspond to the strong mechanical facies and typically have a Leeb hardness value of > 600. The basal section of the Lower Marcellus is also characterized by high to medium strength rock. A couple of weak strength intervals can be identified in the basal section of the lower Marcellus. Core descriptions interpret these weak layers as bentonites. These intervals are not readily identified from XRF analysis but are easily picked out from the strength testing and mechanical facies analysis.

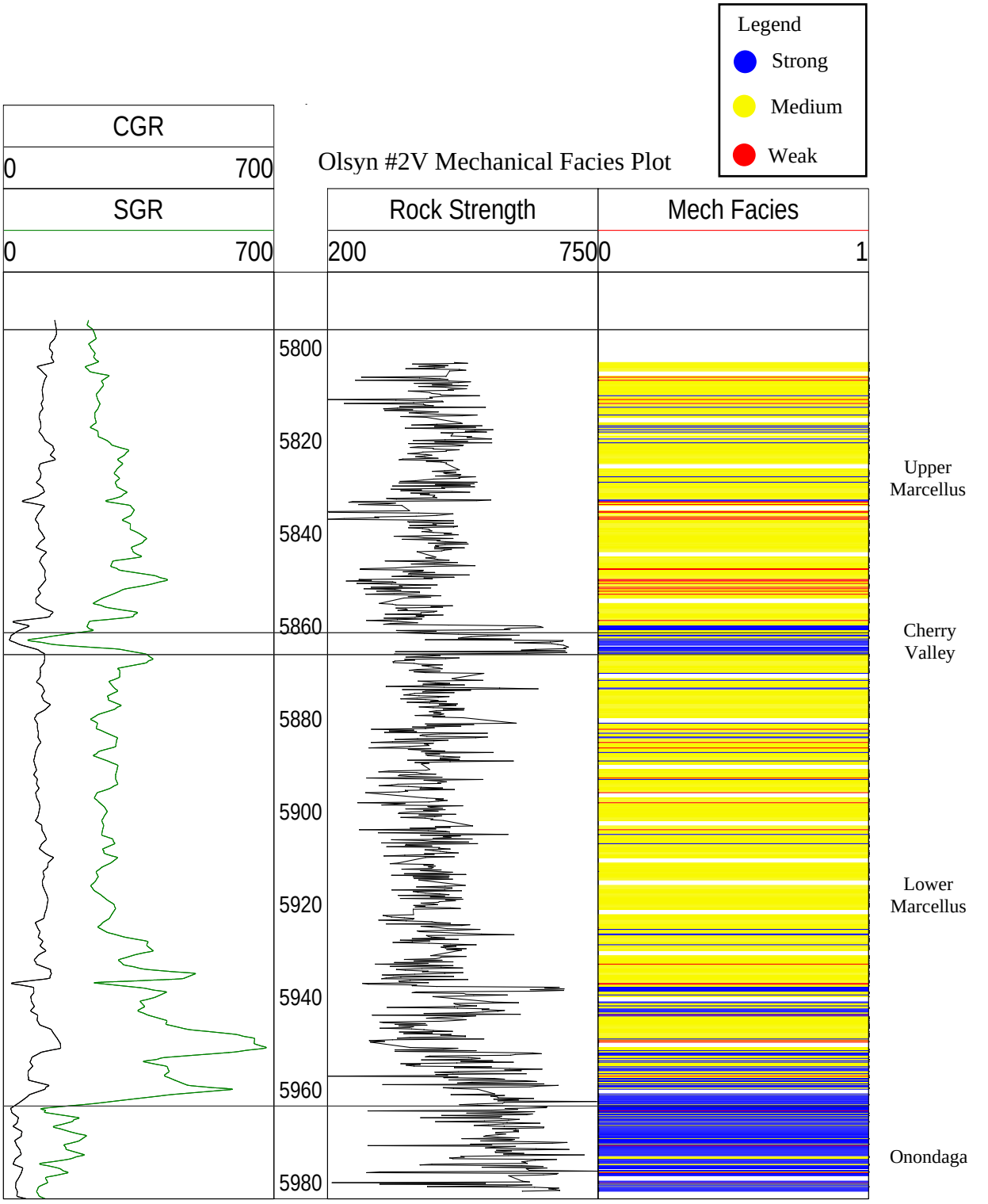

Figure 5.1: Mechanical stratigraphic profile of the Olsyn #2V core showing the three mechanical facies. Hand-held rock strength (Bambino) in Leeb hardness values is plotted in track 2. Standard gamma ray (SGR) in green and computed gamma ray (SGR minus uranium contribution) are plotted in first track.

The middle to upper section of the Lower Marcellus is characterized by mostly medium strength rock. The base of the Upper Marcellus Formation is characterized by medium strength rock and grades into weak rocks at approximately 5850 ft, which corresponds to a spike in the gamma ray log. The Upper Marcellus is characterized by a higher percentage of medium strength rock just as the Lower Marcellus. A 2-ft-thick (0.6 m) interval of high strength rock occurs at 5820 ft with interlayered medium strength rock. The top of the cored section is comprised of weak and medium strength rock intervals.

The high rock strength in the Onondaga, Cherry Valley, basal section of the Lower Marcellus is most likely due to the low clay concentrations in these formations as interpreted from the XRF clay proxies. The depth at 5850 ft in the Upper Marcellus with the high gamma ray value is interpreted to be a flooding surface and from XRF analysis is characterized by a significant increase in clay proxies, which is most likely responsible for the lower rock strength.

5.1.2: SRC #1V Mechanical Stratigraphy

The SRC #1V core is characterized by a higher variation in rock strength than the Olsyn #2V core. As mentioned in the previous chapter, the Onondaga Formation and the basal section of the Lower Marcellus are not present in this well. The cored section of the Lower Marcellus is characterized by medium strength rock with several layers of weak and strong rock (Fig 5.2). Unlike the Olsyn core, the Cherry Valley Formation in the SRC core is characterized by medium to weak mechanical facies with a few strong mechanical layers.

The basal 10 ft (3m) of the Upper Marcellus is characterized by weak strength rocks and is capped by an approximately 2 ft (0.6m) interval of strong rock. The remaining section of the Upper Marcellus is characterized by medium strength rock with interlayered weak rocks.

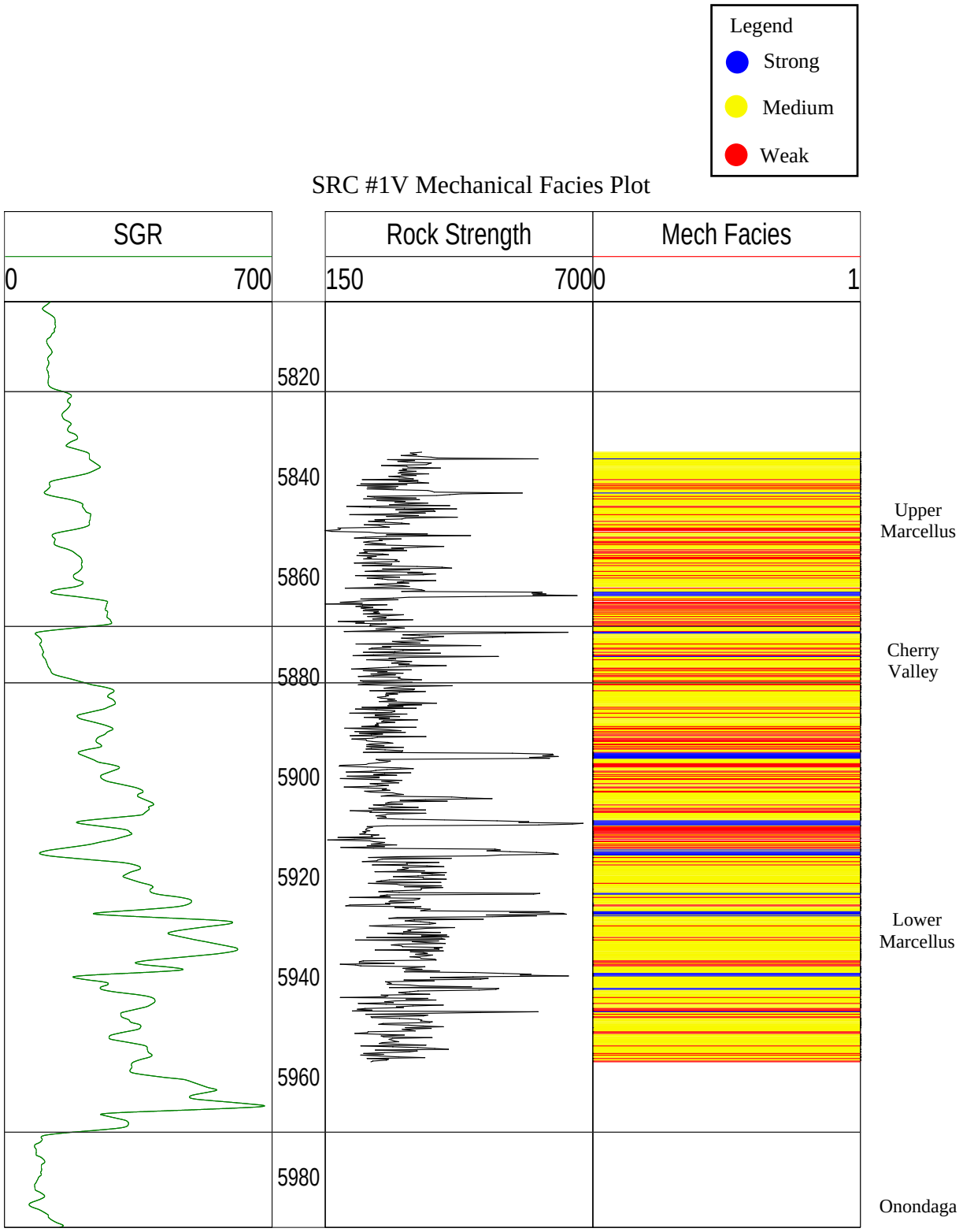

Figure 5.2: Mechanical stratigraphic profile of the SRC #1V core showing the three mechanical facies (strong, medium, and weak). Hand-held rock strength (bambino) in Leeb hardness values is plotted in track 2. Standard gamma ray log is plotted in track 1.

The strong mechanical facies identified across the Lower Marcellus in the SRC core correspond to high Ca concentrations and cleaner gamma ray intervals and have Leeb hardness values that are > 600. An explanation for the lower rock strength in the SRC core as compared to the Olsyn core is most likely due to the higher clay content as observed in the XRF proxies and XRD data, and the possibility of the rock being micro-fractured from bedding plane slippage due to the highly inter-bedded nature of the rock (Aydin, 2012).

5.2: Correlations between Mechanical Stratigraphy and Elastic Moduli

Elastic behavior of a rock refers to the ability of a rock to recover its original shape and volume after an applied stress is removed (Fossen, 2010). Stress and strain are two important terms that govern the elastic behavior of rocks. Stress is defined as force per unit area and strain is the amount of deformation an object experiences due to an applied stress. Stress has a unit of pressure and strain is dimensionless. Young's modulus, Bulk modulus, Shear modulus, and Poisson's ratio are the elastic properties that dictate how a rock will behave and respond to stress. The focus of this study will be on Young's modulus and Poisson's ratio because those are the elastic properties that can be used to determine the rigidity/strength and possibly infer brittleness of a rock (Perez and Marfurt, 2013). They are also important geomechanical properties that influence reservoir quality and the effectiveness of a hydraulic fracture stimulation operation.

Young's modulus (YM) is a measure of the stiffness of a solid elastic material. It is the ratio of stress to strain and its unit of measurement is usually given in megapascals (MPa). It describes how a material will lengthen or shorten when a tensile or compressive stress is applied. If a large applied stress only produces a small extension or strain, then the material is stiff and the YM is a large value. Therefore, a material with a high YM will resist deformation and eventually break when its strength is exceeded, whereas a material with low YM will more easily deform, but

will bounce back after deformation. Brittle materials typically have higher YM than ductile materials (Perez and Marfurt, 2013).

Poisson's ratio (PR) is the ratio of the relative transverse strain to the relative axial strain and is unitless. In other words, when a material is compressed in one direction, it measures the ability of that material to expand in a direction perpendicular to the direction of compression. Most materials have a Possion's ratio value of between 0 and 0.5 (Zoback, 2007). Poisson's ratio has implications on the reservoir and completions quality of a rock because a rock with low PR will be able to withstand significant applied stress without serious deformation in the transverse direction. While a rock with high PR will show significant horizontal or lateral expansion when compressed.

The brittleness of a rock refers to the ability of a rock to break without significant plastic deformation when its strength is exceeded. In contrast, a ductile rock is a rock that will plastically deform before breaking when its strength is exceeded. In this study, brittleness (BRIT) is defined as Young's modulus divided by Poisson's ratio and is a good indicator of the tendency of a rock to fracture under hydraulic stimulation (Perez and Marfurt, 2013). Based on this, a high Young's modulus value and a low Poisson's ratio generally indicates that a rock is brittle in nature and will break or shatter with minimal plastic deformation when hydraulically stimulated.

Young's modulus and Poisson's ratio are calculated for the Olsyn #2V well using the compressional/shear sonic and bulk density logs provided in the log suites. Brittleness is then calculated from the YM and PR log for the well. Because of the poor quality of the shear sonic log obtained from the SRC #1V well, only the Olsyn #2V well is discussed below.

Leeb Hardness values (HLD) are plotted against Poisson's ratio, Young's modulus, and brittleness to investigate if the HLD values can be used to predict these elastic moduli and the brittleness of the rock. The HLD values do not show any relationship with Poisson's ratio, but show weak positive relationship with both Young's modulus and brittleness (Fig. 5.3). The low correlation between HLD and the elastic moduli computed from wireline logs could be due to the differences in vertical resolution of both measurements. The volume of rock characterized by the equotip hardness tester is much smaller than the wireline log measurement.

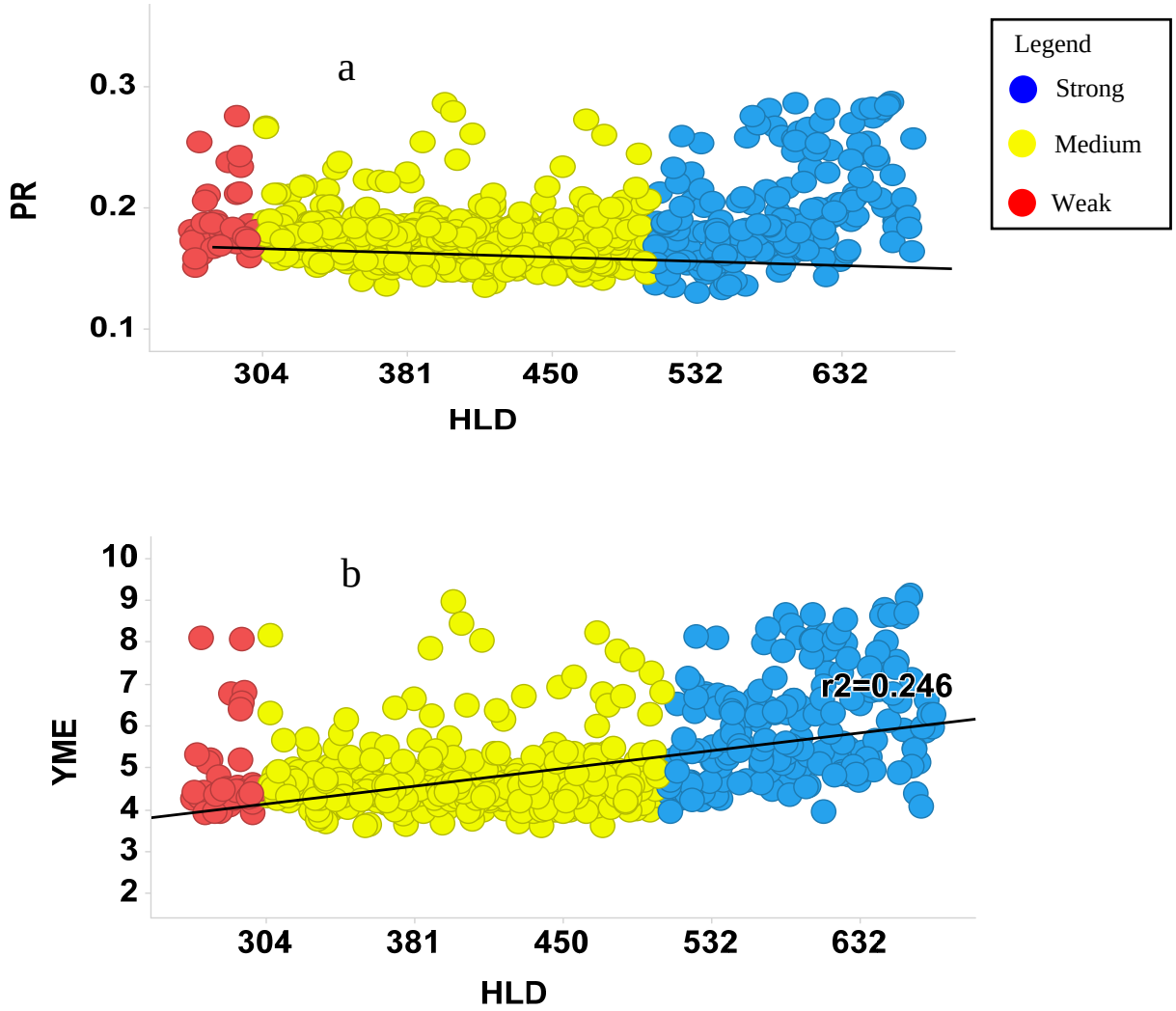

Figure 5.3: Cross plots of elastic parameter versus Leeb Hardness value for the Olsyn #2V well. a) Cross plot of Poisson's Ratio versus HLD shows no relationship, b) Cross plot of Young's Modulus in MPa against HLD shows a weak positive relationship (R^2 = 0.246).

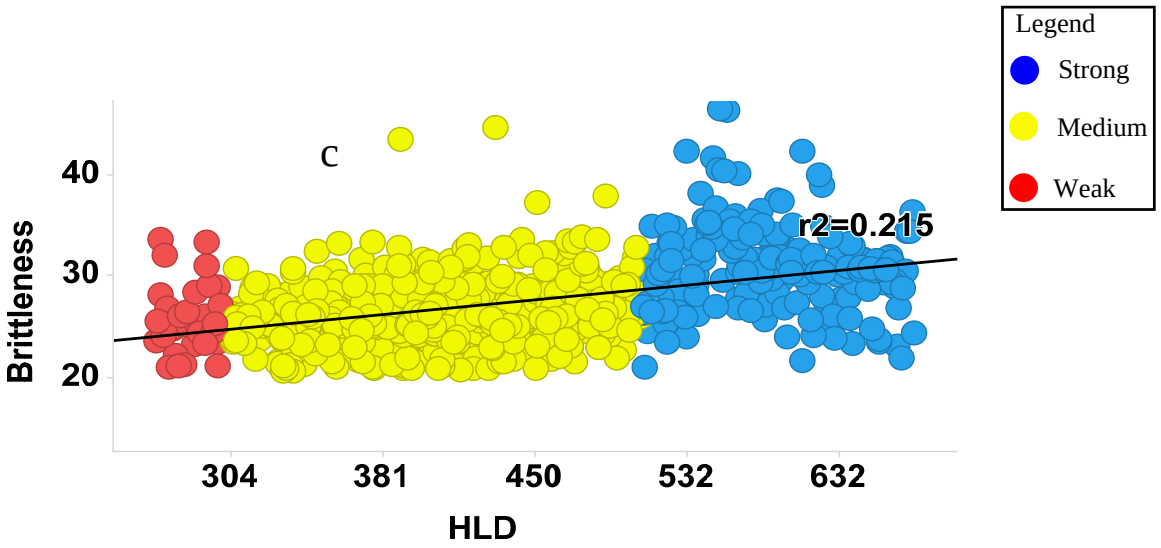

Figure 5.3: c) Cross plot of Brittleness versus HLD shows a weak positive relationship.

Zahm and Sonnenfeld (in review) in their work on the Niobrara Formation showed that they can improve the correlations between elastic moduli and HLD values by smoothing the HLD values to match wireline log resolution. Therefore, the HLD values from the Olsyn core were smoothed using a 10-point running average to match wireline log resolution and this improves the relationship between the HLD values and YME/BRIT (Fig. 5.4). This relationship indicates that rocks with high HLD values will have higher YM values and also higher brittleness than rocks with low HLD values. Thus, the medium to strong mechanical facies should be more brittle and will most likely respond to fracture stimulation more efficiently than the weak mechanical facies. The Onondaga, basal section of the Lower Marcellus and the Cherry Valley have higher HLD, calculated YM, and brittleness values than the upper section of the Lower Marcellus and the Upper Marcellus (Fig 5.5). Therefore, these brittle intervals are expected to respond more positively to hydraulic stimulation/fracturing than the other Marcellus intervals.

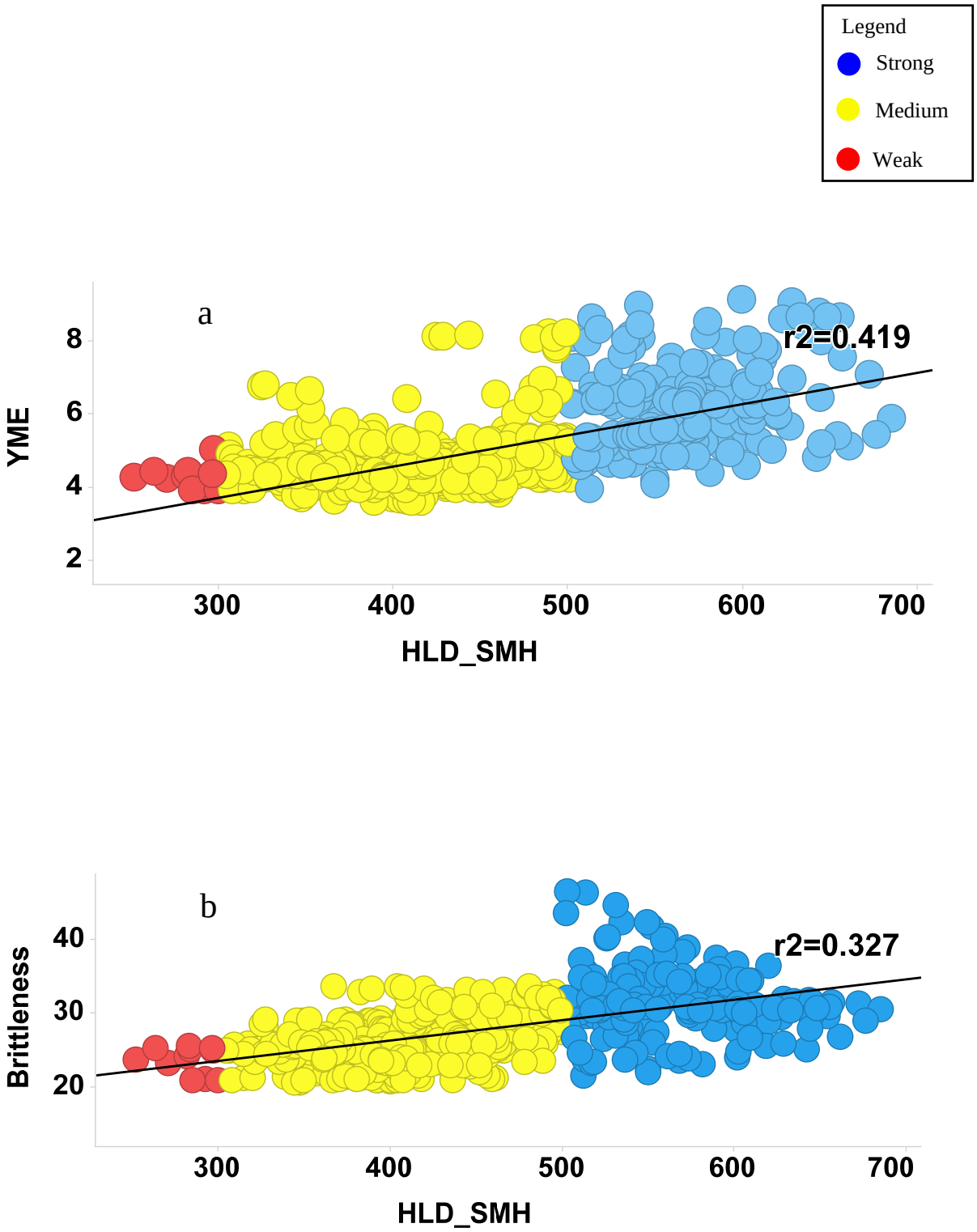

Figure 5.4: a) Cross plot of YME in MPa versus smoothed HLD showing a higher positive relationship (R^2 = 0.42), b) Cross plot of Brittleness against smoothed HLD showing a slightly higher positive relationship (R^2 = 0.33).

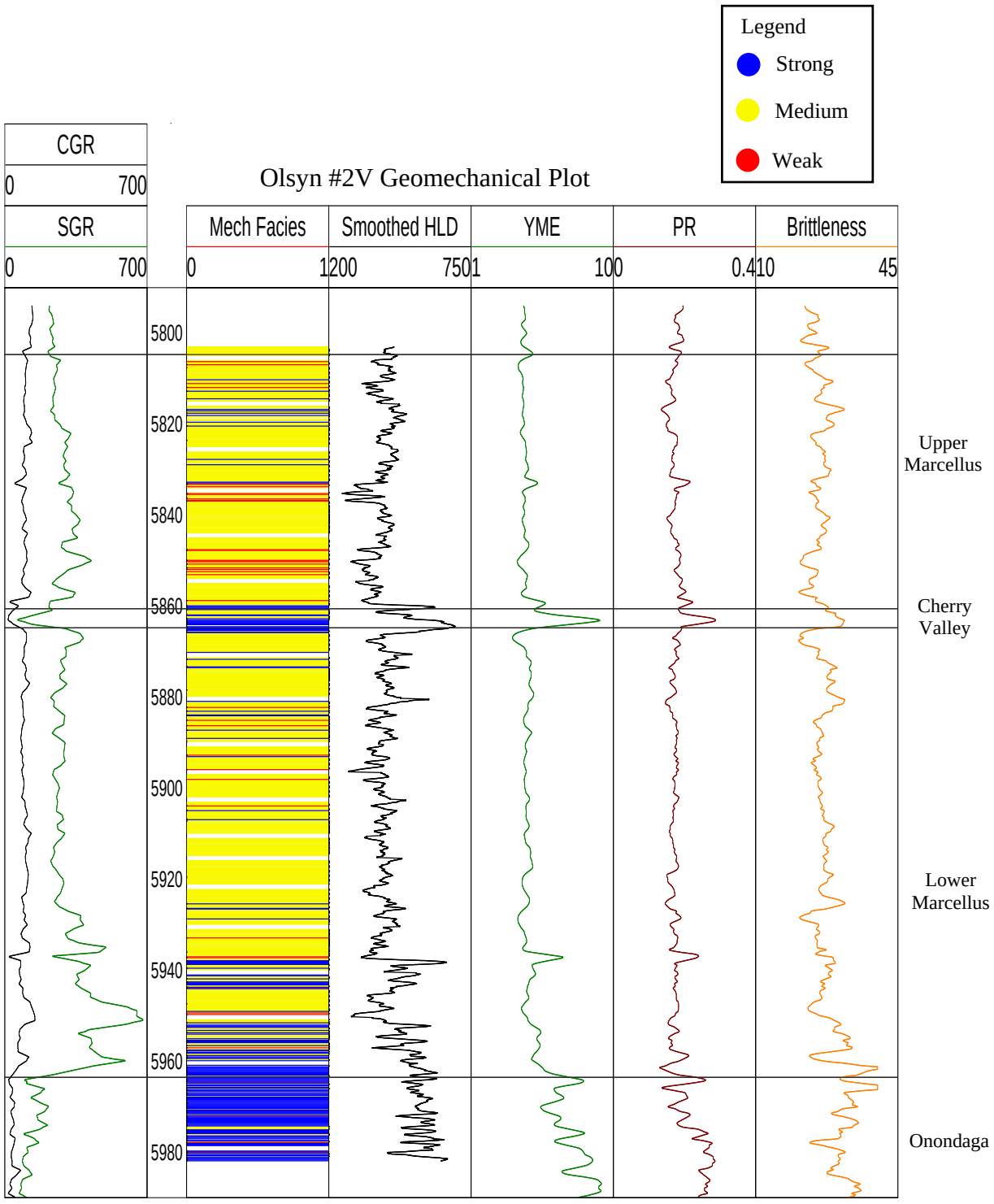

Figure 5.5: Mechanical stratigraphic profile, elastic moduli, and brittleness of the Marcellus in Olsyn #2V well. Gamma Ray, mechanical facies, smoothed Leeb hardness values, Young's Modulus, Poisson's Ratio, and Brittleness are shown.

5.3: Unconfined Compressive Strength (UCS) Determination

The unconfined compressive strength (UCS) of a rock is a crucial parameter that is required to address several geomechanical issues such as wellbore stability during drilling, production induced compaction, sand production, and stress magnitude estimation using observations of wellbore failure (Zoback et al., 2006). UCS is usually determined in the laboratory through triaxial tests on core plugs. Several authors have shown that the Leeb hardness values (L-values) can be used to estimate UCS (Aoki and Matsukura, 2008). However, no triaxial testing has been performed on either of cores in this study to obtain reliable UCS measurements to correlate to the Leeb hardness values.

The HLD measurements from the Olsyn #2V core are converted to UCS values using empirical relationships developed by Zahm and Sonnenfeld (in review) and Enderlin (pers. comm., 2016). Zahm and Sonnenfeld (in review) correlated UCS measurements from triaxial test to HLD values from Niobrara cores and developed the following empirical equation below:

$$UCS\ (psi) = (0.000000683 * HLD^{2.9}) * 145$$

Enderlin (pers. comm., 2016) correlated UCS measurements from triaxial test to HLD values from Barnett cores and developed the following empirical equation:

$$UCS\ (psi) = 0.0000000746 * (0.99725158^{HLD}) * (HLD^{4.2961784})$$

Both equations are utilized on the Olsyn #2V and SRC #1V HLD dataset to estimate UCS in the absence of triaxial measurements. Both equations show similar results for UCS for these wells (Fig 5.6 & Fig 5.7). The calculated UCS values for the Olsyn #2V well are higher than the SRC #1V UCS values.

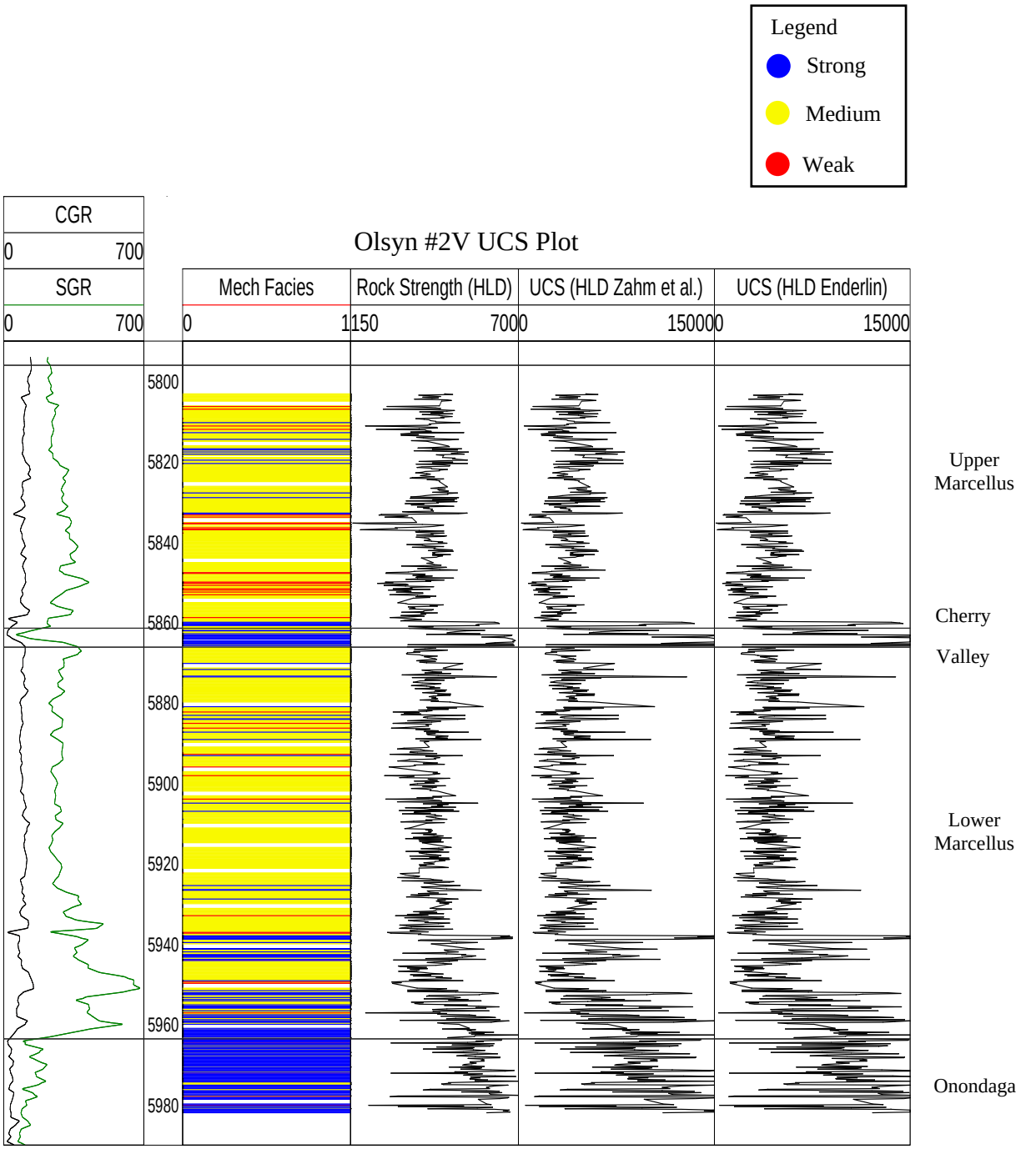

Figure 5.6: Mechanical stratigraphic profile, HLD and UCS of the Marcellus in Olsyn #2V well. Gamma ray, mechanical facies, Leeb hardness values, UCS using the Zahm & Sonnenfeld (in review) equation and UCS using the Enderlin (Pers. Comm., 2016) equation are shown.

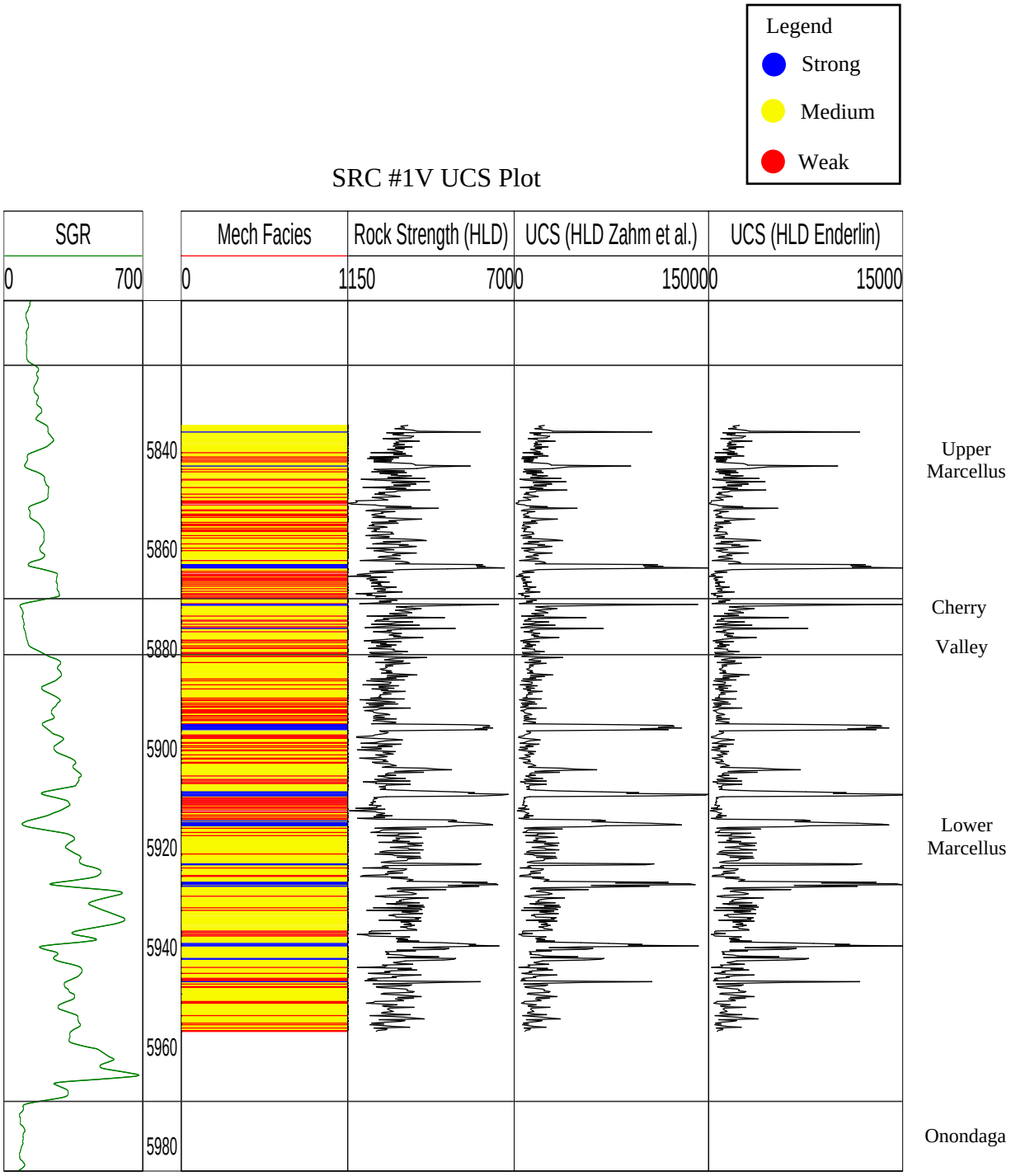

Figure 5.7: Mechanical stratigraphic profile, HLD and UCS of the Marcellus in SRC #1V well. Gamma ray, mechanical facies, Leeb hardness values, UCS using the Zahm & Sonnenfeld (in review) equation and UCS using the Enderlin (Pers. Comm., 2016) equation are shown.

The Onondaga, Cherry Valley and lowermost section of the Lower Marcellus have much higher calculated UCS values than the other intervals in the Olsyn #2V well (Fig 5.6). The UCS values for upper section of the Lower Marcellus and the Upper Marcellus are lower than the Onondaga, basal section of the Lower Marcellus and Cherry Valley and show slight variability throughout those intervals. In contrast, the UCS values for the SRC #1V are more variable across the Lower and Upper Marcellus (Fig 5.7).

CHAPTER 6

DISCUSSION AND SUMMARY

The fine-grained nature of the Marcellus Shale necessitates the use of core description, petrographic, XRF, and Bambino analyses for identification of mineralogy, elemental proportions, and rock strength. This chapter will link the lithological, geochemical, and mechanical characteristics of the Marcellus Shale with available petrophysical logs to provide a framework in which this information can be applied to the rest of the Appalachian Basin. Findings suggest that the Marcellus Shale was deposited in predominantly anoxic bottom water conditions, and stratigraphy varies vertically and laterally between the Olsyn #2V and SRC #1V, which are approximately 94 miles (150 km) apart.

6.1: Well Correlation

In order to identify and correlate different Marcellus Shale facies across the Appalachian Basin, geologists typically use petrophysical logs. For this process, geologists observe changes in gamma ray logs noting that shale units typically have higher gamma ray values compared to carbonate or sandstone units. In this study, lithostratigraphy, chemostratigraphy and mechanical stratigraphy are investigated as alternative correlation methods between both wells.

Six and four lithofacies are identified in the Olsyn #2V and SRC #1V cored intervals, respectively. Figure 6.1 shows a lithologic cross-section of both wells. Despite the usefulness of lithofacies in terms of understanding sediment provenance, hydrodynamic conditions, environment of deposition, and reservoir quality, correlating lithologies poses problems (Wang and Carr, 2013). A major issue is that lithologies have no relation to time or length of time a rock

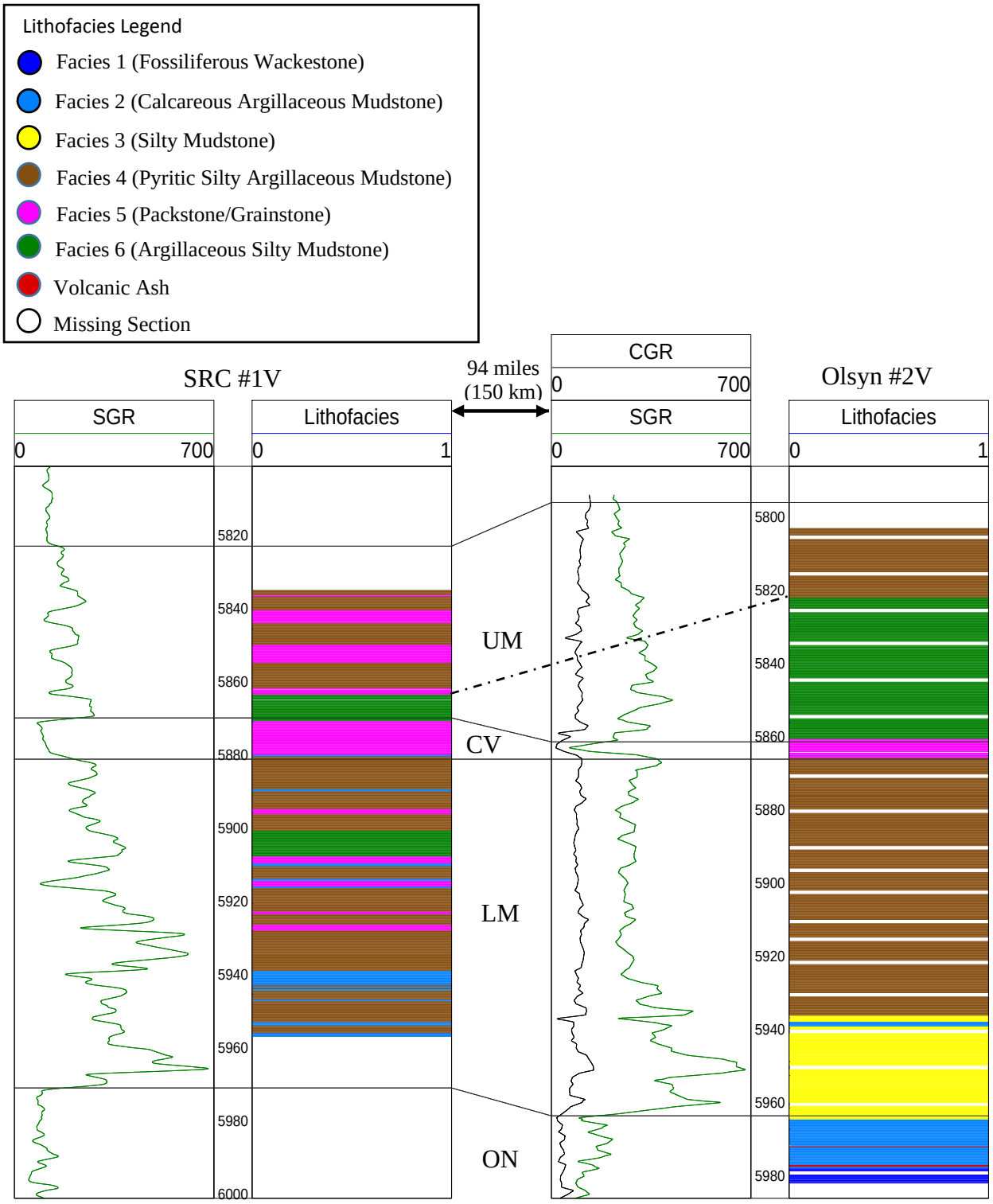

Figure 6.1: Lithostratigraphic correlation of the SRC #1V and Olsyn #2V wells. Datum = Top of Lower Marcellus. ON = Onondaga, LM = Lower Marcellus, CV = Cherry Valley, UM = Upper Marcellus.

was deposited, which means that two seemingly correlative lithologies may not have been deposited at the same time.

As is the case, most of the lithofacies are not correlative between the two wells in the Marcellus. The SRC #1V well has several packstone/grainstone facies in the Lower Marcellus which do not occur in the Olsyn #2V and this makes it difficult to correlate between both wells. The fossiliferous packstone/grainstone facies in the Cherry Valley can be correlated between both wells. The argillaceous silty mudstone facies in the Upper Marcellus can be correlated between both wells and is much thicker in the Olsyn #2V well. The pyritic silty argillaceous mudstone facies in the SRC #1V at the top of the Upper Marcellus is interbedded with fossiliferous packstone/grainstone and cannot be individually correlated to the Olsyn #2V well.

The next possible correlation is to use chemostratigraphy that is developed from cluster analysis of the major and trace elements. The individual chemofacies in the SRC #1V and Olsyn #2V wells do not correlate in the Lower and Upper Marcellus (Fig. 6.2). As noticed with the lithofacies. the SRC well has a higher frequency of limestone chemofacies across the Lower and Upper Marcellus, which affects the ability to correlate between both wells. The limestone chemofacies in the Cherry Valley can be correlated between both wells.

Finally, mechanical stratigraphy also proves to be a poor method to use for correlation. The mechanical facies are not correlative between the two wells in the Lower Marcellus, Cherry Valley or Upper Marcellus (Fig. 6.3). The SRC #1V rock strength is weaker in the Cherry Valley as compared to strong rock strength in Olsyn #2V. The lateral heterogeneity in the Marcellus Shale is the most likely reason why none of the three methods can be used for correlation in this study.

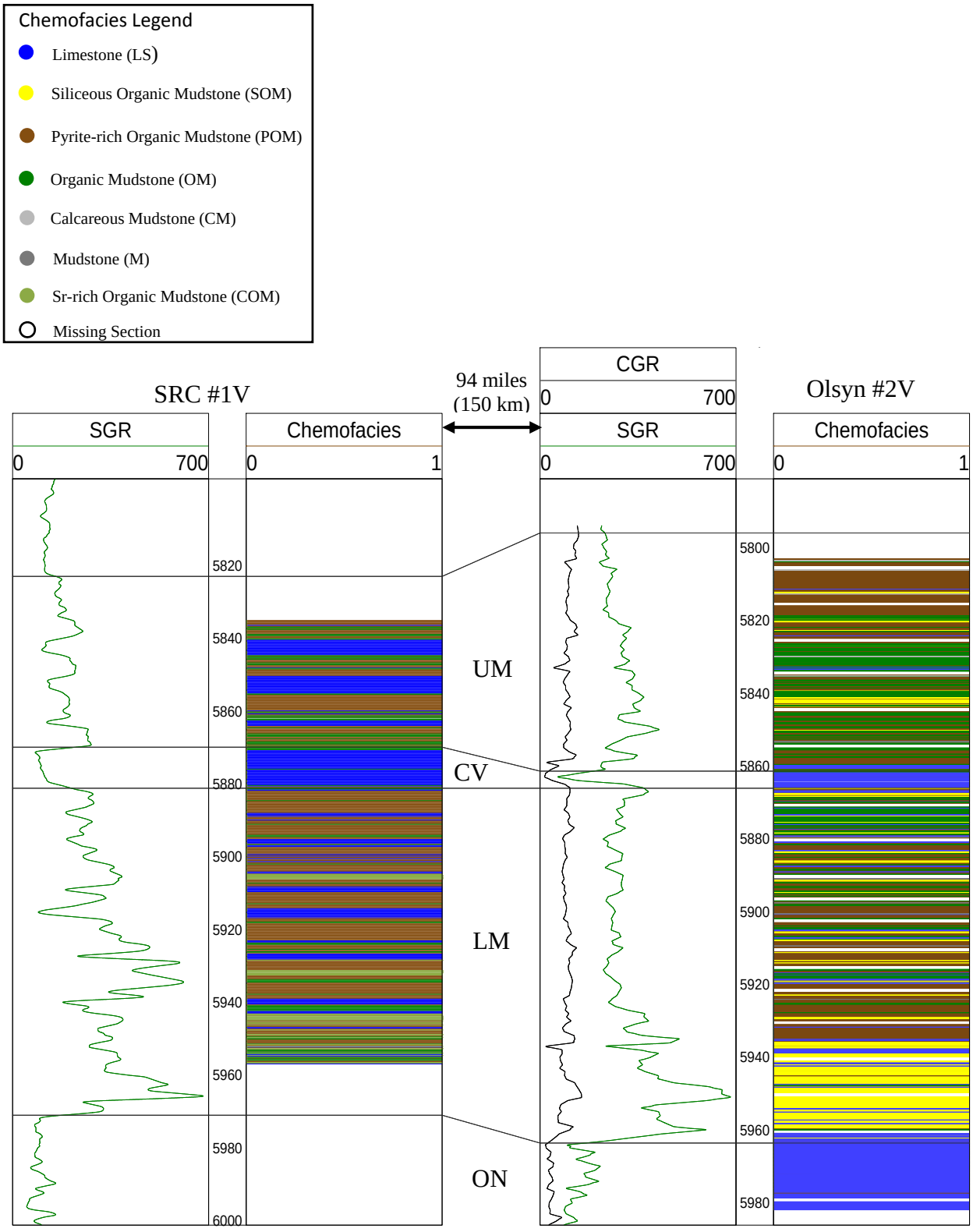

Figure 6.2: Chemostratigraphic correlation of the SRC #1V and Olsyn #2V wells. Datum = Top of Lower Marcellus. ON = Onondaga, LM = Lower Marcellus, CV = Cherry Valley, UM = Upper Marcellus.

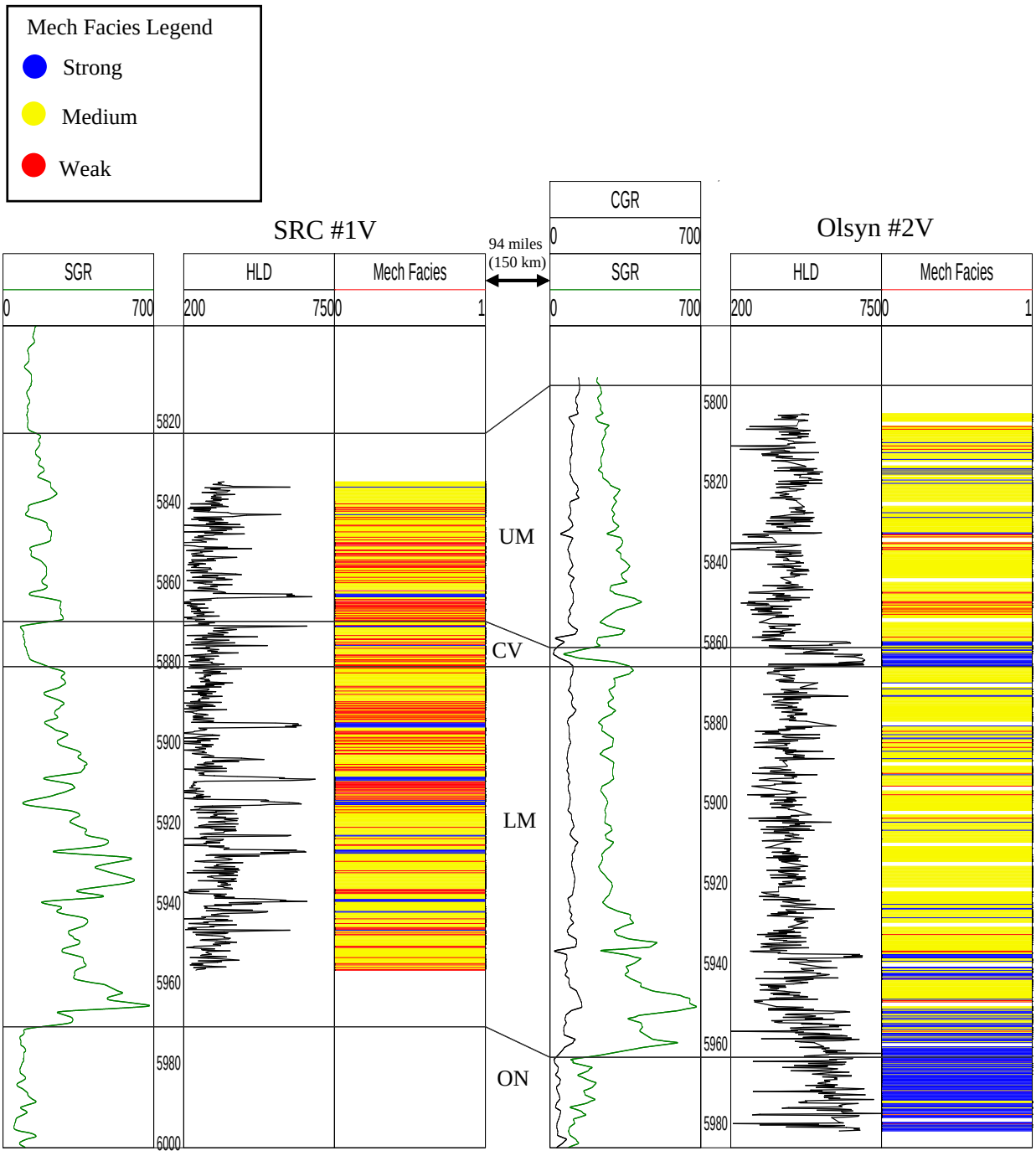

Figure 6.3: Mechanical stratigraphic correlation of the SRC #1V and Olsyn #2V wells. Datum = Top of Lower Marcellus. ON = Onondaga, LM = Lower Marcellus, CV = Cherry Valley, UM = Upper Marcellus.

6.2: Facies Interpretation

Chemical element concentrations and ratios of concentrations are utilized in this section to help identfy mineralogy trends or shifts in mineralogy between the different lithofacies, chemofacies, and mechanical facies. A Ca-Al-Si ternary diagram (Brumsack, 1989), which is assumed to reflect bulk mineralogy of calcite, clay, and quartz is used to predict the dominant mineralogy in each facies. Most mudstone facies contain significant amounts of calcite, clay, and quartz, which makes this type of diagram ideal in defining their bulk mineralogical variations (Rowe et al., 2012).

Mineralogical analysis of the lithofacies in both wells shows that the calcareous argillaceous mudstone identified in the Olsyn #2V and fossiliferous packstone/grainstone facies in SRC #1V display the most diverse mineralogical character (Figs. 6.4 and 6.5). The pyritic silty argillaceous mudstone and argillaceous silty mudstone facies display the highest concentration of clay minerals and lowest calcite concentrations. The silty mudstone facies identified in the Olsyn #2V shows the highest amount of quartz content (Fig. 6.4).

Similarly to the lithofacies, chemofacies can be compared based on their main mineralogical components (Figs. 6.6 and 6.7). The pyrite-rich organic mudstone, organic mudstone, Sr-rich organic mudstone, and calcareous mudstone chemofacies all exhibit higher clay content and lower calcite content. The siliceous organic mudstone chemofacies shows the highest quartz content and has a similar profile to the silty mudstone lithofacies (Fig. 6.4 and 6.6). The high quartz content observed in the siliceous organic mudstone chemofacies and silty mudstone lithofacies, which correspond to the same interval in the lower section of the Lower Marcellus confirms work performed by Emmanuel (2013).

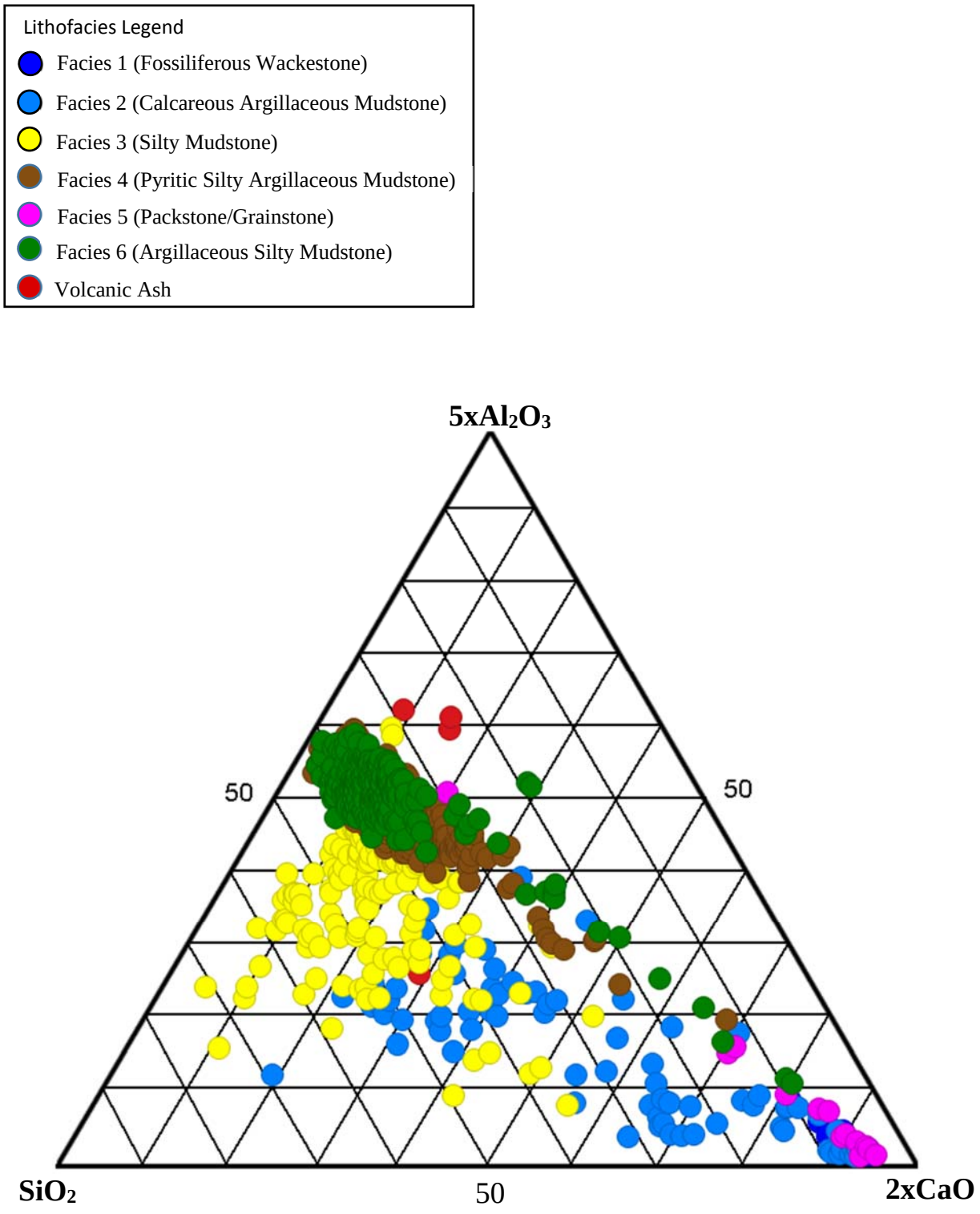

Figure 6.4: Ternary plot of major chemical elements colored by lithofacies from Olsyn #2V. See text for discussion.

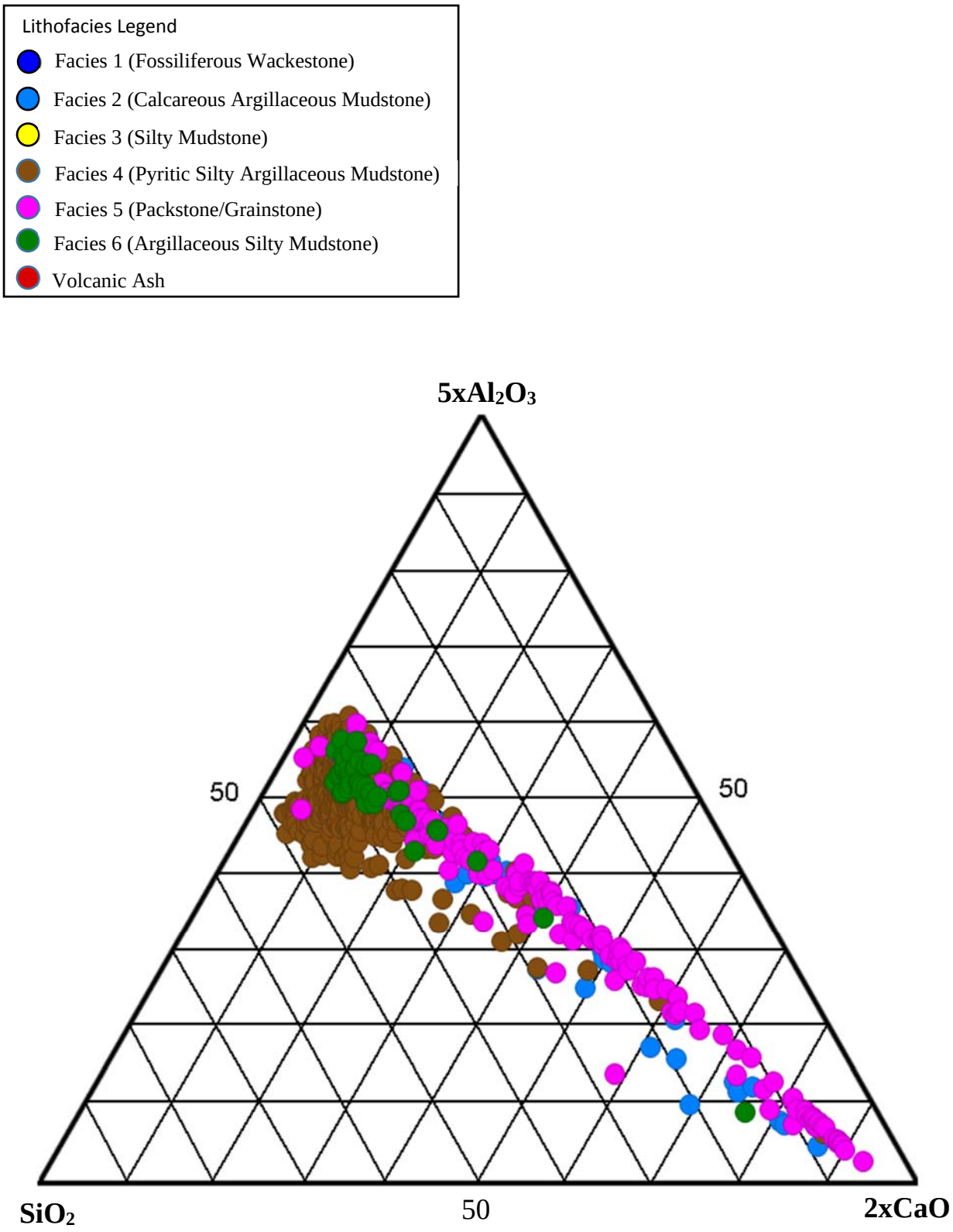

Figure 6.5: Ternary plot of major chemical elements colored by lithofacies from SRC #1V. Only four lithofacies are identified in this well. See text for discussion.

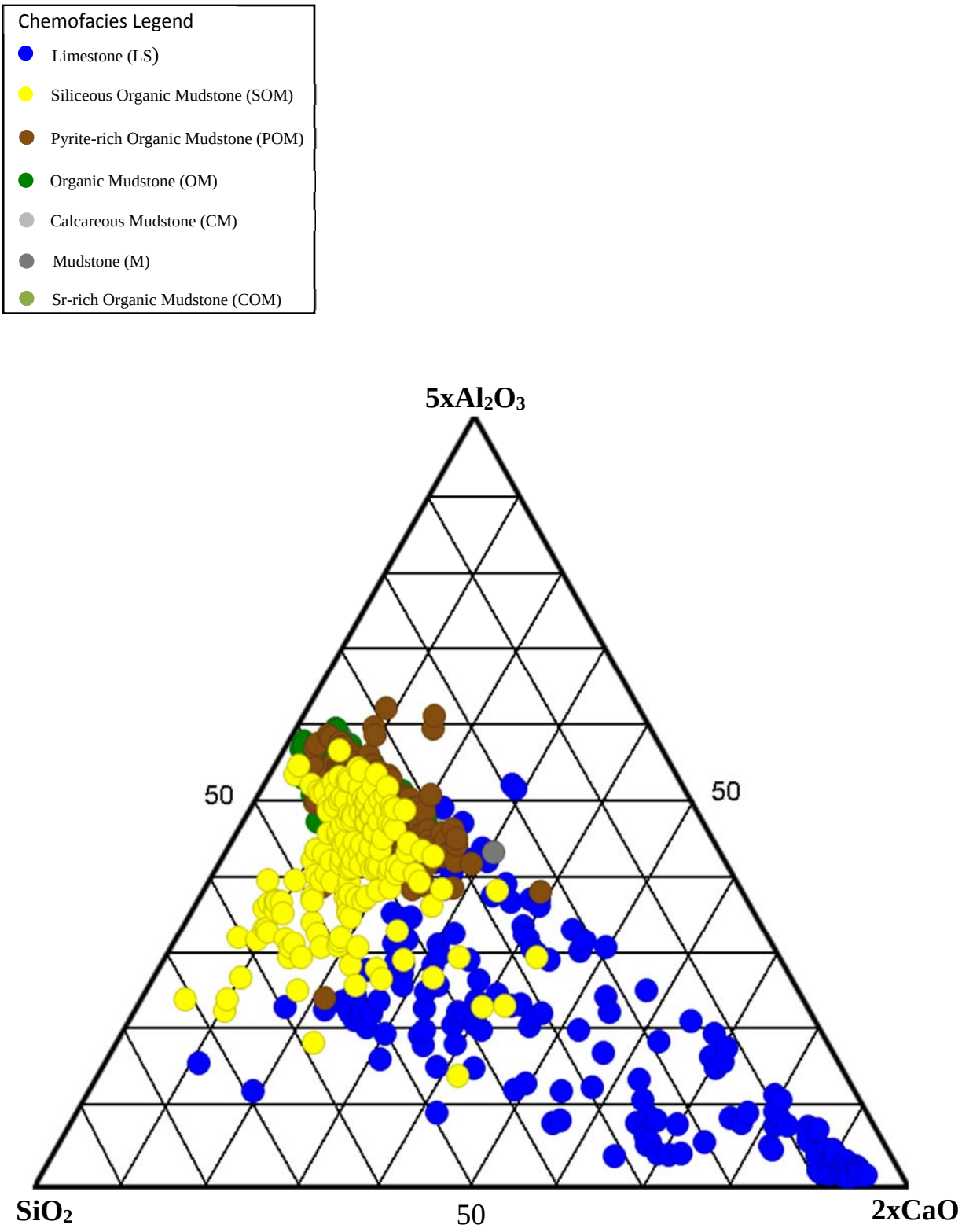

Figure 6.6: Ternary plot of major chemical elements colored by chemofacies from Olsyn #2V.

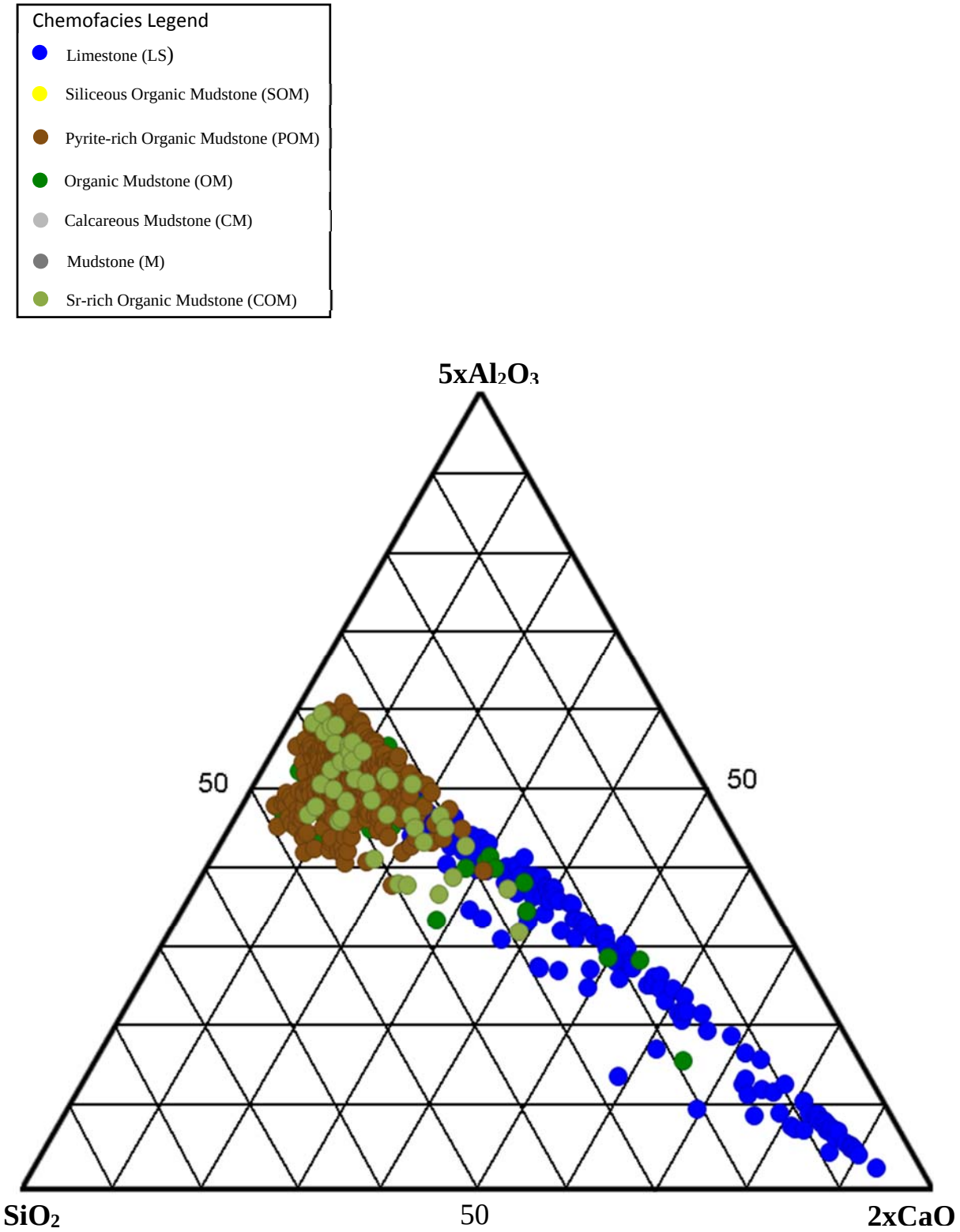

Figure 6.7: Ternary plot of major chemical elements colored by chemofacies from SRC #1V.

In that study, Emmanuel (2013) identified a similar siliceous mudstone lithofacies interval in the Lower Marcellus and estimated high quartz content (> 43 wt %) based on XRD analysis. He also identified most of the quartz to be of biogenic origin and suggests that the biogenic quartz grains are derived mainly from sponge spicules and radiolarians.

Mineralogical analysis of the mechanical facies in both wells shows that the high rock strength/strong intervals mostly correspond to high calcite and quartz intervals. (Figs. 6.8 and 6.9). Very few high strength intervals can be observed to have lower calcite and higher clay content. The medium strength rock intervals display a more diverse mineralogical character, whereas the low strength rocks intervals mostly correspond to high clay and low calcite concentrations.

Box plot diagrams (Figs. 6-10a-d) are created to identify the lithofacies with optimum total porosity, TOC, Leeb's HLD (rock strength), and wt. % Al. Only the Olsyn #2V well is discussed because it contains all the lithofacies identified in this study. The silty mudstone lithofacies has the highest wt. % TOC value with a mean value of about 6% (Fig. 6.10a). The silty mudstone lithofacies also has the highest total porosity with a mean value of 7.6 % (Fig. 6.10b). The pyritic silty argillaceous mudstone lithofacies also has good total porosity with a mean value of 7 %. The fossiliferous wackestones, packstone/grainstone, and calcareous argillaceous mudstone lithofacies have the lowest total porosity values.

Emmanuel (2013) performed Quantitative Evaluation of Minerals by Scanning electron microscope (QEMSCAN) and Tight Rock Analysis (TRA) on Marcellus Shale cores across eight wells to quantify porosity. He observed that the porosity within the Marcellus Shales facies is directly influenced by the mineralogy of the facies. His results show that the higher the quartz content, the higher the porosity. His explanation for this is that a good portion of calcite in the

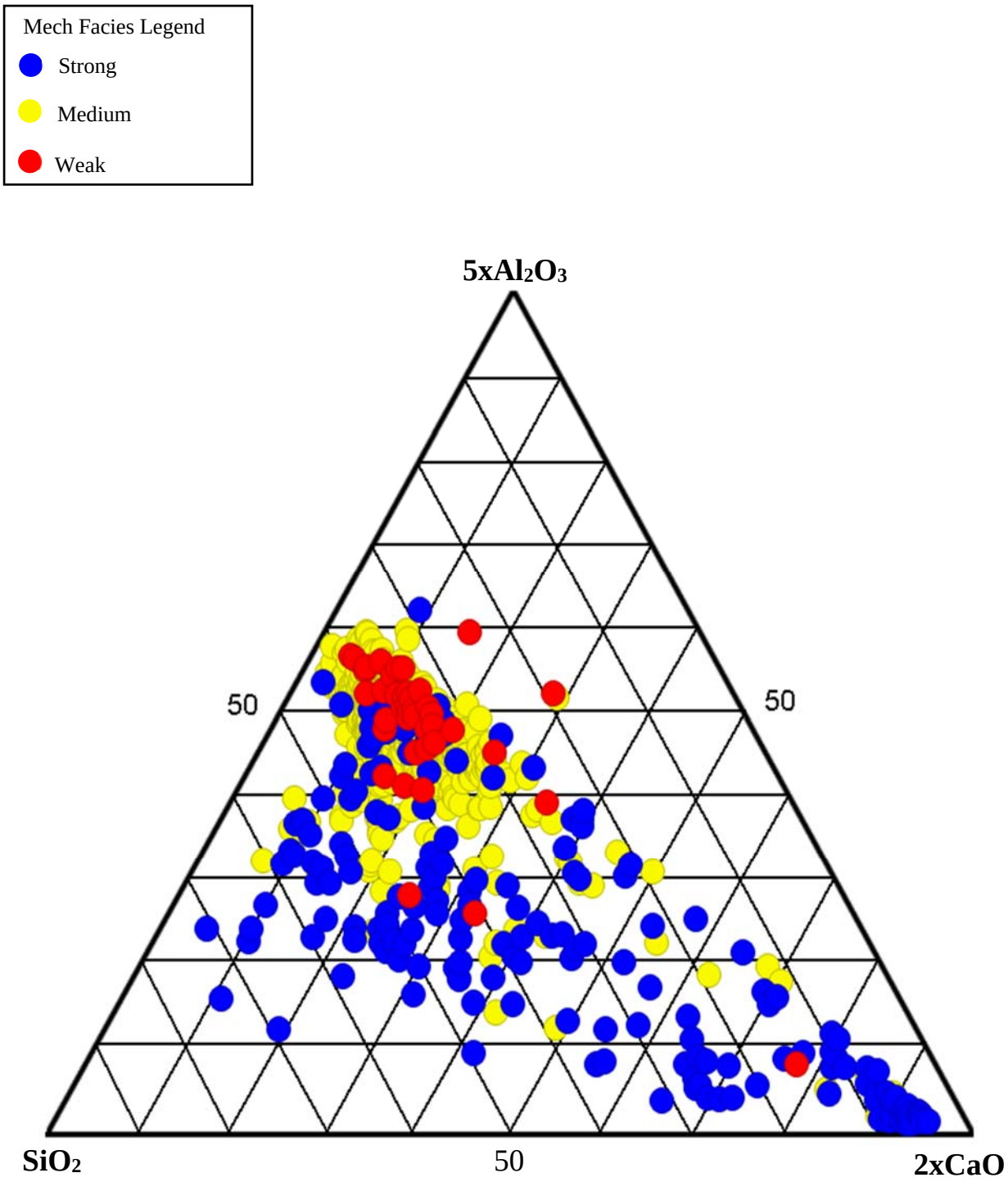

Figure 6.8: Ternary plot of major chemical elements colored by mechanical facies from Olsyn #2V.

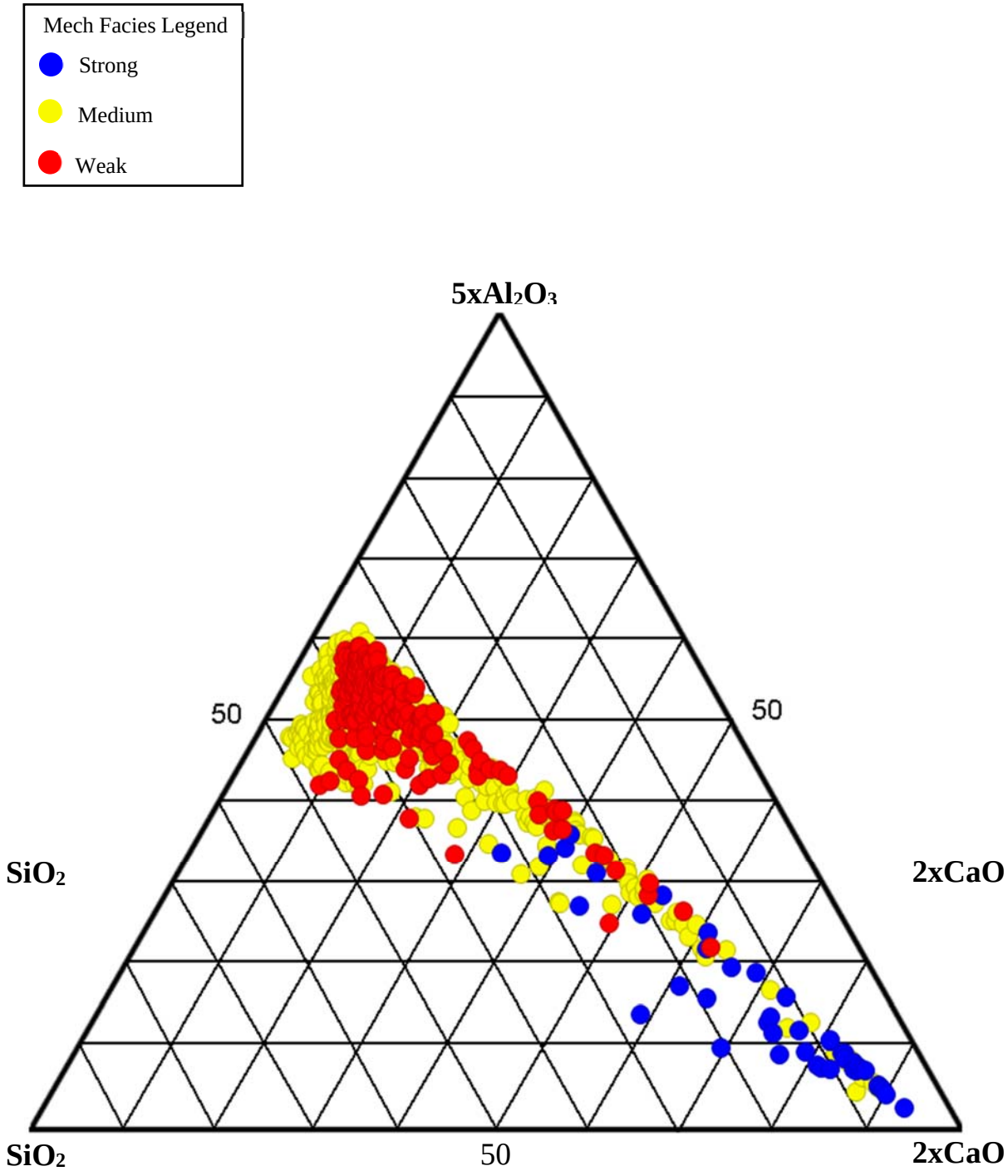

Figure 6.9: Ternary plot of major chemical elements colored by mechanical facies from SRC #1V.

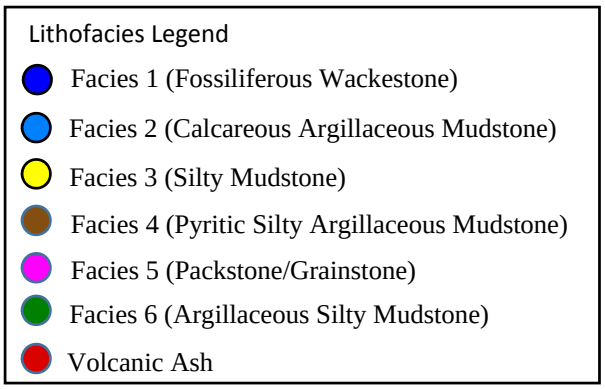

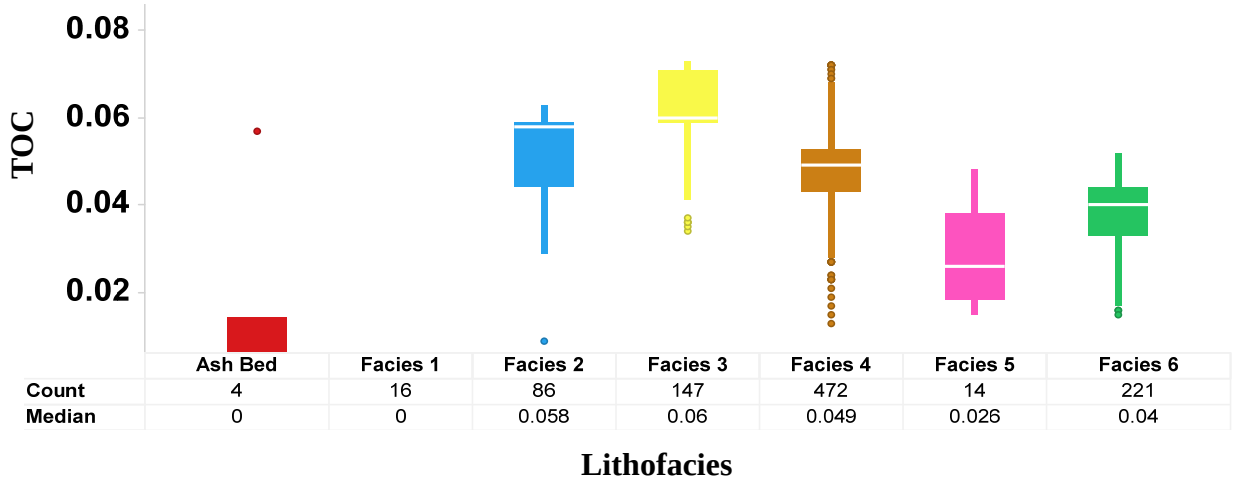

	Ash Bed	Facies 1	Facies 2	Facies 3	Facies 4	Facies 5	Facies 6
Count	4	16	86	147	472	14	221
Median	0	0	0.058	0.06	0.049	0.026	0.04

Lithofacies

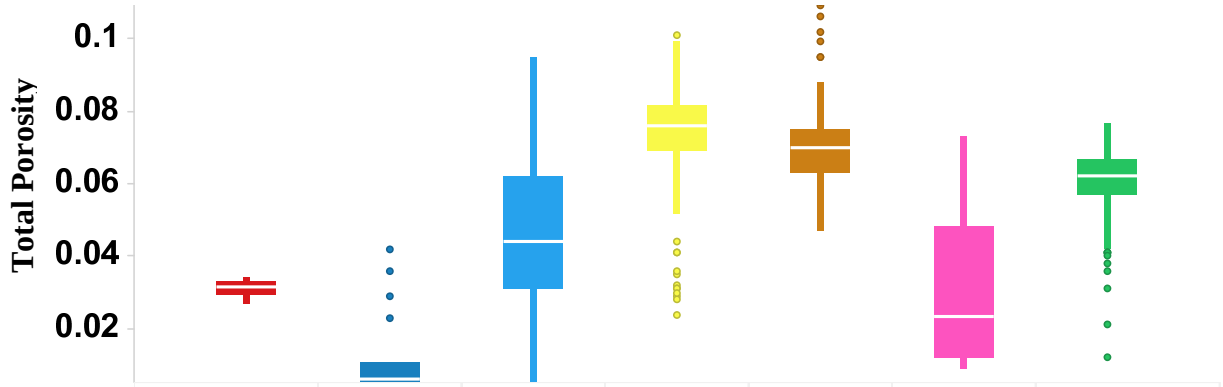

	Ash Bed	Facies 1	Facies 2	Facies 3	Facies 4	Facies 5	Facies 6
Count	4	16	86	147	472	14	221
Median	0.0315	0.006	0.044	0.076	0.07	0.0235	0.062

Lithofacies

Figure 6.10: a) Box plot of the Olsyn #2V well showing how TOC varies with lithofacies, b) Box plot of the Olsyn #2V well showing how total porosity varies with lithofacies. Median is the median value from TOC and total porosity, respectively.

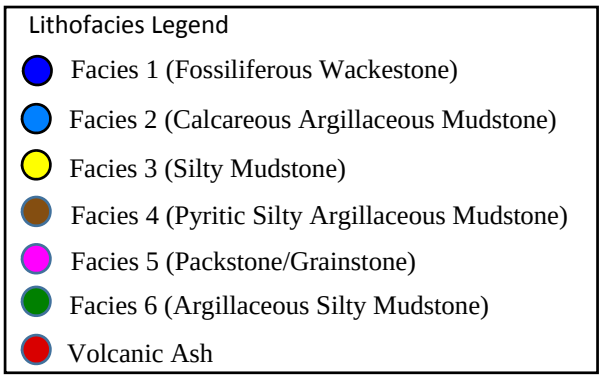

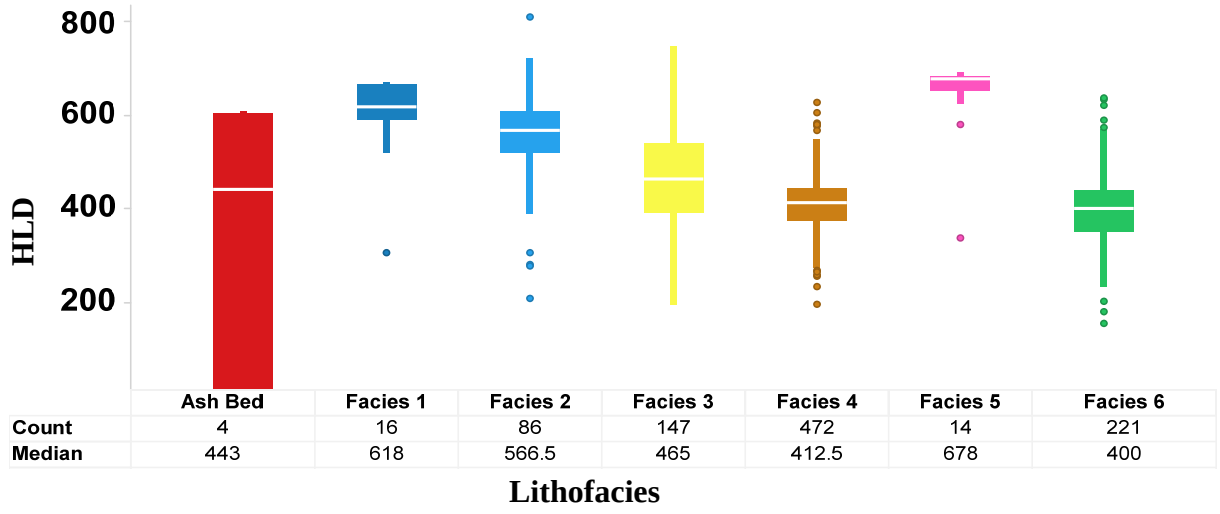

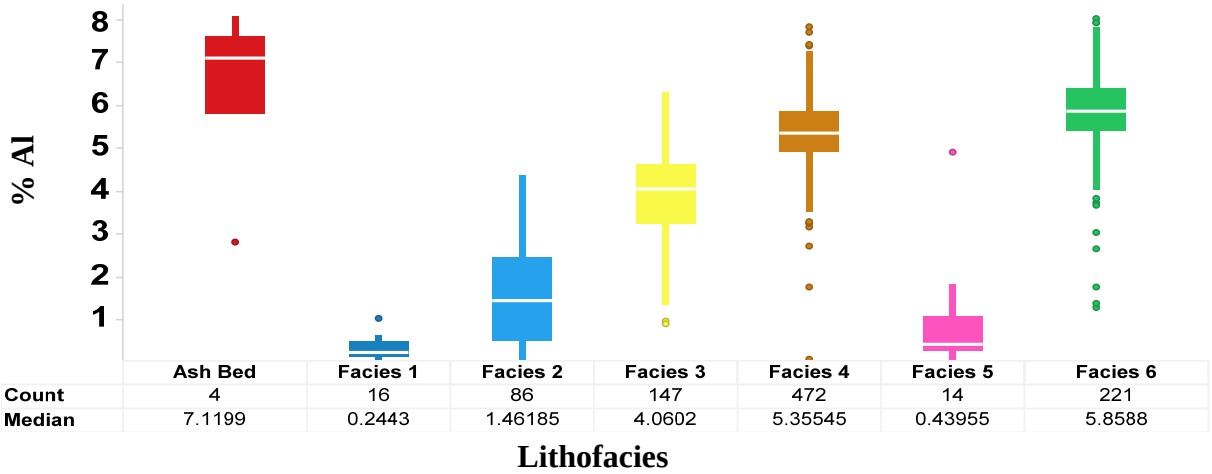

Figure 6.10: c) Box plot of the Olsyn #2V well showing how HLD varies with lithofacies, d) Box plot of the Olsyn #2V well showing how wt. % Al varies with lithofacies.

Marcellus Shale is present as cement material and occludes a significant portion of the pore space, whereas quartz occurs as siliceous matrix, which facilitates the development of equant micropores because the competency of quartz minerals prevents full compaction of matrix material unlike clay minerals (Emmanuel, 2013).

The fossiliferous wackestone and packstone/grainstone facies have the highest Leeb's HLD values with the calcareous argillaceous mudstone and silty mudstone being the next two facies with significant hardness values (Fig. 6.10c). Finally the calcareous-rich intervals have low wt. % Al values. The silty mudstone lithofacies has lower wt. % Al concentrations as compared to the pyritic silty argillaceous mudstone and argillaceous silty mudstone lithofacies (Fig. 6.10d).

6.3: Redox Conditions

Molybdenum (Mo), and uranium (U) concentrations may be used as reduction and oxidation (redox) proxies (Tribovillard et al., 2006), providing insight into the chemical composition of bottom waters at the time of Marcellus Shale deposition. Mo and U values for the Marcellus Shale in this study are compared to gray shale mean values (GSM) values (Raiswell et al., 1988; Sageman et al., 2003) to determine the extent of enrichment from background oxic values. By comparing the concentrations of the redox proxies to the GSM values, it is possible to identify the environmental conditions that existed during the deposition of the Marcellus Shale. Redox proxies from Olsyn #2V and SRC #1V suggest that a significant portion of the Marcellus Shale was deposited under anoxic bottom water conditions. However, evidence of euxinic bottom water conditions does not exist.

Mo concentrations are generally greater than the GSM value of 0.22 parts per million (ppm) in the Olsyn #2V for most of the Marcellus except at the base of the cored Onondaga and in the

Cherry Valley (Fig. 6.11). Mo concentrations are highest at the base of the Lower Marcellus and range from 100 to 260 ppm and decreases in the upper section of the Lower Marcellus. Molybdenum concentrations slightly increases in the Upper Marcellus with an average value of approximately 120 ppm. A similar Mo profile can be observed in the SRC #1V well but with several intervals in the Lower Marcellus and Upper Marcellus below the GSM average. The Mo concentrations in the Cherry Valley for both wells mostly fall below the GSM value.

Uranium concentrations are generally similar to the Mo concentrations for both wells. The concentrations are highest in the lower section of the Lower Marcellus and decreases in the upper section of the Lower Marcellus (Fig. 6.11). Just as with Mo, U slightly increases in the Upper Marcellus and is below the GSM value in the Cherry Valley.

Based on the comparison of Mo and U with GSM values, it appears that the Lower and Upper Marcellus were most likely deposited in predominantly anoxic deep water conditions, whereas the Cherry Valley was most likely deposited in oxic shallower water conditions. The SRC #1V anoxic conditions in the Lower and Upper Marcellus may have been periodically interrupted by oxic conditions, which suggests that it might have been closer to the basin edge or shelf margin. The anoxic conditions in the Olsyn #2V appear to be less interrupted in the Lower and Upper Marcellus, which indicates the rocks were deposited in a deeper portion of the basin.

This study confirms work by Wendt et al., (2015), who performed high-resolution XRF analyses on a transect of cores in central Pennsylvania and concluded that the Lower Marcellus Shale section was deposited predominantly under anoxic to euxinic bottom water conditions. They also suggest that the Lower Marcellus was most likely deposited under a stratified water column, in which the water column was at least 330 ft (100 m) deep in the central part of the basin to prevent wind mixing to the bottom sediments.

SRC #1V and Olsyn #2V Redox-sensitive Elements

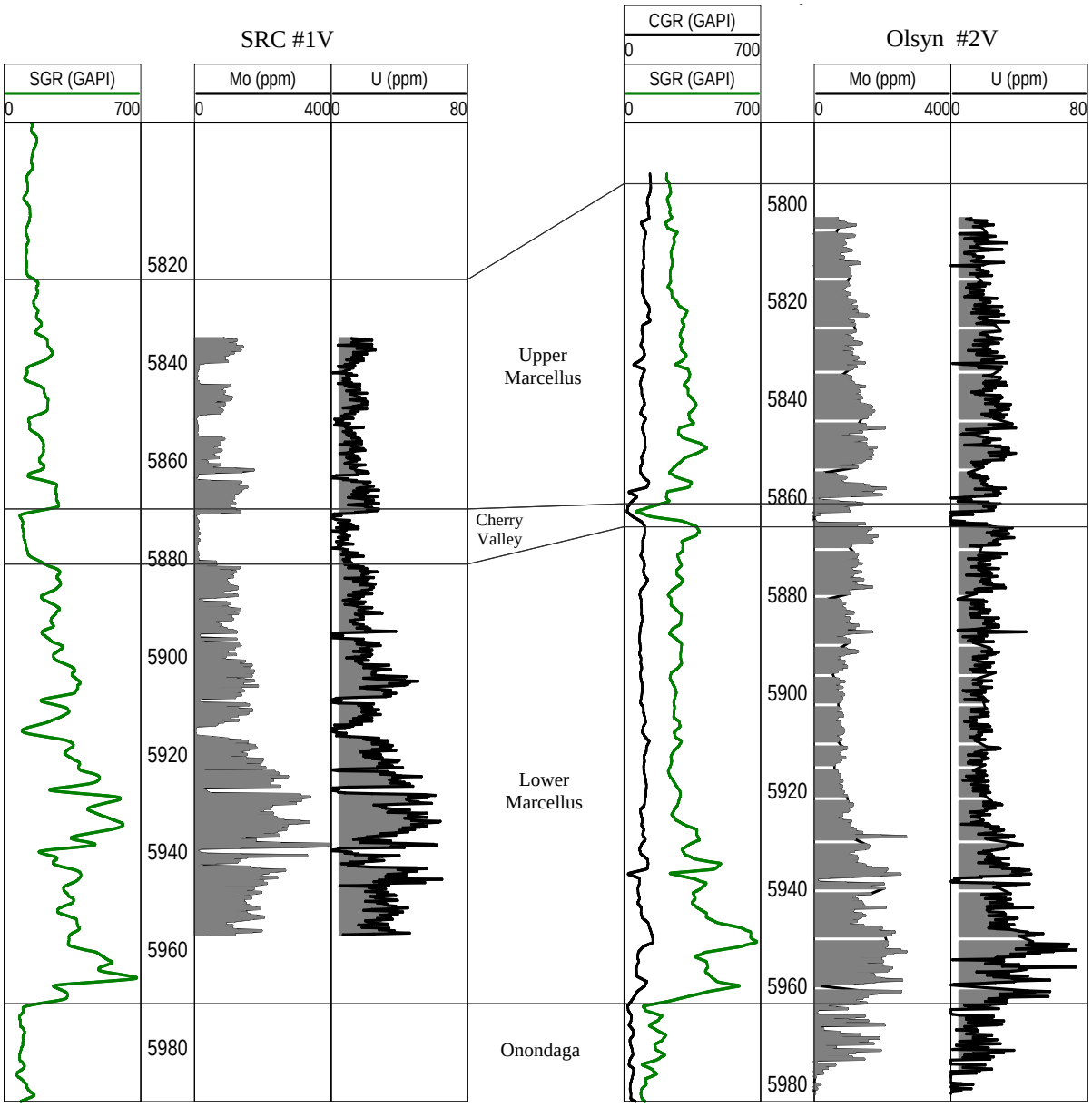

Figure 6.11: Redox-sensitive element chemostratigraphy of the SRC #1V and Olsyn #2V wells. Mo, and U are shaded grey when enriched with respect to the gray shale mean (GSM) value of 0.22 and 5 ppm, respectively as defined by Raiswell et al., (1988) and Sageman et al., (2003).

6.4: Wireline Log Character of Marcellus Shale Lithofacies

As mentioned in the well log correlation section, high gamma ray responses can be used to differentiate shale units or siliceous/argillaceous facies from calcareous facies, which typically have lower gamma ray values. Additionally, the combination of several petrophysical log responses with gamma ray facilitates the recognition of the various Marcellus Shale lithofacies (Wang and Carr, 2013). The recognition of the Marcellus Shale lithofacies by petrophysical logs extends the lithofacies from the well scale to a broad or regional scale, making the various lithofacies mappable

Lithofacies identification are made using a combination of gamma ray (GR), resistivity (AT90), neutron-porosity (NPHI), and density-porosity (DPHI) logs (Figs. 6.12a and 6.12b). Both neutron and density porosity logs were analyzed on a limestone matrix. In the Olsyn #2V well, the calcareous argillaceous mudstone, silty mudstone, and fossiliferous packstone/grainstone lithofacies can be easily identified from the petrophysical logs. The pyritic silty argillaceous mudstone and argillaceous silty mudstone facies have less distinct responses and identifying them is not as straightforward. The calcareous argillaceous mudstone lithofacies is identified as having a GR reading around 152 API, AT90 value between 200 and 2000 ohmm, and low to no separation between NPHI and DPHI porosity logs (Fig. 6.12a). The lack of separation between both porosity logs correlates with the high calcite concentration of this interval. High GR values of around 470 API, AT90 between 40 and 300 ohmm, NPHI values between 15 and 22 % and DPHI values between 6 and 14 % are used to identify the silty mudstone lithofacies. This interval has an NPHI and DPHI separation of about 6-8 % (Fig. 6.12a). The fossiliferous packstone/grainstone lithofacies has GR readings between 80 and 350 API, high AT90 readings greater than 1000 ohmm, NPHI between 4 and 14 percent and DPHI value around 4 %.

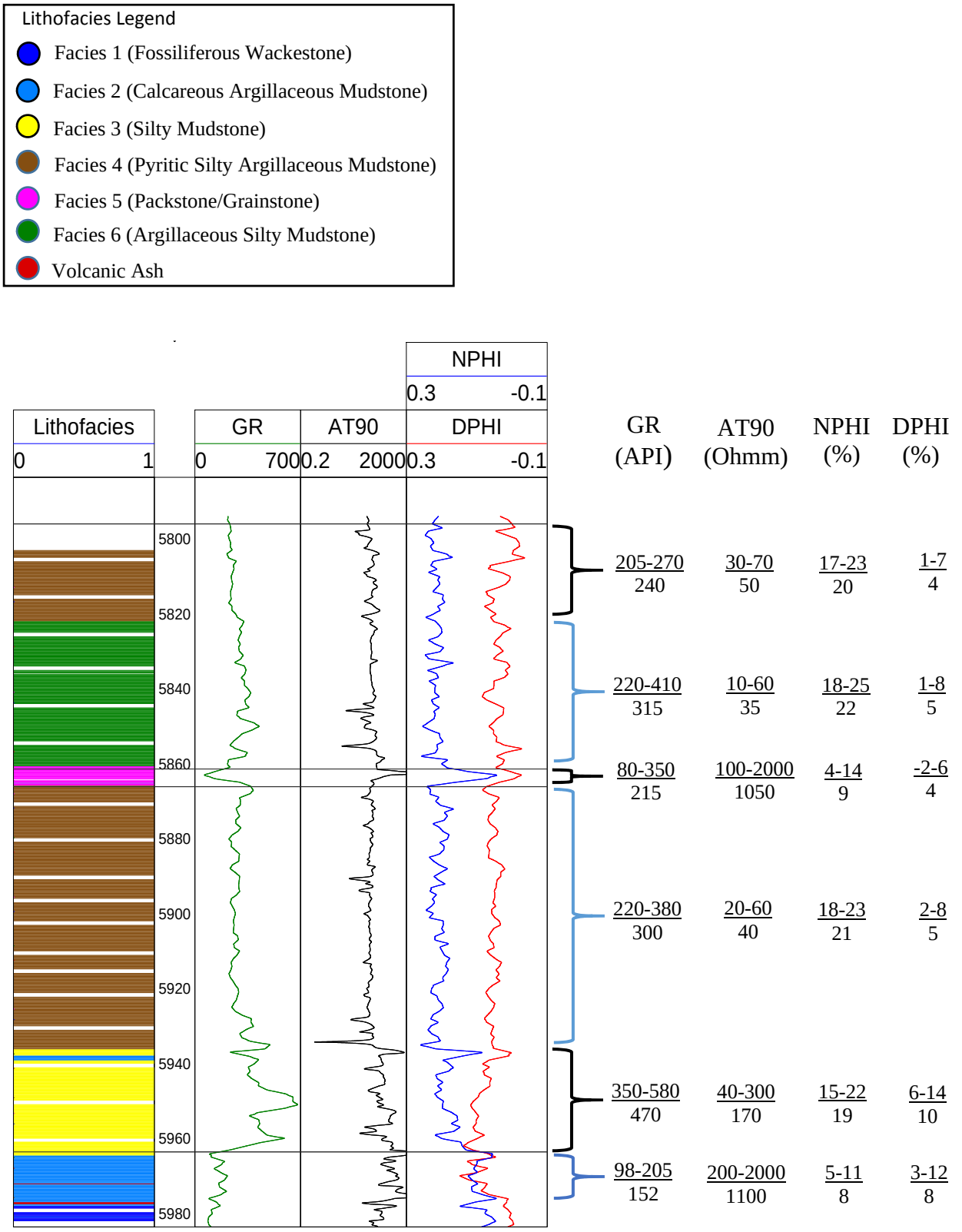

Figure 6.12a: Summary of log responses of the different lithofacies defined from core/petrographic analysis of the Marcellus Shale in the Olsyn #2V well.

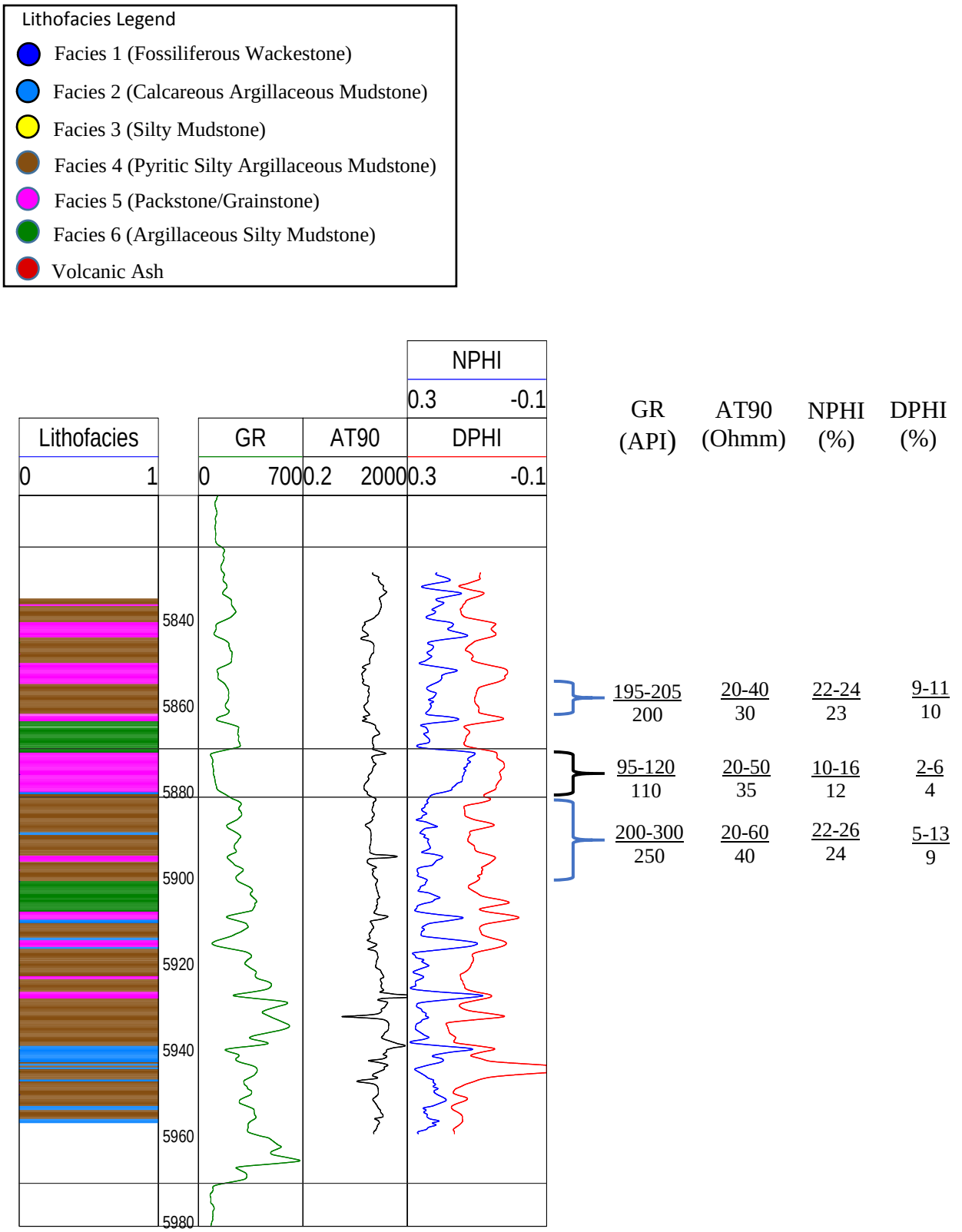

Figure 6.12b: Summary of log responses of the different lithofacies defined from core/petrographic analysis of the Marcellus Shale in the SRC #1V well.

The pyritic silty argillaceous mudstone and argillaceous silty mudstone lithofacies have similar log responses with GR values between 220-410 API, AT90 values between 10 and 70 ohmm, NPHI values between 17 and 25 % and DPHI values between 1 and 8 %. Differentiating between the two lithofacies can be accomplished by analyzing the separation between NPHI and DPHI porosity logs. A high separation between NPHI and DPHI in a shale or siliceous mudstone usually indicates a high clay content. The pyritic silty argillaceous mudstone has an NPHI to DPHI separation between 14 and 16 %, whereas the argillaceous silty mudstone has a separation of 16-20 %.

Identifying the various lithofacies using petrophysical logs in the SRC #1V well is slightly more problematic due to the fact that lithofacies alternate more frequently especially the fossiliferous packstone/grainstone lithofacies (Fig. 6.12b). This thinly bedded lithofacies makes it difficult for the petrophysical logs, which typically have a vertical resolution of 2-4 ft (0.6 – 1.2 m) to resolve. Nevertheless, several thick pyritic argillaceous mudstone and fossiliferous packstone/grainstone sections can be identified using similar log responses as in the Olsyn #2V (Fig. 6.12b).

CHAPTER 7

CONCLUSIONS

Detailed observation of lithology, chemostratigraphy, mechanical stratigraphy, and petrophysical logs indicate that the Marcellus Shale is heterogenous. Six major lithologic units are identified on the basis of their textural fabric, grain type, size and abundance, biota and sedimentary structures. These lithofacies include fossiliferous wackestone, calcareous argillaceous mudstone, silty mudstone, pyritic silty argillaceous mudstone, fossiliferous packstone/grainstone, and argillaceous silty mudstone. Seven chemofacies are also identified from major and trace elements, which include limestone, siliceous organic mudstone, pyrite-rich organic mudstone, organic mudstone, Sr-rich organic mudstone, calcareous mudstone, and mudstone. Three mechanical units, which include strong, medium, and weak intervals are also identified in the Marcellus Shale based on the Bambino analysis. These facies have different mineralogy, porosity, TOC content, and mechanical properties and understanding the facies distribution may help operators improve their target interval within the Marcellus Shale.

The silty mudstone lithofacies/siliceous organic mudstone chemofacies appears to be the interval with the best reservoir quality in the Olsyn #2V from a mineralogy, TOC content, porosity, and mechanical properties perspective. This interval has the highest quartz content > 35 wt. %, 7 - 8 wt. % TOC, 6 – 8 % porosity, and high rock strength values. Also, high Si to Al ratio in this interval suggest that some of the quartz content might be of biogenic origin.

Redox-sensitive trace elements suggest that the Lower and Upper Marcellus intervals were most likely deposited in predominantly anoxic deep water conditions, whereas the Cherry Valley was deposited in oxic shallower water conditions. Anoxic conditions in the Lower and Upper Marcellus at the location of the SRC #1V well seems to have been periodically interrupted by oxic

conditions, which suggests that it could have been closer to the basin edge. In contrast, the anoxic conditions in the Olsyn #2V appear to have persevered during the deposition of the Lower and Upper Marcellus, which indicates that deposition occured in a deeper portion of the basin.

Analysis of petrophysical log curves show that a combination of log curves can be used to identify and possibly map the thickness of the various lithofacies within the study area or regionally. The calcareous argillaceous mudstone, silty mudstone, and fossiliferous packstone/grainstone lithofacies have distinct log charcteristics, whereas the pyritic silty argillaceous mudstone and argillaceous silty mudstone facies have less distinct log characteristics.

This study sheds some light onto the heterogeneity of the Marcellus Shale. Results from this study would support similar studies in other unconventional reservoir plays, which are probably more heterogeneous than they initially appear. A better understanding of the heterogeneities would allow operators to more efficiently drill, target, and complete wells to get the best production.

References Cited

Algeo, T., Maynard, J., 2004, Trace-element behavior and redox facies in core shales of Upper Pennsylvanian Kansas-type cyclothems. Chemical Geology, v. 206, p. 289-318.

Aoki, H., Matsukura, Y., 2008, Estimating the Unconfined Compressive Strength of Intact Rocks from Equitop Hardness: Bulletin of Engineering Geology and Environment, v. 67, p. 23-29.

Arthur, M.A., Dean, W.E., 1991, A holistic geochemical approach to cyclomania: examples from Cretaceous and pelagic limestone sequences *in* Einsele, G., Ricken, W., and Seilacher, A., (eds.) *Cycles and Events in Stratigraphy*, Springer-Verlag, Berlin, p. 126-166.

Aydin, M. G., 2012, Revisiting the Hubbert-Rubey Hypothesis for Overthrusting Faulting: Inferences from Progressive Mineralization on Bedding Slip Surfaces during Flexural Slip Folding of Devonian Shale, the Appalachian Basin, Master's thesis, Pennsylvania State University, Pennsylvania.

Benelli, P., 2012, Comparison between Whole Rock Lithogeochemistry and fine Lithogeochemistry of Marcellus Shale, Master's thesis, University at Buffalo, State University of New York, Buffalo, New York.

Brookins, D. G., 1988, Eh-pH diagrams for geochemistry: *in* Kesler, S. E., *Geochimica et Cosmochimica Acta vol.* 53(3), Springer-Verlag, New York p. 763.

Brumsack, H. J., 1989, Geochemistry of recent TOC-rich sediments from the Gulf of California and the Black Sea. Geologische Rundschau, v. 78, p. 851-882.

Calvert, S.E., Pedersen, T.F., 1993, Geochemistry of recent oxic and anoxic sediments: implications for the geological record. Marine Geology, v. 113, p. 67-88.

Cate, A. S., 1963, Lithostratigraphy of some Middle and Upper Devonian rocks in the subsurface of southwestern Pennsylvania, Symposium of Middle and Upper Devonian Stratigraphy of Pennsylvania and adjacent states, Pennsylvania Geological Survey General Geology Report, 4th series, no. G39, p. 229-240.

Carter, K. M., Haper, J. A., Schmid, K. W., Kostelnik, J., 2011, Unconventional natural gas resources in Pennsylvania: The backstory of the modern Marcellus Shale play, Environmental Geosciences, v. 18, no 4, p. 217-257.

Collins, H. R., 1979, Devonian Bentonites in Eastern Ohio: Geologic Notes, American Association of Petroleum Geologist Bulletin, v. 63, p. 655–660.

Conrey, R. M., Wolff, J. A., 2011, Application of portable X-ray fluorescence spectrometry to problems in volcanology, Geological Society of America, v. 43, no. 5, p. 231-250.

Daniels, G., McPhee, C., McCurdy, P., Sorrentino, Y., 2012, Non-Destructive Strength Index Testing Applications for Sand Failure Evaluation: Society of Petroleum Engineers paper 158326, 12p.

De Witt Jr., W., Roen, J. B., Wallace, L. G., 1993, Stratigraphy of the Devonian Black Shales and Associated Rocks in the Appalachian Basin, Petroleum Geology of the Devonian and Mississippian Black Shale of Eastern North America: U.S. Geological Survey Bulletin 1909B, p. B1-B57.

Emmanuel, O. O., 2013, Geologic Characterization and the Recognition of Cyclicity in the Middle Devonian Marcellus Shale, Appalachian Basin, NE USA, Doctoral Dissertation, Colorado School of Mines, Golden, Colorado.

Enderlin, M., 2016, Personal communication on equation to compute unconfined compressive strength (UCS) from Bambino Leeb's hardness values. July, 2016.

Ettensohn, F. R., 1985, The Appalachian Foreland Basin in Eastern United States, The Sedimentary Basin of United States and Canada, 594p.

Fortson, L., 2012, Geochemical and Spatial Investigation of Uranium in the Marcellus Shale, Master's thesis, University at Buffalo, State University of New York, Buffalo, New York.

Fossen, H., 2010, Structural Geology. Cambridge, United Kingdom: Cambridge University Press.

Hall, J., 1839, Third annual report of the fourth geological district of the state of New York: New York Geological Survey Annual Report, p. 287-339

Harris, L. D., 1978, The eastern interior aulacogen and its relation to Devonian Shale-gas production, Eastern Gas Shale Symposium, v. 2, p. 55-72.

Hasson, K. O., Dennison, J. M., 1988, Devonian Shale Lithostratigraphy, central Appalachians, U.S.A, *in* McMillian, N.J., Embry, A. F., and Glass, D.J., (eds.) *Devonian of the world: Proceedings of the Second International Symposium on the Devonian System*: *Canadian Society of Petroleum Geologists Memoir 14*, v. 2, p. 157 – 177.

Katz, A., Sass, E., Holland, H. D., Starinsky, A., 1972, Strontium behavior in the aragonite-calcite transformation: An experiment study at 40-98^{o}C, Geochemica et Cosmochemica Acta, vol. 36, no. 4, Abstract.

Kiesel, M., 2013, Chemostratigraphy and Elemental Analysis of the Mississippian Barnett Shale Formation using Energy-dispersive X-ray Fluorescence Spectrometry, Fort Worth Basin, Johnson County, Texas, Master's thesis, Texas Christian University, Fort Worth, Texas, 80p.

Lash, G. G., Blood, R., 2011, Chemostratigraphic Trends of the Middle Devonian Shale, Appalachian Basin: Preliminary Observations, Search and Discovery Article #80198.

Lash, G. G., Engelder, T. E., 2011, Thickness trends and Sequence Stratigraphy of the Middle Devonian Marcellus Formation, Appalachian Basin: Implications for Acadian Foreland Basin evolution, American Association of Petroleum Geologist Bulletin, v. 95, no. 1, p. 61-103.

McLennan, S. M., Taylor, S. R., 1995, The geochemical evolution of the continental crust, Reviews of Geophysics, v. 33, p. 241-265.

Milici, R. C., 1977, Blue Ridge Thrust Belts (068), Piedmont Province (069), Atlantic Coastal Plain Province (070), Adirondack Province (071), and New England Province (072).

Milici, R. C., Swezey, C. S., 2006, Assessment of Appalachian Basin Oil and Gas Resources: Devonian Shale-Middle and Upper Paleozoic Total Petroleum System, U.S Department of the Interior, U.S. Geological Survey, Open-File Report Series 2006-1237.

Milliken, K. L., Rudnicki, M., Awwiller, D. N., Zhang, T., 2013, Organic matter-hosted pore system, Marcellus Formation (Devonian), Pennsylvania, American Association of Petroleum Geologist Bulletin, v. 97, no. 2, p. 177-200.

O'Neal, D. L., 2015, Chemostratigraphic and Depositional Characterization of the Niobrara Formation, Cemex Quarry, Lyons, Colorado, Master's thesis, Colorado School of Mines, Golden, Colorado, 95p.

Perez, R., Marfurt, K., 2013, Calibration of brittleness to elastic rock properties via mineralogy logs in unconventional reservoirs, American Association of Petroleum Geologist Search and Discovery Article # 41237.

Phillips, N. D., 1991, Refined subsidence analyses as a means to constrain Late Cenozoic fault movement, Ventura basin, California, Master's thesis, University of Texas, Austin, Texas.

Phillips, N. D., 2015, Personal communication on technique to determine chemofacies type from average concentrations of chemical elements. June, 2015.

Raiswell, R., Buckley, F., Berner, R. A., Anderson, T. F., 1988, Degree of pyritization of iron as a paleoenvironmental indicator of bottom-water oxygenation, Journal of Sedimentary Petrology, v. 58, p. 812-819.

Reed, J. D., Zumberge, J. E., Ferworn, K. A., Dunbar, D. C., 2007, Appalachian Basin Petroleum System Study, Geomark Research, p. B-2.

Richard, G. A., 2007, Adirondack Geology: Old Rocks and New Mountains, Stony Brook Mineral Physics Institute Research.

Rodgers, J., 1990, Fold and Thrust belts in Sedimentary Rocks, Part 1: Typical examples, American Journal of Science, v. 290, no. 4, p. 321–359.

Roen, B. J., 1984, Geology of the Devonian black shales of the Appalachian Basin, Organic Geochemistry, v. 5, no. 4, p. 241–254.

Rowe, H., 2016, Personal communication regarding the inability to resolve Ti, V and Cr peaks in intervals with high barium concentrations. March 2016.

Rowe, H., Hughes, N., Robinson, K., 2012, The quantification and application of handheld energy-dispersive x-ray fluorescence (ED-XRF) in mudrock chemostratigraphy and geochemistry, Chemical Geology, v. 324-325, p. 121-131.

Ryder, R.T., 2008, Assessment of the Appalachian Basin Oil and Gas Resources, Utica-Lower Paleozoic Total Petroleum System: U.S. Geological Survey Open-File Report 2008-1287, 29p.

Sageman, B. B., Murphy, A. E., Werne, J. P., Ver Straeten, C. A., Hollander, D. J., Lyons, T. W., 2003, A tale of shales: The relative roles of production, decomposition, and dilution in the accumulation of organic-rich strata, Middle-Upper Devonian, Appalachian Basin, Chemical Geology, v. 195, p. 229-273.

Sageman, B. B., Lyons, T. W., 2009, Geochemistry of Fine-grained Sediments and Sedimentary Rocks *in* Holland, H. D., Turekian, K. K., (eds.) *Readings from Treatise on Geochemistry*, Elsevier, p. 424-456.

Salminen R., Batista, M. J., Bidovec, M., Demetriades, A., De Vivo, B., De Vos, W., Duris, M., Gilucis, A., Gregorauskiene, V., Halamic, J., Heitzmann, P., Lima, A., Jordan, G., Klaver, G., Klein, P., Lis, J., Locutura, J., Marsina, K., Mazreku, A., O'Connor, P. J., Olsson, S. A., Ottesen, R. T., Petersell, V., Plant, J. A., Reeder, S., 2005, Geochemical Atlas of Europe, Part 1: Background Information, Methodology and Maps. Geological Survey of Finland, Espoo, 526 pp. Available online at: http://www.gtk.fi/publ/foregsatlas/ (last accessed on 5/15/2016).

Thomas, W. A., 1991, The Appalachian-Ouachita rifted margin of southeastern North America, Geological Society of America Bulletin, v. 103, no. 3, p. 415-431.

Tribovillard, N., Algeo, T. J., Lyons, T., Riboulleau, A., 2006, Trace metals as paleoredox and paleoproductivity proxies, An update. Chemical Geology, v. 232, p. 12-32.

U.S Energy Information Administration, 2016, Drilling productivity report for key tight oil and shale gas regions (http://www.eia.gov/petroleum/drilling/pdf/marcellus.pdf).

VanMeter, J., 2013, Regional Mapping and Reservoir Analysis of the Middle Devonian Marcellus Shale in the Appalachian Basin, Master's thesis, West Virginia University, Morgantown, West Virginia.

Ver Straeten, C., Baird, G., Brett, C., Lash, G., Over, J., Karaca, C., Jordan, T., Blood, R., 2011, The Marcellus Subgroup in its Type Area, Finger Lakes Area of New York, and Beyond. Report prepared for New York Geological Association, Albany, New York.

Verwaal, W., Mulder, A., 1993, Estimating Rock Strength with the Equotip Hardness Tester, International Journal of Rock Mechanics and Mining Sciences, v. 30, p. 659-662.

Walker-Milani, M. E., 2011, Outcrop Lithostratigraphy and Petrophysics of the Middle Devonian Marcellus Shale in West Virginia and Adjacent State, Master's thesis, West Virginia University, Morgantown, West Virginia.

Wang, G., 2012, Black Shale Lithofacies Prediction and Distribution Pattern Analysis of Middle Devonian Marcellus Shale in the Appalachian Basin, Doctoral Dissertation, West Virginia University, Morgantown, West Virginia.

Wang, G., Carr, T. R., 2013, Organic-rich Marcellus Shale lithofacies modeling and distribution pattern analysis in the Appalachian Basin, American Association of Petroleum Geologist Bulletin, v. 97, no. 12, p. 2173-2205.

Wendt, K. A., Arthur, A. M., Slingerland, R., Kohl, D., Bracht, R., Engelder, T., 2015, Geochemistry and depositional history of the Union Springs Member, Marcellus Formation in central Pennsylvania, Interpretation, v. 3, no. 3, p. SV17-SV33.

Yanni, A., 2010, Subsurface Stratigraphy and Petrophysical Analysis of the Middle Devonian Interval, Including the Marcellus Shale, of the Central Appalachian Basin: Northwestern Pennsylvania, Master's thesis, West Virginia University, Morgantown, West Virginia.

Zagorski, W. A., Wrightstone, G. R., Bowman, D. C., 2012, The Appalachian Basin Marcellus gas play: its history of Development, geologic controls on production, and future potential as a world-class reservoir, in AAPG memoir, Breyer J. A.,, ed., Shale reservoirs – giant resources for the 21st Century.

Zahm, C. K., Enderlin, M., 2010, Characterization of rock strength in cretaceous strata along the Stuart City Trend, Texas, Gulf Coast Association of Geological Societies Transactions, v. 60, p. 693-702.

Zahm, C. K., Sonnenfeld, M., in review, Measurement of UCS in thin, low-strength bentonite zones within the Niobrara Formation, submitted to Rock Mechanics and Rock Engineering.

Zoback, M. D., Chang, C., Khaksar, A., 2006, Empirical relations between rock strength and physical properties in sedimentary rocks, Journal of Petroleum Science and Engineering, v. 51, p. 223-237.

Zoback, M. D., 2007, Reservoir Geomechanics. Cambridge, United Kingdom: Cambridge University Press.

APPENDIX

Appendix 1: Chemical Element Cross Plots from Olsyn #2V and SRC #1V wells

Appendix 1

Olsyn #2V Chemical Element Cross Plots

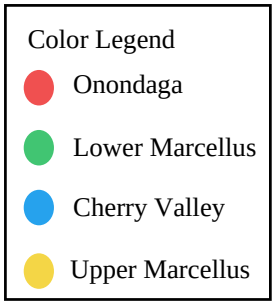

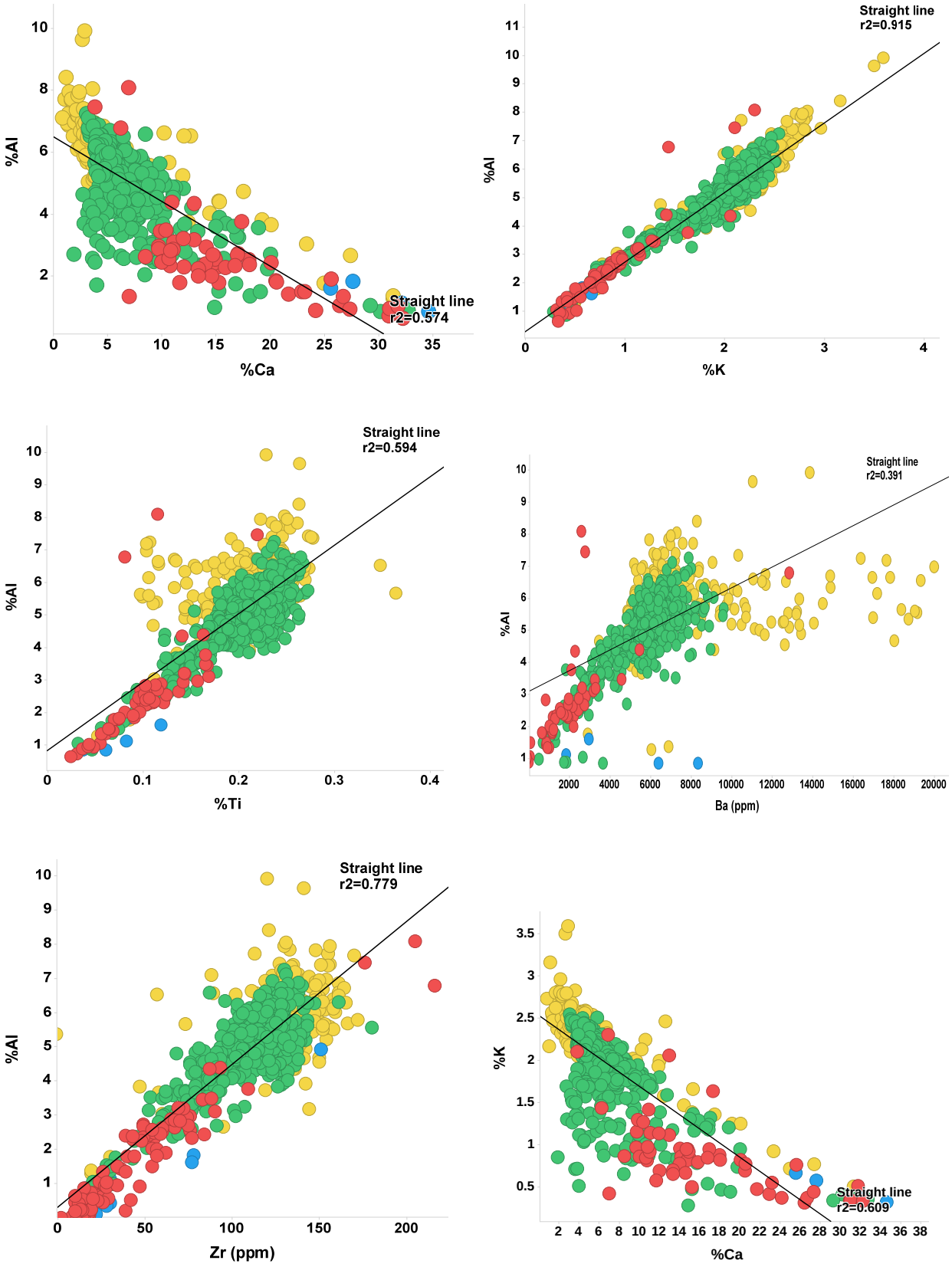

Cross plots of XRF-derived data for the Olsyn #2V.

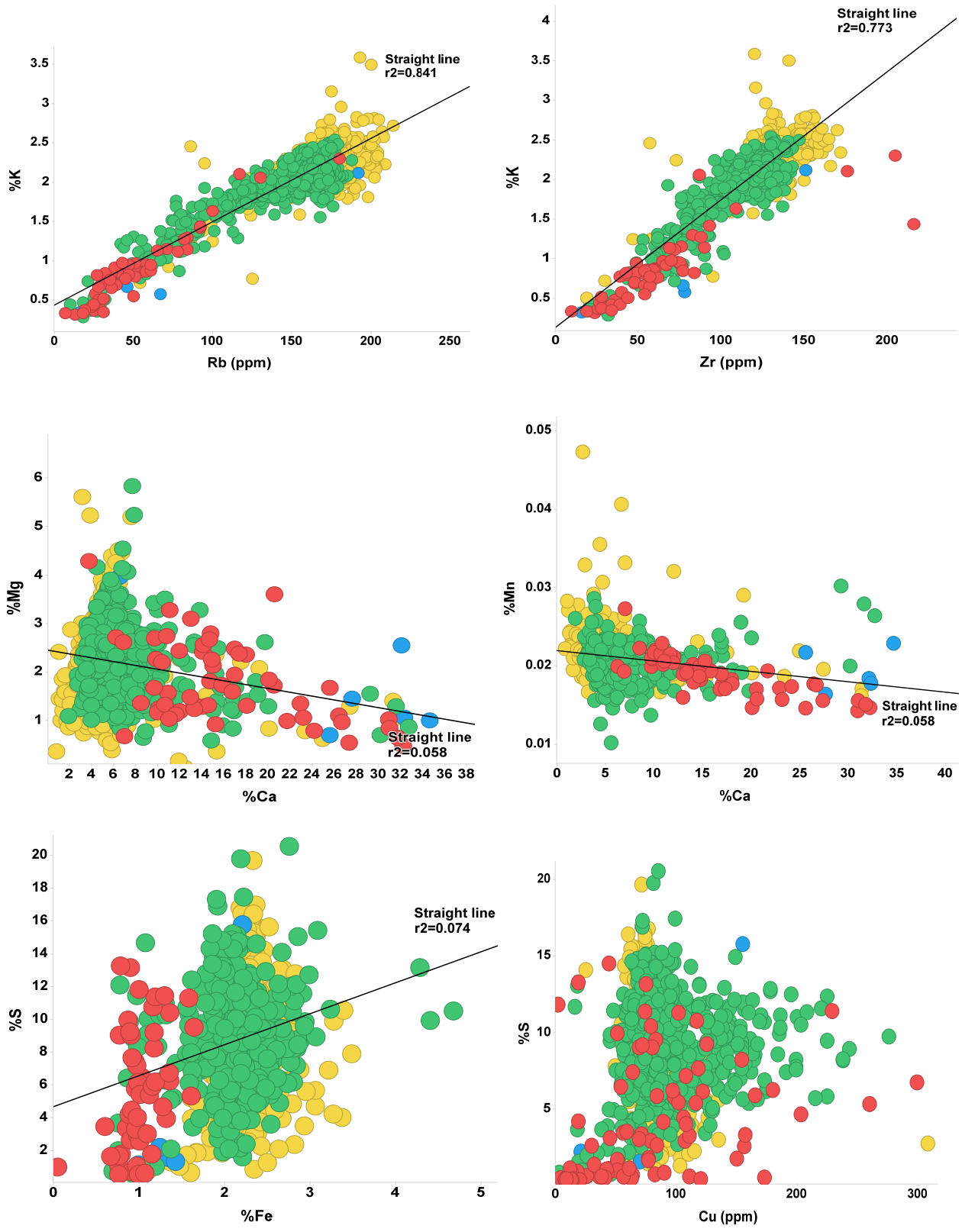

Cross plots of XRF-derived data for the Olsyn #2V.

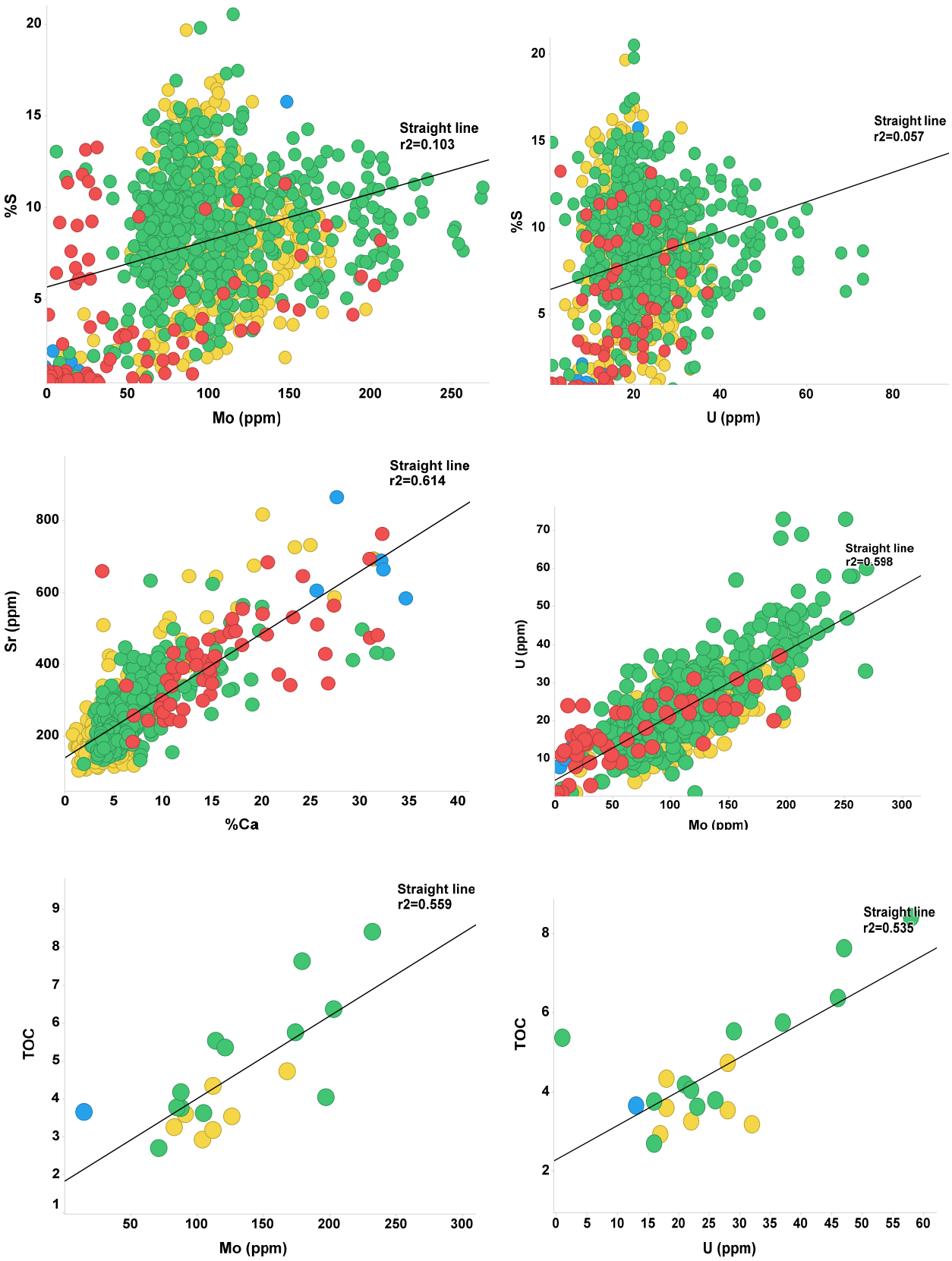

Cross plots of XRF-derived data for the Olsyn #2V.

SRC #1V Chemical Element Cross Plots

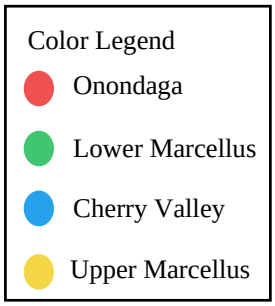

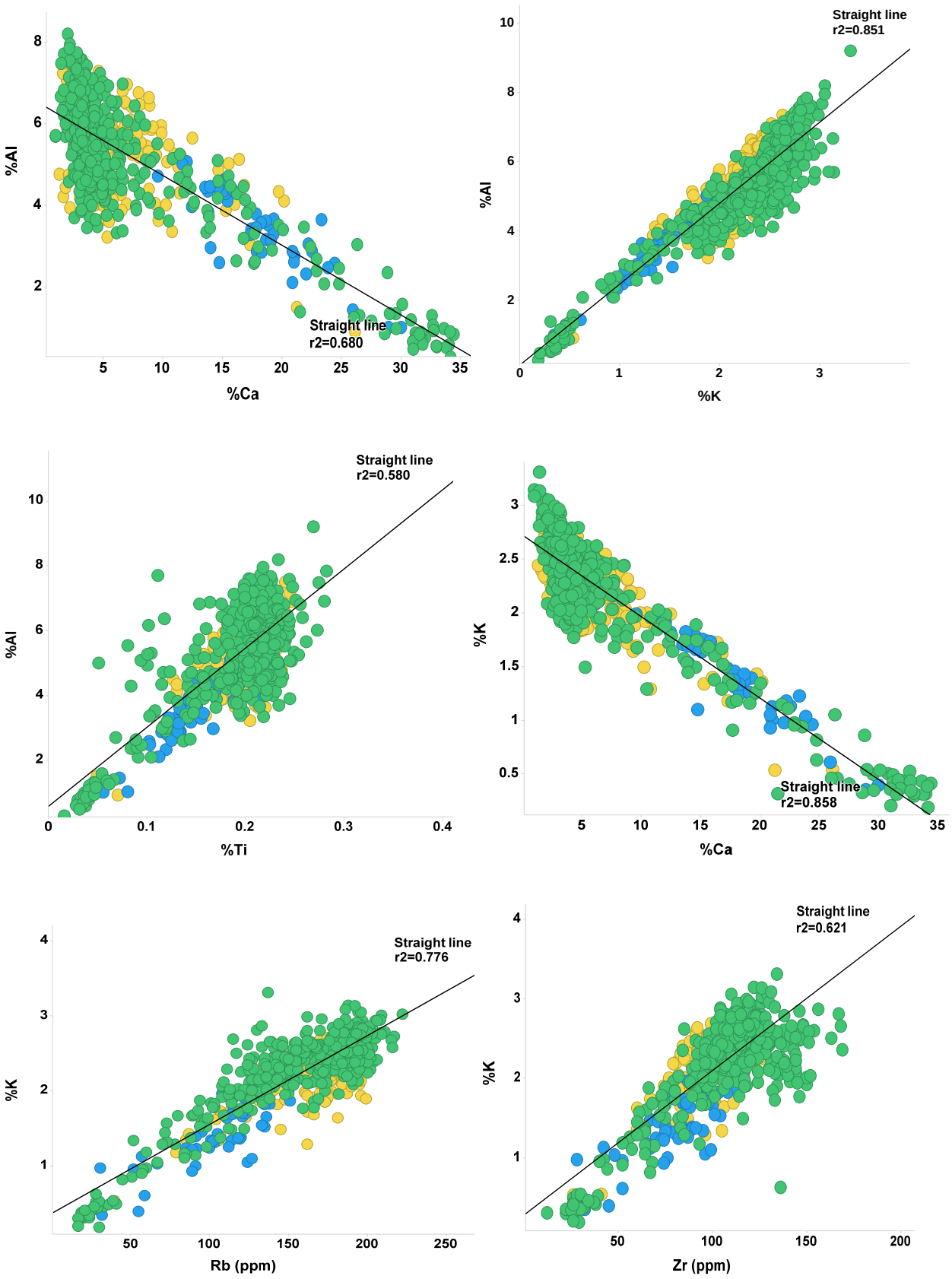

Cross plots of XRF-derived data for the SRC #1V.

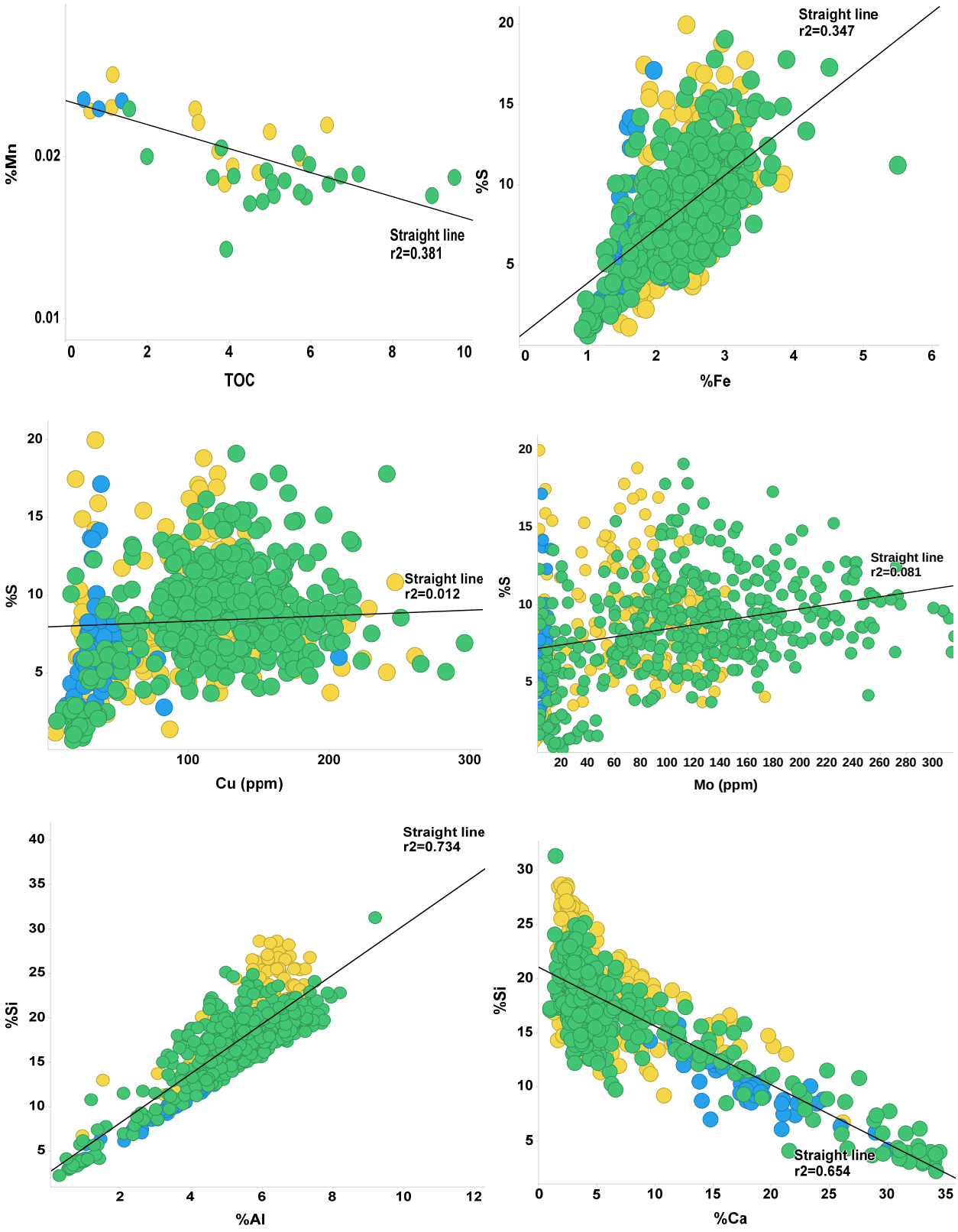

Cross plots of XRF-derived data for the SRC #1V.

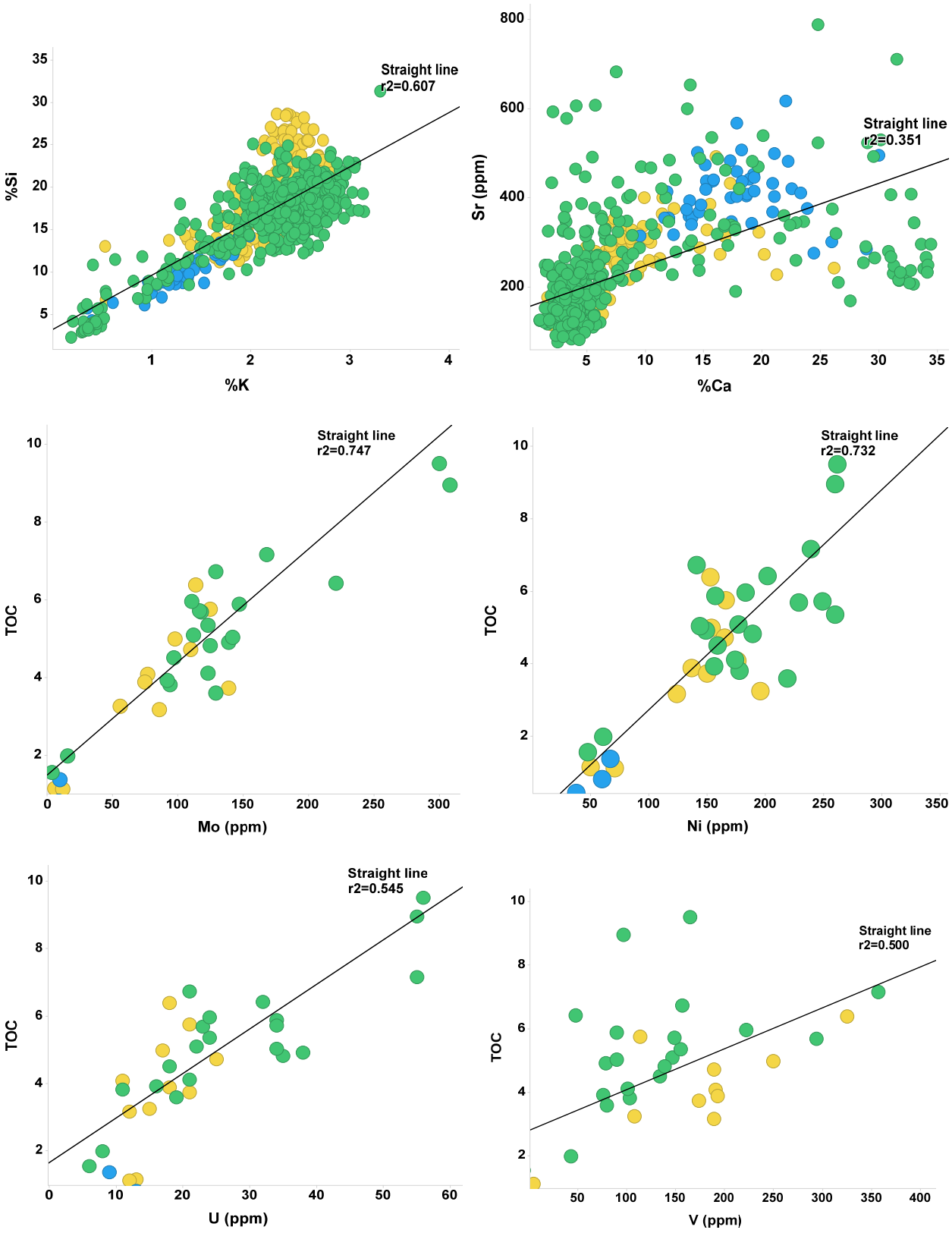

Cross plots of XRF-derived data for the SRC #1V.

VITA

Personal Background	Chieke Gregory Offurum Fort Worth, Texas Son of Benedict and Helen Offurum Married to Adanna N. Offurum, April 26, 2014
Education	Bachelor of Science, Geology, 2004, University of Port Harcourt, Nigeria Master of Science, Geology, 2016, Texas Christian University
Experience	Field Engineer, Baker Hughes Inc., 2008-2011 Senior Geoscientist, Baker Hughes Inc., 2011-2012 Senior Petrophysicist, EOG Resources, 2012-Present
Professional Memberships	American Association of Petroleum Geologists (AAPG)

ABSTRACT

INTEGRATED GEOCHEMICAL, MECHANICAL, AND LITHOLOGICAL CHARACTERIZATION OF THE MARCELLUS SHALE, PENNSYLVANIA

Chieke Gregory Offurum, M.S., 2016
Department of Geology
Texas Christian University

Dr. Helge Alsleben, Associate Professor of Geology

The middle Devonian (392-387 Ma) Marcellus Shale is one of the primary targets for unconventional drilling in the Appalachian basin. Despite its often homogenous and fine-grained appearance, the Marcellus Shale was deposited under varying environmental conditions, which can lead to subtle differences in fabric and texture not readily identifiable by conventional low resolution sampling and analysis. This study incorporates high resolution geochemical, mechanical, and lithological characterization from two vertical cores to assess vertical and lateral heterogeneity of the Marcellus Shale in northern Appalachian basin. Detailed analysis were also performed to understand the sediment flux, paleoproductivity and paleoredox conditions during Marcellus deposition. Interpretation of the various analytical results suggests that the Marcellus Shale is vertically and laterally heterogeneous. Redox-sensitive trace elements also suggest that the Marcellus Shale was most likely deposited in predominantly anoxic deep-water conditions.